OPTIMIZING FLOTATION PERFORMANCE USING EXTREMUM SEEKING CONTROL

by

Daniël Adriaan Wepener

Submitted in partial fulfillment of the requirements for the degree
Master of Engineering (Electronic Engineering)

in the

Department of Electrical, Electronic and Computer Engineering
Faculty of Engineering, Built Environment and Information Technology

UNIVERSITY OF PRETORIA

February 2023

SUMMARY

OPTIMIZING FLOTATION PERFORMANCE USING EXTREMUM SEEKING CONTROL

by

Daniël Adriaan Wepener

Supervisor:	Prof J. D. le Roux
Co-supervisor:	Prof I. K. Craig
Department:	Electrical, Electronic and Computer Engineering
University:	University of Pretoria
Degree:	Master of Engineering (Electronic Engineering)
Keywords:	Extremum seeking control, optimization, flotation circuit, peak air recovery, process control

In this dissertation, a flotation circuit is controlled in simulation using an extremum seeking control (ESC) approach to optimize the flotation performance of the circuit using peak air recovery. Flotation is a separation process in the mineral processing chain. A comminution process such as a grinding circuit first grounds the raw ore from a mine into fine particles, then the flotation circuit is responsible for separating the valuable minerals from the waste material or gangue. A flotation process achieves this by exploiting the difference in hydrophobicity between the valuable minerals and the gangue. Air is pumped into the bottom of the flotation cell to create bubbles in the cell. Chemical reagents such as collectors are added to the slurry to ensure the valuable minerals are hydrophobic, and the gangue is hydrophilic. As the bubbles rise through the slurry, the valuable minerals attach to the bubbles and rise to a froth layer at the top of the cell, from where it overflows and can be concentrated.

The flotation process has two important performance properties: the grade is how pure the final product is, and the recovery is how much of the valuable minerals have been concentrated. Grade and recovery are inversely proportional, which creates the control challenge of selecting

the optimal grade and recovery operating points. A solution to this control challenge is to maximize air recovery. Air recovery is the fraction of air introduced to the cell that overflows in unburst bubbles and has been shown to be a measure of froth stability. It is assumed that optimal performance is achieved at the operating point where the air recovery is maximized as the froth layer is stable and the mineral recovery of the flotation cell is optimized.

A model-free adaptive control strategy in the form of ESC is proposed to control the flotation circuit at the peak air recovery operating point and optimize the flotation performance. The ESC controller explores an unknown static map of the objective function and searches for the extremum. Two gradient-based ESCs, a classical perturbation-based ESC and a time-varying ESC, as well as a non-gradient-based direct search Nelder-Mead simplex ESC, are implemented on a model that simulates a flotation circuit and used to steer the plant towards the peak in air recovery. The three ESC methods do not depend on a process model to optimize the plant and only use the online measurement of the objective function to optimize the process.

Two control strategies are implemented: a single-input perturbation and a multiple-input perturbation strategy. The implemented ESC controllers are evaluated in two simulation scenarios that investigate the optimization ability of the ESC controllers and the disturbance rejection ability of the ESC controllers. The three ESCs can respectively optimize the flotation circuit in both strategies and find the peak air recovery operating point. The simplex ESC can converge quickly to the optimum but does not adapt to changing conditions. The gradient-based ESCs can track the time-varying peak air recovery operating point in the presence of an external disturbance.

The convergence time of the gradient-based controllers is relatively slow due to the time scale separation required between the flotation dynamics and the optimization rate. The multiple-input perturbation strategy resulted in slightly faster convergence in the gradient-based controllers, but with slightly worse performance compared to the single-input perturbation strategy. The convergence time of the simplex ESC becomes much slower when the second input is also perturbed due to the added complexity. The ESCs are ideally suited for model-independent long-term automated optimization of a flotation circuit with a slow time-varying optimal operating point.

ACKNOWLEDGMENTS

I am thankful for the financial support for this work provided by the National Research Foundation of South Africa (Grant number 130380). I would also like to thank the South African Council for Automation and Control as well as the IFAC Foundation for their sponsorships, allowing me to attend the CCA2021 and the MMM2022 conferences.

I would like to thank my supervisors, Prof Derik le Roux and Prof Ian Craig, for their support, patience and guidance throughout my studies. I am grateful for everything I learned from them and all the opportunities they gave me, it has been a privilege to pursue my studies under their supervision.

I would also like to thank Kobus Oosthuizen for the generous knowledge and insight he shared about the flotation process and his willingness to share his research which proved instrumental to the completion of this work.

Thank you to my parents for giving me the opportunity to study and for their support and encouragement throughout my studies. Lastly, I would also like to thank God for allowing me the ability and strength to undertake this task.

LIST OF ABBREVIATIONS

ESC	Extremum Seeking Control
MISO	Multiple-Input Single-Output
MPC	Model Predictive Control
PAR	Peak Air Recovery
PESC	Perturbation-based Extremum Seeking Control
PID	Proportional-Integral-Derivative
ROM	Run-Of-Mine
SESC	Simplex Extremum Seeking Control
SISO	Single-Input Single-Output
TESC	Time-varying Extremum Seeking Control

TABLE OF CONTENTS

LIST OF FIGURES

LIST OF TABLES

CHAPTER 1 INTRODUCTION

1.1 PROBLEM STATEMENT

1.1.1 Context of the problem

Flotation is a separation process in the mineral processing chain responsible for separating valuable mineral particles from the gangue. Inside a flotation cell, air is pumped from the bottom of the cell and forms bubbles that rise to the top of the cell and form a froth layer. The desired mineral particles are hydrophobic (or they are made hydrophobic through the addition of chemicals) and attach to the bubbles that rise to the top of the cell, where the froth overflows and collects in the launder.

The main goals of a flotation cell are to firstly recover as much as possible of the desired mineral and secondly to keep the final product as concentrated as possible. These two goals represent two of the important performance metrics of a flotation circuit called the mineral recovery and grade. Recovery is the fraction of the desired minerals in the feed that are concentrated, and grade is the mass ratio of the desired mineral to the gangue in the final product. Both grade and recovery should be maximized to optimize the performance of the flotation circuit. However, grade and recovery are inversely proportional (Wills and Finch, 2015), and it remains a challenge to select the best operating point on the grade-recovery curve.

One way to select the operating point is by using another metric called air recovery. Air recovery is the fraction of the air that enters the flotation cell that overflows the lip of the cell inside unburst bubbles. Hadler and Cilliers (2009) report that the optimal performance of a flotation cell can be found by maximizing the air recovery of the cell and operating at the peak air recovery point. At this optimal operating point, the froth is stabilized, and the

mineral recovery is maximized while the grade is kept at an acceptable level (Hadler et al., 2010).

An impediment to using peak air recovery for optimization control is that the peak is time-varying, and the required aeration rate that results in peak air recovery continuously shifts (Phillpotts et al., 2020). The fluctuation in air recovery may be due to changing ore characteristics or upstream conditions that propagate to the flotation circuit (Wepener et al., 2021). This makes it difficult to operate the flotation plant optimally at all times, and manual selection of the setpoints could result in reduced performance.

Model-based control is a possible solution to the optimization problem, but it is dependent on a model of the flotation process, which is a complicated metallurgical process and is difficult to model accurately. There are good flotation models that can be used to optimize the process, but the models are often very large, difficult to fit to a processing plant and are dependent on accurate, fast and reliable online measurements, which are not always available (Oosthuizen et al., 2017).

In the mineral processing industry, there is an incentive for improved optimization control, especially long-term automated advanced optimization (Shean and Cilliers, 2011; Bergh and Yianatos, 2011; Smith et al., 2010). The focus of this study is a model-free flotation optimization controller that ensures that the process autonomously operates at the optimal operating point even under changing conditions.

1.1.2 Research gap

In the mineral processing industry, there is a need for automation to reduce the dependence of the processing plant on experienced operators and to improve the economic performance of the plant. This is highlighted in a survey on the degree of automation in the mineral processing industry (Olivier and Craig, 2017). More than 90 % of the respondents indicated that operator actions are required at least once every 30 min, and more than 20 % of the respondents indicated that operators are constantly busy. About 50 % of the operator actions are changes in operating conditions. If these operator actions can be replaced with a real-time optimization control layer, the performance of the plant can be improved, and the plant can be operated more autonomously without the need for constant operator actions. This

optimization control layer would be a step towards the goal of a completely autonomous processing plant.

Air recovery has been shown to be an important metric to use in the optimization of a flotation circuit because it is a measure of froth stability, and mineral recovery is optimized at the peak in air recovery (Hadler and Cilliers, 2009; Hadler et al., 2010; Smith et al., 2010). However, limited evidence has been found of air recovery being used in flotation control (Shean et al., 2017), and no literature could be found that describes air recovery actively being used to control an industrial plant. Phillpotts et al. (2020) demonstrated on an industrial plant that the peak in air recovery corresponds to maximum mineral recovery during normal flotation, confirming that an optimization controller using air recovery would be a feasible solution. The research gap that is addressed in this dissertation is the need for a model-free real-time controller that can optimize a flotation circuit autonomously using peak air recovery.

Extremum seeking control (ESC) is an optimization technique that maximizes an objective function by exploring an unknown static map and steering the system towards the optimal operating condition (Krstić and Wang, 2000; Guay et al., 2015). ESC is a model-free adaptive controller and does not use any explicit knowledge of the process dynamics. The research gap is addressed in this study by using an ESC controller to optimize a flotation circuit by continuously operating the circuit at peak air recovery. An ESC optimization layer on a flotation control structure could potentially replace the need for regular operator actions and allow the plant to operate optimally autonomously.

1.2 RESEARCH OBJECTIVE AND QUESTIONS

The main research objectives of this dissertation are to:

- Implement a flotation simulation platform with a sufficient dynamic flotation model that can be used to simulate different controllers and evaluate the performance of the controllers.
- Design different ESC controllers to optimize the performance of a flotation circuit.
- Simulate the controllers on the simulation platform and evaluate and compare the flotation performance under varying operating conditions.

The resulting research questions that stem from these objectives are:

1. What is a sufficient dynamic flotation model to use in the simulation platform that will enable accurate simulation and evaluation of different controllers on a flotation circuit?
2. Is air recovery a viable objective function to use for flotation optimization using an ESC?
3. Which ESC controllers would be best suited for flotation optimization, i.e., do gradient-based or direct search controllers work better?
4. What manipulated variables should be used by the ESC controller to optimize the flotation circuit?
5. Which optimization strategies would be best suited for air recovery optimization?
6. Can an ESC controller successfully optimize the performance of a flotation circuit when starting from a suboptimal operating point in the presence of external disturbances and noise?
7. Is an ESC controller fast enough to track a time-varying optimum as the operating conditions change?

1.3 HYPOTHESIS AND APPROACH

The hypothesis is that an ESC will be able to successfully optimize a flotation circuit and track a time-varying optimal operating point. Including air recovery in an objective function is expected to result in optimal mineral recovery and flotation performance by operating the flotation cell at the peak in air recovery. The ESC controller is not expected to perform as well as a model-based controller in terms of convergence time, but it should be able to effectively steer the plant towards the unknown optimum even in the presence of some external disturbances and noise.

The following approach will be taken in this study:

1. A literature study will be conducted on flotation modelling and control to get a better understanding of how the process work, what types of models exists and how flotation circuits are controlled. A literature study will also be conducted on ESC to understand how ESC works and what types of ESC controllers can be used to control the flotation circuit.
2. From the literature study, a suitable flotation model will be identified to use for the simulation platform.

3. The simulation platform will be implemented using the identified flotation model and appropriate flotation plant data. Regulatory controllers will also be implemented on the platform to stabilize the flotation cell and hopper levels. The platform will make it possible to test a variety of optimization controllers and operating conditions in a controlled environment.
4. From the literature study, at least two different ESC controllers will be identified that can be used to optimize the flotation circuit.
5. The ESC controllers will be implemented on the simulation platform and tuned to work well and control the flotation circuit successfully.
6. At least two different optimization strategies using the ESC controllers will be tested in simulation.
7. The performance of the flotation circuit under the control of each of the ESC controllers will be analyzed and compared. Specific attention will be given to how the grade, recovery and air recovery compare when the optimization starts from a suboptimal operating point and in the presence of disturbances and noise.
8. The study will be concluded by evaluating the effectiveness, benefits and drawbacks of the model-free optimization of the flotation circuit using ESC.

1.4 RESEARCH GOALS

The research goals of the study can be summarized as follow:

- Design and implement a flotation simulation platform using a suitable dynamic flotation model, including regulatory controllers, that can be used to simulate and evaluate flotation optimization controllers.
- Implement and tune different ESC controllers on a simulation platform that can successfully control a flotation circuit.
- Demonstrate that ESC can successfully be used for model-free optimization of a flotation circuit and that the ESC controllers can track a time-varying optimal operating point in the presence of disturbances and noise.

1.5 RESEARCH CONTRIBUTION

The contribution of this work is the demonstration of a successful implementation of an ESC optimization controller on a flotation circuit in simulation. This work describes the first application of different ESC controllers to a flotation circuit model. In particular, a newly

developed flotation circuit model (Oosthuizen et al., 2021), verified on industrial data, is used to illustrate the feasibility of applying ESC to flotation and the impact that it has on optimizing the process. This study explores three different ESC methods: two gradient-based methods (a perturbation-based and a time-varying method), and a non-gradient-based Nelder-Mead simplex method. The ESC controllers optimize the flotation circuit performance by maximizing the air recovery in each cell.

1.6 RESEARCH OUTPUTS

The following publications resulted from this study:

- Wepener, D. A., le Roux, J. D. and Craig, I. K. (2021). Disturbance propagation through a grinding-flotation circuit, *IFAC-PapersOnLine* **54**(21): 19–24.
- Wepener, D. A., le Roux, J. D. and Craig, I. K. (2022). Extremum seeking control of a flotation circuit using peak air recovery, *IFAC-PapersOnLine* **55**(21): 61–66.
- Wepener, D. A., le Roux, J. D. and Craig, I. K. (2022). Extremum seeking control to optimize mineral recovery of a flotation circuit using peak air recovery, submitted to *Journal of Process Control*.

1.7 OVERVIEW OF STUDY

The dissertation is organized as follows:

- Chapter 2 provides a review of the relevant flotation literature. The chapter includes an overview of the flotation process, modelling of flotation circuits and flotation control. The literature on air recovery and its significance in flotation optimization is reviewed.
- Chapter 3 describes the literature and history of ESC. The chapter also gives the design methodology and implementation of the three different ESC controllers: two gradient-based methods (a perturbation-based and a time-varying method), and a non-gradient-based Nelder-Mead simplex method.
- Chapter 4 presents the flotation circuit model used in the study as well as the steady-state simulation of the model showing the relationships between the parameters.
- Chapter 5 shows the simulation setup of the regulatory controllers and ESC controllers in the simulation platform. The simulation results of the optimization by the different ESC are presented and discussed.
- Chapter 6 gives the concluding remarks of the research project and highlights the significant findings.

CHAPTER 2 FLOTATION

2.1 CHAPTER OVERVIEW

This chapter presents the flotation literature study for this dissertation. Section 2.2 discusses how the flotation process works and what the objectives of the process are. Section 2.3 provides a literature survey of different types of flotation models and gives examples of flotation models that are being used for flotation control. In Section 2.4, the literature on flotation control is discussed using four levels of stratification: instrumentation, regulatory control, advanced control, and optimization control. Section 2.5 concludes the chapter.

2.2 FLOTATION PROCESS DESCRIPTION AND OBJECTIVES

2.2.1 Mineral processing plant description and objectives

The mineral processing chain consists of two main stages: the comminution stage and the separation stage. Figure 2.1 show the entire chain from the mining operation to the final product. The run-of-mine (ROM) ore from the mining operation first passes through the

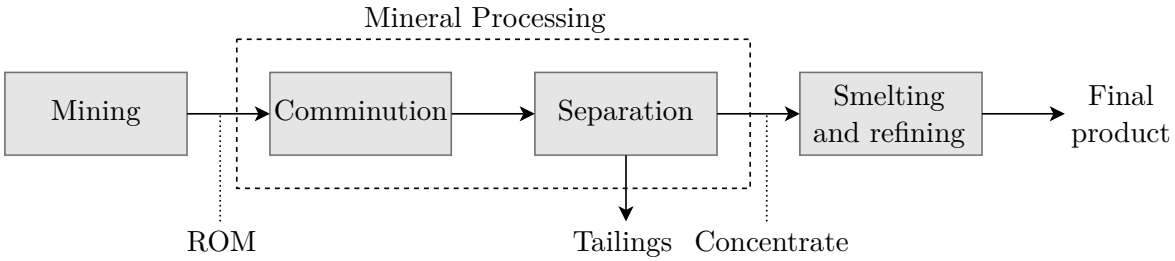

Figure 2.1. Diagram of a mineral processing plant.

comminution stage, where the ore is broken into fine particles and mixed with water to form a slurry. The comminution circuit consists of several processes that are required to liberate valuable minerals. Next, the slurry flows to a separation stage where the valuable minerals are separated from the grange. As can be seen from Figure 2.1, the comminution and

separation processes are closely linked, and it is not uncommon for disturbances to propagate from the comminution to the flotation circuit as discussed in Wepener et al. (2021) and Addendum B. Separation processes are capable of selecting particles based on their physical or chemical properties. There are many different types of separation circuits: flotation, magnetic separation, gravimetric separation, dense medium separation, sorting or leaching. This study will focus on flotation only. The flotation process is discussed in Section 2.2.3. The tailings from the separation stage are discarded and flow to tailings dams while the concentrate is pumped to the next stage in the chain. The smelting and refining stage consists of many sub-processes where the grade of the concentrate is increased until only the final pure product remains.

The control objectives of the overall mineral processing plant play an important role in the control strategies of the individual processes in the chain. The objective can be to maximize the throughput, the net revenue or the recovery at a constant grade (le Roux and Craig, 2019). When determining the profit of the plant, the operating costs are subtracted from the net smelter return. It has been shown that higher throughput translated to better profitability despite a lower quality product (Thivierge et al., 2019). The control objective of the liberation process should ideally be set according to the plant-wide objective but is usually set to maintain a percentage of particles smaller than a given size (Hodouin, 2011). There is a trade-off between the liberation of the particles and the cost of comminution. The desired product size distribution is therefore set to an acceptable compromise.

2.2.2 Comminution by means of grinding

A typical comminution circuit starts with a crusher to crush the ROM ore into smaller rocks. These rocks then feed into a grinding mill along with water and steel balls to be grounded into fine particles. The grinding mill is a large rotating drum lined on the inside with raised sections or mill liners that provide lift to the charge in the mill as it rotates. As the charge falls back down from the load shoulder to the toe at the bottom of the mill, it crashes into other rocks and steel balls which causes impact breakage of the ore (Wills and Finch, 2015). Other methods of grinding that also happen in the mill include attrition and abrasion.

The slurry in the mill can be discharged by means of a discharge screen or overflow. The screen has a mesh with apertures that only allow particles smaller than a specific size through.

Any particle larger than the aperture will pass over the screen and is circulated back for regrinding. After discharging the mill, the slurry is collected in a sump and further diluted with water. The sump level can vary, allowing for the absorption of some of the irregularities and disturbances in the throughput of the mill. From the sump, the slurry is pumped to a classifier such as a hydrocyclone. The hydrocyclone is used to separate finer particles from coarser particles in the slurry. The slurry is fed into the cyclone, where it travels in a spiral around the cyclone which creates a vortex. The lighter particles are carried upwards by the vortex and exit at the top in the cyclone overflow. The heavier, denser particles are pushed to the walls of the cyclone by centrifugal forces and travel downwards to the bottom of the cyclone, where it exits in the underflow stream from where it is recycled into the mill to be ground finer.

The cyclone overflow with the finer particles is the final product of the comminution circuit and flows to the separation stage where the valuable mineral particles can be separated from the gangue.

2.2.3 Separation by means of flotation

Flotation is a separation process that concentrates minerals by using their hydrophobicity properties. A flotation cell is used to separate the hydrophobic particles from the hydrophilic particles in a three-phase system (Jovanović and Miljanović, 2015a). The three phases refer to the mineral particles (solid), water (liquid) and air (gas) that interacts with each other inside a flotation cell. Some minerals are not naturally hydrophobic, in which case chemicals called collectors are added to the slurry to improve the hydrophobicity properties of these minerals. Collectors are organic compounds that attach to the surface of a mineral particle and make the particle water-repellent. Reagents called frothers are also added to the slurry. Frothers help in the formation of bubbles and keep the bubbles from bursting when they reach the top of the cell, which is essential for a stable froth that can overflow the cell lip. The frothers also reduce the bubble size and, as a result of the reduced size, the bubbles slow down as they rise through the slurry allowing more particles to attach to the bubbles (Wills and Finch, 2015). Other reagents called modifiers or regulators can also be added to the slurry to further enhance the flotation process through a number of mechanisms.

After the raw ore is liberated in the comminution stage and the water is added to form a

slurry, the ore is pumped into the flotation cell, where the flotation process takes place. The flotation tank size can vary from small laboratory tanks up to large 300 m^3 industrial tanks (Yianatos et al., 2012). Air can be introduced into the tank in different ways depending on the type of flotation cell. In a self-aerated mechanical cell, the air is sucked into the cell by an impeller due to the difference in pressure that is created when the impeller is rotated. In a forced-air mechanical cell, compressed air is released into the cell from an air sparger located underneath the impeller. Column flotation cells were developed in the 1960s and, unlike mechanical cells, contain no moving parts (Wang et al., 2018). In a column cell, the air is pumped into the cell through spargers at the bottom of the cell and mixed with the slurry as the bubbles move to the surface. Another type of flotation cell is the Jameson cell, where the air is mixed with the slurry in a vertical pipe called a downcomer before it reaches the flotation cell (Jameson, 1998).

The aim of the flotation process is to separate valuable particles from gangue. This is achieved when the valuable mineral particles attach to air bubbles introduced in the flotation tank and flow to the top of the tank while the gangue flows to the bottom[1]. This process divides the cell into two sections, the froth and the pulp. The pulp volume contains the liquid slurry with the bubbles flowing through the liquid and the gangue material remaining in the pulp to flow out of the cell through the tailings stream. The froth volume contains the bubbles that float on top of the pulp, and the valuable mineral particles collect in the froth to flow out of the cell through the concentrate stream. The way that the valuable material flow to the froth from the pulp can be divided into three mechanisms:

- True flotation - the particles attach to the rising air bubbles because they are hydrophobic.
- Entrainment - the particles are entrained in the water between the bubbles that rise to the froth.
- Entrapment - the particles are trapped between other particles that are attached to a bubble and flow to the froth with these particles.

True flotation is the most important mechanism that is responsible for the majority of the recovered material. Entrainment and entrapment are also important because it is possible for both valuable particles and gangue particles to become entrained or entrapped, which will affect the efficiency of the process. Detachment can also happen when valuable particles

[1] In some cases, the gangue is hydrophobic and the valuable minerals hydrophilic, which is called reverse flotation (Wang et al., 2018).

become detached from the bubbles in the froth phase and drain back to the pulp phase, which will negatively affect the flotation efficiency. Because of the likelihood that some gangue particles will be recovered with the valuable mineral in the concentrate and that some of the valuable particles will not be concentrated, a single flotation cell is uncommon, and multiple flotation cells are arranged together in flotation circuits.

In industry, flotation circuits comprise of cells connected in series to form a flotation bank. Different flotation banks are then connected together, with each bank performing a specific function. The functions of the flotations banks can usually be divided into three sections: rougher, scavenger and cleaner banks (Laurila et al., 2002). The slurry from the liberation process flows into the rougher flotation bank, where the fast-floating valuable mineral particles are concentrated. Therefore the function of the rougher is to have a high recovery. The tailings of the rougher cell flow into the scavenger bank, where the slowly floating particles are concentrated. The concentrate of the rougher and scavenger cells flows to the cleaner cells, where the grade of the concentrate is increased. The scavenger and cleaner tailings form the final tailings to flow out of the flotation plant.

2.2.4 Flotation objectives

The flotation process is generally evaluated based on two main performance indicators: product grade and mineral recovery. The grade is the ratio of valuable minerals to gangue in the final product, and recovery is the fraction of the total amount of valuable minerals in the feed that are concentrated. The control objective of each flotation cell is to maximize grade and recovery. However, there is an inverse relationship between grade and recovery (Laurila et al., 2002; Craig and Koch, 2003). The relationship between grade and recovery can be illustrated using a grade-recovery curve as shown in Figure 2.2 where each curve shows the range of operating points that are possible under certain operating conditions. The high-level control objective would be to improve the metallurgical efficiency of the process by moving the grade-recovery relationship in the direction of the control objective arrow. The goal is to get the best grade-recovery curve that results in the highest recovery at the highest grade.

The selection of the specific optimal operating point on the grade-recovery curve is an important choice to make and is dependent on the control objective of the wider processing plant and can be affected by many factors such as commodity prices, reagent and treatment costs, ore

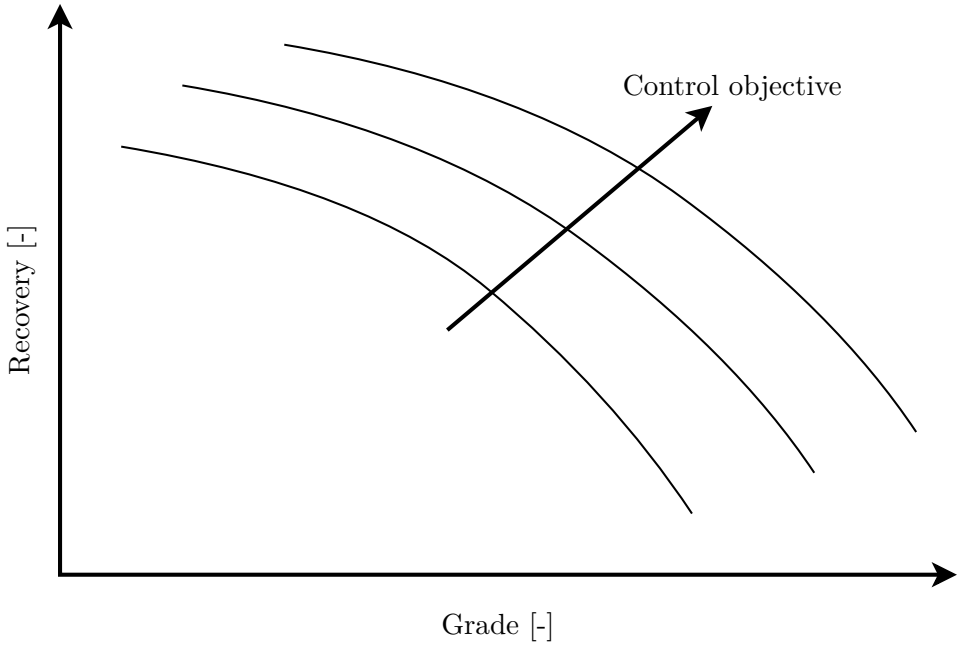

Figure 2.2. Flotation grade-recovery curve showing the control objective. Adapted from Wills and Finch (2015), with permission.

feed rate into the comminution circuit and transportation costs (Wills and Finch, 2015). The operation objective can vary over time as these factors change. Some possible strategies include setting a target grade and maximizing the recovery (Oosthuizen, 2023) or selecting the optimal point based on isoeconomic contours (Laurila et al., 2002). Mass-pull is the mass flow rate of the concentrate from a flotation cell and can be used as a control objective by setting a target mass-pull for the flotation circuit. Supomo et al. (2008) used a machine vision system to control the mass pull of a rougher flotation bank, and the increase in mass pull resulted in an increase in recovery. According to Hadler et al. (2010) however, the increased mass pull can also result in decreased recovery.

Optimizing air recovery is another flotation control objective that will be utilized in this study. Air recovery is the fraction of the air that enters the flotation cell and overflows the lip of the cell inside unburst bubbles. Air recovery has been shown to be linked to the stability of the froth in the flotation cell, and air recovery can be used to measure the froth stability (Ventura-Medina and Cilliers, 2002; Barbian et al., 2003; 2005; 2006). Therefore, air recovery (α) is an indicator that can be used to evaluate the efficiency and performance of the flotation

process. The equation for air recovery is given by (Neethling et al., 2003),

$$\alpha = \frac{v_f \cdot h \cdot w}{Q_{Air}}, \tag{2.1}$$

where v_f is the overflow velocity of the froth, h is the overflow froth height above the cell lip, w is the weir lip length, and Q_{Air} is the inlet airflow rate. In industrial flotation plants, the air recovery can be measured with a froth vision system and laser-based froth height measurement (Shean et al., 2017; Phillpotts et al., 2020). Since the camera only looks at a section of the total cell lip where the froth overflows, the froth velocity and overflow height in this section must be representative of the average froth velocity and overflow height of the entire cell to be accurate (Neethling et al., 2003). Froth velocity measurements can become a problem if the concentrate launder layout is complex and not uniform around the cell or the overflow lip is not horizontal. The froth velocities in the section where the camera can be different from the average froth velocity of the entire cell and thus creating incorrect air recovery measurements.

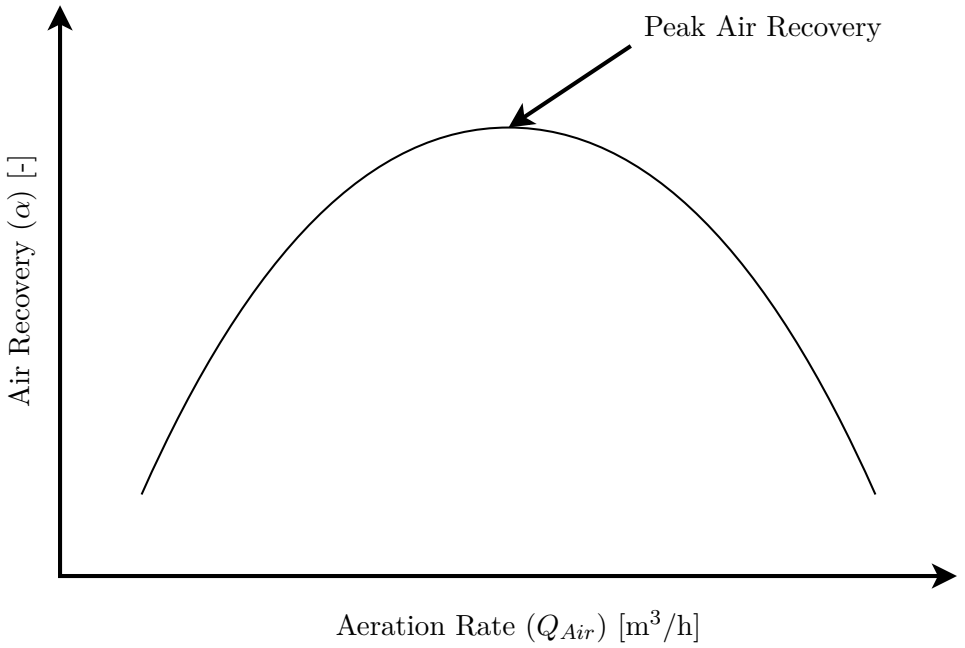

Figure 2.3. Air recovery as a function of aeration rate.

Peak air recovery (PAR) is the maximum air recovery measured in a flotation cell as the aeration rate varies, as shown in the study by Hadler and Cilliers (2009). This peak was confirmed using fundamental physics-based modelling and has been observed experimentally (Neethling and Cilliers, 2008). More importantly, studies also showed that when operating the cell at PAR, the flotation performance improved, causing higher mineral recovery or higher

grade or higher recovery and grade (Smith et al., 2010; Hadler et al., 2010). Figure 2.3 shows the relationship between air recovery and aeration rate, highlighting the PAR point.

At low air rates, below the PAR air rate, the bubbles move slowly through the slurry creating highly laden, well-drained froths, but some bubbles collapse before overflowing the cell lip. At these low air rates, the mineral recovery and mass pull are low, but the mineral grade is high. At high air rates, above the PAR air rate, the bubbles rise quickly through the slurry creating high water content in the froth and low bubble loading. The bubble tends to burst before overflowing, leading to low concentrate grade, but reasonable recovery and high mass pull (Hadler et al., 2010).

At the PAR air rate, there is a balance between the bubble loading and froth mobility which leads to a stable froth, high mineral recovery at an acceptable grade and a reasonable mass pull. Smith et al. (2010) noted that air recovery optimization is a robust and generic technique to find the optimum total air addition to a bank of cells and the optimum distribution of air to the bank. Therefore using PAR as an operational objective gives a single optimization goal that can be used to optimize the process in terms of mineral recovery. PAR optimization has been successfully demonstrated in a single laboratory flotation cell using a direct search optimization algorithm (Shean et al., 2017). In this study, the air rate was the only manipulated variable, and all the other variables were kept constant. The flotation tank used was a closed-loop two-phase system with only a surfactant solution and air. There were no mineral particles in the system, so no separation took place, and the pulp flow rate was set to zero. This setup is not comparable with flotation at an industrial scale, where it might be more challenging for a direct search algorithm to find the peak in the presence of disturbances and changing conditions.

The peak in air recovery is not limited to only variations in the aeration rate as other operating variables can also be used to optimize the air recovery. Surveys by Hadler et al. (2012) showed that air recovery passes through a peak as froth depth is varied at a constant air rate and that froth depth should increase as the air rate increases for the highest possible air recovery. Qu et al. (2013) demonstrated that there exists a strong correlation between air recovery and product ash content in coal flotation by varying the reagent concentrations, and Norori-McCormac et al. (2017) showed that the particle size distribution has an effect on the air recovery and that

there is an optimal air rate for each particle size distribution.

Changes in the flotation circuit due to disturbances or changing feed conditions, such as a change in the particle size distribution, can cause the peak in the air recovery to be time-varying and shift around continuously. Phillpotts et al. (2020) showed the transient nature of the PAR value on an industrial flotation plant. These different peak values at different aeration rates pose a problem with using PAR as a control objective as it requires online air recovery measurements and a process control algorithm to adapt to the changing PAR value to ensure continuous flotation optimization.

2.3 FLOTATION MODELLING

Flotation is a complicated process with many interacting variables that makes the process difficult to model accurately. The process is multi-phased, containing a pulp phase and a froth phase, and it is inherently unstable with complex dynamics (Quintanilla et al., 2021a). A motivation behind the development of accurate dynamic flotation models is to enable the use of advanced model-based control such as Model Predictive Control (MPC). MPC can be effectively used to optimize the flotation process and improve performance. The efficiency of MPC will however deteriorate when the plant model used is no longer an accurate representation of the actual plant dynamics.

Flotation modelling can be classified under two categories, macro-scale and micro-scale models. Micro-scale models are models of the sub-processes in a flotation cell that represent the chemical and physical relationships between the variables in these processes. Due to the many sub-processes with complicated interactions between the variables, it is difficult to identify and model these cause-and-effect relationships (Polat and Chander, 2000). Macro-scale models are simplifications or combinations of micro-scale models to form an overall model for the entire flotation cell. The response of the flotation system is related to various operating parameters through a set of mathematical equations that are dependent on experimental data, plant design layout and control strategies. Only macro-scale models will be discussed, which can be subdivided into theoretical and deterministic models (Gharai and Venugopal, 2016). Theoretical models are of interest and are divided into two main types of models: phenomenological and empirical models. Empirical and phenomenological models can often overlap and be combined together, for example, when the form of an empirical model is

influenced by phenomenological considerations or when empirical parameters are included in phenomenological models (Quintanilla et al., 2021a). The models can also be used alongside each other in one large flotation model - for example, the dynamic model by Quintanilla et al. (2021c) contains both phenomenological and empirical models.

Phenomenological models can further be divided into kinetic models, population balance models and probabilistic models. Apart from the aforementioned basic classification, the models can also be classified based on the characteristics of the model defined by whether the model is (Brogan, 1991; Hodouin, 2011):

- steady-state or dynamic
- stochastic or deterministic
- continuous time or discrete time
- causal or non-causal
- linear or non-linear
- time-varying or constant coefficient
- based on mathematical equations or fuzzy rules.

Another way to organize models is according to the aim of the model (Bouchard et al., 2009):

- prediction of the recovery
- analysis of dynamic behaviour
- development of soft sensors.

A description of each basic model type is given in the next sections.

2.3.1 Phenomenological models

Phenomenological models are based on the fundamental physics and chemistry theory of the sub-processes taking place in flotation and are derived from the conservation of mass, momentum and energy equations. Phenomenological models are usually accurate over a wide range of operating conditions and are not specific to one type of flotation plant.

2.3.1.1 Kinetic models

Kinetics refers to the rate of change of an output variable due to change in the input variable as a function of time (Gharai and Venugopal, 2016). Flotation is intrinsically a rate process because the rate at which the valuable particles are concentrated is proportional to the

concentration of those particles in the pulp. The rate of the particle-bubble collision process is assumed to be first-order with regards to the number of particles, and the bubble concentration remains constant (Polat and Chander, 2000). The actual order of the flotation kinetics is widely discussed (Somasundaran and Lin, 1973; Hernáinz and Calero, 2001; Brożek and Młynarczykowska, 2007; Li et al., 2013), but the first-order rate equation is the most widely accepted approach among researchers (Jovanović and Miljanović, 2015b). The solution of this rate equation results in a first-order flotation model. Kinetic models depend on determining the flotation rate constant, k, which depends on many flotation properties and is thus very difficult to determine.

An example of a kinetic flotation model used for the optimal control of a flotation circuit is given in Maldonado et al. (2007) - this work is based on the dynamic simulator developed by Casali et al. (2002). Putz and Cipriano (2015) made use of kinetic models to develop mass balance models that use the attachment and detachment processes and Tian et al. (2018) followed a similar approach by using kinetic models for the froth phase in an MPC control strategy.

2.3.1.2 Population balance models

A population balance model is a type of discrete kinetic model based on the idea that every particle belongs to a specific group according to its state in the slurry (Bascur, 1982). A particle is either free in the pulp, attached to a bubble in the pulp, free in the froth or attached to a bubble in the froth. Kinetic equations can be used to describe the movement of the particles between these states based on particle-bubble and water transport mechanics. The hydrodynamic characteristics of the flotation cell can be built into a population balance model making simulations of the effect of manipulated variables on the flotation process possible. Population balance models can represent the attachment and detachment of particles as well as the transfer of particles between the pulp and froth, but do not fully represent all the phenomena that occur in a flotation cell (Quintanilla et al., 2021a).

The model in Bascur (1982) is a detailed population balance model that provides an understanding of flotation operations at the expense of increasing complexity (Oosthuizen et al., 2017). A simpler hydraulic model based on mass and volume balances can be found in Jämsä-Jounela (1992), which was later improved by taking the structure of flotation cells and

valve sizing into account (Kämpjärvi and Jämsä-Jounela, 2003). Putz and Cipriano (2015) used a similar hydraulic approach to model the dynamics of the pulp level.

2.3.1.3 Probabilistic models

Probabilistic models are based on the probability of occurrence of the sub-processes in the flotation process, such as the collision, adhesion and detachment of particles and air bubbles. These sub-processes all form part of a sequence of events that needs to happen for a valuable mineral particle to be recovered. The probabilities of the sub-processes can be added together to form a probabilistic model to predict the probability of a particle being successfully recovered (Gharai and Venugopal, 2016). Schuhmann (1942) presented a probabilistic flotation model to predict the successful transfer of a particle to the concentrate based on the probabilities of particle-air bubble collision and adhesion.

2.3.2 Empirical models

Empirical models are based on data collected from the process that are used to form relationships between process variables without determining the theoretical causes of the relationships. These data-driven flotation models mainly involve one of three purposes (Oosthuizen et al., 2017):

- Performance evaluation by modelling the relationship between froth features and flotation performance.
- Grade or recovery prediction from inlet conditions and operational variables.
- Creating a model-based soft sensor to estimate a key process variable.

Mathematical equations are used to describe the correlation between the amount of material floated and the input and output variables. These equations contain curve-fitting parameters that are estimated using statistical methods to relate dependent and independent variables. The parameters do not necessarily have any physical significance (Polat and Chander, 2000). Empirical models require data from flotation plants to use in the statistical methods, and as a result, the model is specific to a particular plant. Empirical models have the advantage of being cheaper and easier to develop but are not always reliable in the long term due to changing operating conditions. Phenomenological models are therefore preferred if available (Oosthuizen et al., 2017).

An example of an empirical model is the model by Pérez-Correa et al. (1998) where mass balances and empirical relationships were used to create a non-linear dynamic model used

in a simulation to reproduce the dynamic behaviour of a plant. This model was also used and expanded on by Putz and Cipriano (2015) for the implementation of a hybrid dynamic simulator to evaluate a hybrid MPC methodology. Savassi et al. (1998) provides an empirical model for entrainment in industrial flotation plants using two empirical parameters. Maldonado et al. (2009) used empirical models fitted with operational data to implement an MPC strategy to control a flotation column. Empirical models are often combined with phenomenological models. Examples include the population balance model in Bascur (1982) that made use of empirical models for some of the relationships and the dynamic simulator in Casali et al. (2002) that combines kinetic models with empirical relationships. The dynamic model in Oosthuizen et al. (2021) includes empirical parameters in some of the equations that model air recovery and bubble size.

2.3.3 Deterministic models

While deterministic models are not often used in control applications, they are useful in modelling the flotation process to better understand how the process works (Gharai and Venugopal, 2016). Computational fluid dynamic (CFD) modelling of the flotation cell is a useful modelling approach to model the bubble-particle attachment (Koh and Schwarz, 2006). CFD modelling applies a probabilistic approach in describing the flotation micro-processes when developing the models for particle adhesion to air bubbles in the pulp (Koh and Schwarz, 2006; Jovanović and Miljanović, 2015b). CFD methods are capable of simulating the flow of liquids, gasses and particles in a flotation tank and solving the time-dependent turbulent flow field (Wang et al., 2018). CFD models provide a wealth of details about the flotation process, like internal velocities and the distribution of phases in a call.

2.4 FLOTATION CONTROL

Plant-wide flotation control consists of interconnected control levels as described in Laurila et al. (2002) and shown in Figure 2.4. The top control level is the optimization level which aims to maximize the profit generated by the flotation process (Bergh and Yianatos, 2011). Other stratification systems have also been proposed (Jovanović and Miljanović, 2015a), but in this review, the focus will be on the four levels shown in Figure 2.4.

2.4.1 Instrumentation and actuators

Instrumentation and actuators form the basis for any control system, and without adequate installation and maintenance of these control elements, none of the advanced control strategies will be possible. The flotation process is a very complex process with a large number of

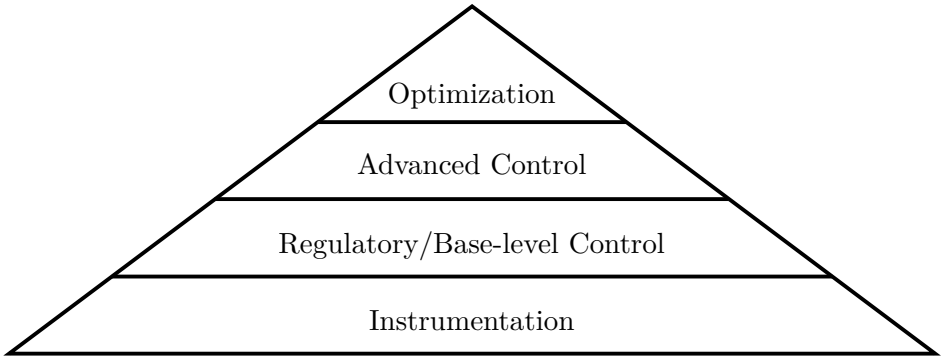

Figure 2.4. Control system level hierarchy for flotation processes.

variables (as many as 100 different variables (Shean and Cilliers, 2011)) that interact with each other physically or chemically in the flotation cell. The most important variables in the process are listed in Laurila et al. (2002) as follows:

- slurry properties (density, solid content and flow rate)
- froth properties (speed, stability and bubble size distribution)
- particle properties (size distribution, degree of liberation and shape)
- electrochemical potentials (acidity, electrochemical potential, and conductivity)
- chemical reagents and their addition rate (collectors, frothers and modifiers)
- pulp level and aeration rates
- mineralogical composition of the ore
- mineral concentrations in the feed, concentrate and tailings
- froth wash water rate.

These variables can generally be divided into three categories (Wright, 1999):

- feed characteristics
- physicochemical factors
- hydrodynamics.

However, it is often better to divide the variables in terms of their function in a process control loop (Hodouin, 2011):

- internal state variables
- manipulated variables
- controlled variables
- disturbance variables.

Examples of typical flotation variables in each of the categories can be found in Hodouin (2011) and Jovanović and Miljanović (2015a). To measure the variables used in the control of a flotation cell and to control the controlled variables, instrumentation and actuators are required. In the following paragraphs, the instrumentation and actuators used in the flotation industry are discussed.

Slurry flow rate measurement: To measure the flow rate of the slurry flowing into the flotation cell, magnetic flow meters are most often used. Magnetic flow meters are based on Faraday's principle of induction to measure the flow of a liquid in a non-obtrusive way. Magnetic flow meters require the fluid to be weakly conductive to work, and it does not work with magnetic solids. Demagnetization is required for magnetic solids like magnetite (Laurila et al., 2002). In the case of an open channel, as is often found in the concentrate stream, the flow can be measured with a dam arrangement. The dam arrangement uses a V-shaped cutout and an ultrasonic level transmitter to roughly estimate the flow rate.

Pulp level measurement: There are many different ways to measure the pulp level, however, the transition from pulp to froth is not always a sharp transition, and accurate level measurement can be troublesome (Laurila et al., 2002). The different measurement methods are as follows:

- Float with target plate and ultrasonic transmitter
- Reflex radar (can be used to measure pulp level and froth thickness)
- Float with angle arms and a capacitive angle transmitter
- Hydrostatic pressure measurement
- Conductivity and capacitance measurement

The level can also be predicted by a model (Shean et al., 2018) that can act as a soft sensor or a validation method to verify the measurements.

Slurry control valves: The slurry control valves are the actuators used in the control of the slurry flow rate and, by extension, the pulp level. Most often, either pinch valves or dart valves are used. The valves must be robust and durable since they must accommodate large flow rates, capacity changes and abrasive minerals.

Airflow rate measurement: There are three typical methods to measure the flow rate of the air entering the flotation cell:

- thermal gas mass flow sensor
- differential pressure transmitter with a venturi tube
- differential pressure transmitter with Pitot or annubar element.

Thermal gas mass flow sensors are relatively expensive, making the differential pressure flow meters more popular, but there can be some installation-related problems with the latter. To control the airflow rate, butterfly valves are used (Laurila et al., 2002).

Gas dispersion measurements: Gas dispersion refers to the measurement of the variables concerning the state of the superficial gas (air) in the flotation cell (Gomez and Finch, 2007). The velocity of the gas bubbles moving upwards inside the cell can be measured with a superficial gas velocity measurement sensor. A gas holdup measurement sensor measures the volumetric fraction of the gas in the gas-slurry mixture. The bubble size distribution in the pulp phase can be measured by a bubble size measurement sensor. The sensors are explained in detail in Gomez and Finch (2007).

Elemental Assaying: An elemental assaying instrument is one of the most important parts of the control of a flotation cell since it can give a compositional analysis of a sample from a slurry stream which can be used to determine the quality of the slurry. The mineral concentration of the concentrate or tailings can be measured with an X-ray fluorescence (XRF) analyzer. The analyzer can measure samples at different stages of the process sequentially and report the composition and proportions of several minerals from the samples. The on-stream analysis of the XRF analyzer provides online information about the performance of flotation in real time. A different (supplementary) way to estimate the element contents is using visual and near-infrared reflectance spectroscopic analysis, which is much faster than an XRF analysis, but not as accurate (Shean and Cilliers, 2011).

Density measurement: Density measurements are important to calculate the mass flow in a flotation cell when the flow rates are known. The XRF analyzers have the ability to measure the density of the slurry, but specific density meters like a nuclear density meter are commonly used. Nuclear density meters are accurate and non-obtrusive, but it does not work when there

are air bubbles present in the liquid, making the installation location of the meter important (Laurila et al., 2002).

Reagent addition measurement and control: The addition of the reagent chemicals into a flotation cell is an important manipulated variable, but the amount of reagents added is a ratio of the ore weight, and the quantity is often very small and difficult to measure and control. One way to add the reagents is with simple on/off valves that estimate the reagent addition flow rate, but this method can be inaccurate. Inductive flow meters and control valves or metering pumps can be used, but this tends to be more expensive.

Acidity (pH), electrochemical potential, and conductivity measurements: The electrochemical measurements give information about the chemistry of the minerals in the process. The pH level of the liquid can be measured using ion-selective electrodes and a pH transmitter. Conductivity is measured using a conductivity probe. The pH and conductivity measurements provide similar information and can thus be interchanged depending on the operating conditions. Both measurements can be used to gather more accurate information. The electrochemical potential (E_h) can be measured with a platinum electrode (redox), but the measurement can be problematic due to the difficult maintenance of the electrode probes (Woods, 2003).

Froth image analysis: Machine vision is used to estimate several variables from the froth surface. Physical, statistical or dynamic features can be extracted from images of the froth using a variety of methods (Aldrich et al., 2010). Some of the froth properties that can be extracted from images include the bubble size distribution, number of bubbles, bubble shape distribution, colour, density, speed and stability of the froth. However, there are some conflicting results when linking these features to the froth grade (Aldrich et al., 2010). Flotation froth image analysis has benefited from breakthroughs in deep learning, with convolutional neural networks (CNN) becoming the state-of-the-art in image processing. Features from froth images can be used in advanced control (Aldrich et al., 2022).

2.4.2 Regulatory or base-level control

Regulatory or base-level control is used to control the fundamental controlled variables to a setpoint. The control objective of the regulatory control layer is to stabilize circuit performance by minimizing the frequency and severity of erratic operation (McKee, 1991).

Plant optimization is strongly dependent on properly controlled regulatory control loops that receive setpoints from a higher-level advanced controller, as shown in Figure 2.4.

For a flotation circuit, the base-level controlled variables include the pulp and froth levels, airflow rate into the cells, reagent addition and, pH. Proportional-integral-derivative (PID) controllers are the most common controllers used for regulatory control in flotation circuits (Olivier and Craig, 2017). Usually, single-input-single-output (SISO) control loops are used where one manipulated variable is used to control one controlled variable, and most of the time in mineral processing plants, the derivative action is not implemented, and only PI-control is used (Hodouin, 2011). Besides PID controllers, model-based multivariable controllers can also be used for regulatory control. For example, Schubert et al. (1995) uses a multivariable controller to control the cell levels in a flotation bank. Such controllers can provide better performance but require more effort in the design stage and more intensive process modelling.

The pulp level in each cell is controlled using the tailings flow rate out of the cell, i.e. by adjusting the slurry outlet valves. Kämpjärvi and Jämsä-Jounela (2003) report on two different control strategies used for level control: SISO and multiple-input-multiple-output (MIMO) level control. The SISO control strategy uses feedback PI control to ensure that the pulp levels remain at the desired setpoints. Feed-forward control is also regularly integrated into the controller to compensate for upstream disturbances (Jämsä-Jounela et al., 2001; 2003). In MISO control strategies, the entire bank of cells is controlled together to improve the level control performance. Decoupling control can be used to eliminate the cross-coupling effects of control loops and prevent a change in level in one cell from affecting the level in the cells before or after the cell (Kämpjärvi and Jämsä-Jounela, 2003). A multivariable model-based feedback controller can manipulate the flows out of each cell simultaneously to minimize the total error continuously. Commercial level control strategies also exist, such as Float-Star™, developed by Mintek, which provides an integrated package for level control of an entire flotation circuit by utilizing a multivariable controller (Schubert et al., 1995).

The airflow rate into a cell is a very important controlled variable and is essential for advanced control to be able to control the air rate to a setpoint. The way that air rate is measured and controlled is dependent on the type of flotation cell, which can be forced air or self-aerated. For

self-aerated cells, the air rate control is more challenging as it depends on the impeller speed. The air rate in forced air cells can be adequately controlled with well-tuned feedback/feed-forward PI/PID control loops by manipulating the control valves (Shean and Cilliers, 2011). The correct sizing of the airflow valves is an important design consideration and valves should not be oversized as it can result in poor airflow control (Laurila et al., 2002).

Reagent addition is controlled at the base level and is commonly controlled using feed-forward ratio control. Reagents addition has a lingering effect on the subsequent operations as it will affect all the flotation cells in the circuit, and thus separate control of reagents for each cell is not possible. The amount of reagents added to the feed is varied based on the feed rate of the valuable mineral in the slurry determined from assays to achieve a target concentration of reagents in the slurry. An increase in collector addition increases the recovery until a plateau is reached. It is important to maintain the addition rate at the leading edge of the plateau, which is not a trivial task as it is difficult to identify this point. Automatic control of collector addition has rarely been successful due to factors such as changes in ore type, and operator input is often required to adjust for ore type changes (Wills and Finch, 2015). Collector addition is sometimes controlled as a ratio of the tonnage of valuable minerals in the flotation feed or the feed grade and depends on assays of the feed. Frother addition is also challenging to control automatically as small changes in the addition rate can result in large effects on the bubble sizes, recovery, grade, mass-pull and entrainment. Therefore, frother addition is usually controlled manually to a setpoint or, less commonly, to a ratio of the feed rate of solids and water.

The pH of the slurry in a flotation cell can be controlled to a setpoint by a base-level regulatory controller through the manipulation of acid or lime addition with a PID controller. The pH addition has a long response time, and a lag time should be included to allow for the appropriate mixing of the acid or lime (Wills and Finch, 2015).

2.4.3 Advanced process control

According to Laurila et al. (2002) the objective of advanced controllers is to control the grade and recovery by manipulating the setpoints of the regulatory controllers. The setpoints for the grade and recovery are determined by the optimization layer or by an operator. Controlling grade and recovery setpoints is one approach to advanced control. Another approach is to

control the mass-pull and re-circulating load.

Grade and recovery are mainly considered as the two degrees of freedom of the flotation process output (Hodouin et al., 2001), and the process can be controlled successfully if both grade and recovery can be kept at the desired operating point (McKee, 1991). There are two types of methods used to control the grade and recovery, model-based methods and expert control systems.

Model-based methods can be very effective for advanced process control and have come a long way (Bergh and Yianatos, 2011), but several issues need to be addressed to ensure their success. Model-based methods are very dependent on good instrumentation and measurements, an acceptable regulatory control layer, and reliable dynamic models. MPC is one of the techniques that has been widely accepted to be capable of advanced control of flotation (Bouchard et al., 2009) and numerous investigations showed that MPC is one of the most efficient advanced control strategies to optimize a multivariable process (Qin and Badgwell, 2003; Camacho and Bordons, 2013). However, the implementation of MPC in industrial flotation circuits remains a challenge due to the reliance on an accurate dynamic model. Modelling for flotation control has received considerable attention recently (Oosthuizen et al., 2017; Quintanilla et al., 2021a), and some recent dynamic models can potentially enable model-based advanced flotation control (Oosthuizen et al., 2021; Quintanilla et al., 2021b;c).

MPC uses a plant model and an objective function to predict what the optimal control inputs are that will result in the minimization of the objective function. This approach is very powerful as a variety of different objective functions can be used, and several control inputs can be manipulated simultaneously. There are some examples where MPC has been used for flotation with some success. Maldonado et al. (2009) used empirical models to implement an MPC strategy to control a flotation column while satisfying operational constraints. Putz and Cipriano (2015) successfully used a hybrid MPC in simulation to show that the MPC strategy is suitable for controlling the final tails grade while constraining the pulp levels. Brooks and Munalula (2017) describe an industrial application of MPC to control an oxide rougher flotation bank using froth velocities to maximize recovery and maintain the concentrate grade above user-entered limits. One of the implementation challenges noted was the validation of measurements which may fail in a number of ways and negatively impact the controller.

Oosthuizen (2023) used an MPC in a simulation study to achieve the desired grade while maximizing the mineral recovery. The study also used a moving horizon estimator (MHE) to estimate unmeasured model states and flotation parameters which can enable more robust models for the use of MPC in industry.

Model-based advanced controllers are not yet widely implemented due to a lack of good measurements, acceptable regulatory control and reliable dynamic models and thus expert control systems are still widely used for advanced process control (Shean and Cilliers, 2011). Expert control systems use some form of artificial intelligence (AI) to automate the decision-making by operators. Many different methods of AI can be used in an expert system, such as fuzzy logic, machine learning, artificial neural networks (ANN), and machine vision.

Fuzzy logic expert systems aim to capture the intelligence of an expert plant operator into a set of fuzzy logic rules that can be used to make decisions on an industrial flotation plant. In fuzzy logic systems, the IF-THEN logic rules determine the response of the system based on the fuzzy set of input parameters. Fuzzy logic expert systems contain probabilistic induction and heuristic rules obtained from domain experts to create a desired control recipe (Jovanović and Miljanović, 2015a). Muller et al. (2010) demonstrated a flotation control approach using a fuzzy logic controller in an expert system advanced process controller that controls the concentrate mass pull by manipulating the cell level and air addition PID setpoints in the regulatory control layer. The fuzzy logic system adapts the control actions based on the detection of different process states. The different states alter the way that the manipulated variables are changed to account for different operating conditions. Another example of a logic-based expert system for the control of a rougher flotation circuit is given by Bergh and Yianatos (2013). The controller aimed to find a froth depth profile to best compromise between grade and recovery. The expert system was able to successfully satisfy the targets in the presence of disturbances in the industrial simulator.

Machine learning uses mathematical models and/or plant data to generate rules and form induced decision trees (Shean and Cilliers, 2011). Decision trees and genetic algorithms can be used to develop knowledge-based systems for the control of the flotation process. One benefit of these decision trees is the classification of different froth structures from plant data that can be incorporated into the plant decision-making support system (Jovanović and Miljanović,

2015a). ANN are neural networks arranged in layers with numerical weights connecting the neurons in adjacent layers. The networks are trained on datasets by iteratively updating the weights such that a set of outputs can be predicted by a set of inputs. An ANN controller can be trained on historical plant data to be able to change plant inputs based on the plant outputs in a way that mimics the operator in the training dataset (Gupta and Yan, 2016).

Machine vision is widely used in flotation systems to monitor froth flotation plants and to assist with flotation control. These vision-based systems use AI methods such as deep neural networks to analyze many different image properties that can be used for control. van Schalkwyk (2002) designed a control system for a rougher flotation circuit using machine vision to extract bubble velocities, bubble area and bubble colour. Supomo et al. (2008) used a machine vision system to control the mass pull of a rougher flotation bank, and the increase in mass pull resulted in an increase in recovery. Machine vision systems can also use dynamic froth image analysis from a video feed to measure properties such as froth velocities that can be used in advanced controllers to calculate and control the mass pull or air recovery of a flotation cell (Phillpotts et al., 2020; Aldrich et al., 2022).

2.4.4 Optimizing flotation control

Optimizing control forms the top control layer and is responsible for controlling the plant at the optimal economic performance by providing specific inputs to the advanced control layer. The aim is to increase economic efficiency and to operate at optimal performance. The boundary between the optimization layer and the advanced control layer is not clear as the two layers can often be combined into one optimizing advanced control layer. There are a couple of different optimization strategies that can be followed. For example, the grade-recovery relationship shown in Figure 2.2 can be optimized by moving the process operation to the top right of this figure as shown by the control objective arrow.

This optimal operating point on the curve can be found with isoeconomic contours which are based on the net smelter return (Laurila et al., 2002). The net smelter return can be calculated from a variety of factors including the grade, recovery, market price of the desired mineral, refining and smelting fee, quality-based fee and other costs. Examples of net smelter return equations are given in Laurila et al. (2002) and Thivierge et al. (2019). For optimal control, the optimal isoeconomic point on the grade-recovery curve can be calculated with a

model-based controller to find the best grade and recovery setpoints to provide to the advanced control layer. As an example, the optimization layer in Muñoz and Cipriano (1999) aims to maximize the financial profit using a model-based control strategy.

Another optimization method consists of using froth stability which leads to air recovery optimization and operating the flotation cell at PAR as discussed in Section 2.2.4. This approach translates the optimization problem to a local problem of finding the gas rate and froth depth that maximizes the air recovery in each cell (Maldonado et al., 2012). Although the optimization ability of air recovery has been confirmed (Smith et al., 2010; Hadler et al., 2010), not many examples exist of air recovery being used in flotation optimization control. Shean et al. (2017) developed a flotation control system to optimize performance using peak air recovery. The algorithm is a direct search algorithm based on the generating set search methodology which makes increasingly smaller steps in the aeration rate while searching before converging to the peak air recovery operating point. The optimization algorithm was successfully implemented on a single laboratory flotation cell and was able to find the PAR air rate.

Adaptive control is an optimization technique that uses time-varying parameters to achieve the desired flotation performance and stability. Adaptive controllers can be divided into mode-based adaptive controllers and model-free adaptive controllers. Model-based methods are efficient and fast because the knowledge of the plant can improve the performance of the controller. However, model-based adaptive controllers are limited by the accuracy of the model which is a problem due to the complex nature of the flotation process and modelling challenges. Desbiens et al. (1994) provide a long-range predictive adaptive controller for a flotation circuit. The controller is an application of a generalized predictive control algorithm implemented in a self-tuning manner that is able to deal with nonlinear, time-varying systems and disturbed systems. Thornton (1991) used a minimum variance adaptive controller with a linear SISO plant model that operates in parallel with a cautious PID controller to regulate the lead assays of a rougher bank tail stream by adjusting the flow rate of the collector. Jämsä-Jounela (1992) presents a simulation study of self-tuning adaptive control for rougher flotation. The study explores explicit and implicit algorithms of SISO self-tuning controllers as well as the corresponding multivariable algorithm. Unlike model-based adaptive controllers, model-free methods do not use any explicit knowledge of the process dynamics and use

online measurements to optimize an objective function. These model-free adaptive controllers are slower than model-based methods and are better suited for the optimization of slowly varying process parameters. Extremum seeking control (ESC) is a type of model-free adaptive controller and is discussed in Section 3.2. Another model-free adaptive control method is reinforcement learning algorithms. The idea behind these algorithms is to build a predictive model by applying many random control actions and learning from the result of these actions. This trial-and-error method can be very effective but comes with some drawbacks like the long required learning period before the model can be useful (Benosman, 2016).

Other optimization methods include air rate profiling and mass-pull profiling (Maldonado et al., 2012). Air rate profiling consists of distributing the air to each cell in a set profile or pattern down the bank. The profile can compensate for changes in floatability down the bank and allow the bank to achieve the target recovery. Mass-pull profiling is commonly used in industry and consists of setting a profile for the solid mass concentrate flow rate. The mass-pull controller is usually implemented by controlling the froth velocity, which is measured using machine vision image analysis methods. Supomo et al. (2008) uses a froth velocity profile for optimization on an industrial plant. The froth velocity is measured with a machine vision system, and then the controller adjusts the froth depth to achieve the required optimal froth velocity and mass-pull profile. The method has resulted in a 1.0 % incremental recovery increase, and novel control logic around the cameras, which included rougher froth velocity profile control, has led to an additional 2.4 % increase in rougher recovery. Muller et al. (2010) uses an MPC optimization controller to maintain a concentrate grade by manipulating the mass-pull setpoints of the flotation cells.

Another approach towards optimization is to optimize the entire mineral processing plants instead of optimizing the flotation circuit separately. Plant-wide control methods can be very beneficial and are discussed in the next section.

2.4.5 Plant-wide control

According to Hodouin et al. (2001), plant-wide economic optimization is the only final goal of the mineral processing industry. In plant-wide control, the grinding and flotation circuits are controlled together to optimize some operational objectives for the entire plant instead of separate objectives for the individual unit operations. Some examples where plant-wide

control has been used in literature are discussed below.

A guide by McIvor and Finch (1991) to the interface between grinding and flotation operations proposes a size-by-size analysis of the recovery of minerals to connect the grinding and flotation circuits. The mineral size distribution of the cyclone overflow is used to categorize the product of the grinding circuit. The size-recovery performance of the flotation circuit is used to connect the recovery to the mineral distribution of the grinding circuit. The economic value of the product from the grinding circuit can then be defined. The size-by-size mineral recovery is relatively invariant to changes in the design and operating conditions like feed size and feed rate. As a result of this invariance, a steady-state grind size can be selected to result in optimal recovery and, therefore also optimal economic performance. McIvor and Finch (1991) also show that for a simple two-phase system, the size region of maximum recovery corresponds to the region of minimum recovery of the gangue and therefore yields the maximum concentrate grade.

The optimal throughput of a copper concentrator is presented by Schena et al. (1996) using a financial principle. The optimization principle requires estimates of the concentrate grade, plant power and material consumption at different throughput levels. A simple empirical model for size reduction is used to relate the feed rate to the size of the grinding product instead of a phenomenological model. For flotation, the recovery was modelled with a simple kinetic model with an empirical relationship between the ultimate recovery and the fineness of the grinding product instead of using a species-specific rate constant model. The economic model for the concentrator uses the revenue generated by a smelter based on the recovery and grade of the concentrate as well as the cost of the plant including operation costs like energy, reagents and grinding media and capital costs to calculate the profit of the plant. A profit-profile curve is created that relates the throughput feed rate of the plant to the profit generated by the plant and can be used to optimize the throughput of the plant.

In Sosa-Blanco et al. (2000) a step-wise procedure is given to tune a grinding circuit to maximize the economic efficiency of a flotation circuit. A plant simulator is used to perform the optimization. The simulator uses phenomenological models for the grinding and flotation circuits, and the economic efficiency of the plant is assessed from the net smelter return or the net revenue of the concentrator. The interface between the grinding and flotation circuit is

modelled empirically. This model links the particle size distribution of the ore to the particle size distribution of the minerals. Therefore on the grinding side, only the size of the particle is used to estimate the size and the type of mineral the particle is made of on the flotation side.

Muñoz and Cipriano (1999) propose a two-level control strategy to dynamically optimize the performance of a mineral concentrator plant. The two levels include a multivariable predictive regulator using dynamic models and an optimization level using a Hammerstein model-based optimizer to supply setpoints to the regulatory level. The control strategy maximizes an economic objective that describes the profit of the plant based on the revenue from the sale of fine copper in the concentrate ore flow of the flotation plant, the variable cost of the grinding and flotation circuits and fixed costs of the plant. The fine copper flow is a function of the smelter recovery, the ore feed grade of the plant and the tailings grade of the plant. Simulations using a dynamic simulator of the grinding-flotation plant showed that the economic optimal control strategy improved the profits compared to an exclusively regulatory strategy.

In Wei and Craig (2009), the economic assessment framework of Bauer and Craig (2008) is used to compare a nonlinear model predictive controller (NMPC) to three single-loop PID controllers for a comminution circuit. The economic performance function used in the economic performance assessment (EPA) is based on the relation between the comminution product particle size and the separation concentrate recovery. This relationship is classified into two stages: the relationship between the recovery and particle size fractions in the flotation circuits and the relation between the recovery in the flotation circuit and the ore particle size distribution of the comminution product. The mill load and sump level are also included in the economic performance function to account for the impact of the load or level exceeding the limits on the economic performance.

Thivierge et al. (2019) presents an economic model of a grinding-flotation circuit that calculates the profit of the plant by subtracting the plant operating costs from the net smelter return. The operating costs include the fixed costs of the plant as well as the variable costs like the grinding media and energy consumption. The net smelter return is calculated using the grade and flow rate of the concentrate. The link between the grinding and flotation circuit is a liberation model (Pérez-García et al., 2020) that estimates the size-liberation distribution

matrix of the grinding product. The size-liberation matrix link with an empirical kinetic flotation model as a flotation rate constant can be calculated for each size-liberation class. The kinetic rate constant is a function of the probability of a particle-bubble collision that depends on the exposed hydrophobic surface which is described by the liberation model. A flotation mass balance model is then used to predict the concentrate grade and flow rate used in the net-smelter-return calculation to calculate the profit of the plant used in the economic model.

le Roux and Craig (2019) propose a plant-wide control framework for a grinding mill circuit. The control framework is structured into two parts: a top-down and a bottom-up analysis (Larsson and Skogestad, 2000; Skogestad, 2004). The economic objective is included in the top-down analysis and determines the optimal steady-state operation of the plant. The bottom-up analysis includes the regulatory control that follows the conditions imposed by the economic objective. The control framework is created for the grinding circuit to operate at the optimal economical operation of the entire plant. The optimal performance of the flotation circuit is defined as the most profitable region on the grade-recovery curve. Mass balance equations are used to relate the recovery to the grade and feed rate of the grinding circuit product and concentrate. The grade-recovery curve is also influenced by the cyclone product particle size estimate. Second-order polynomial equations are used to empirically model the relationship between recovery and the particle size estimate. The economic control is based on the net smelter return, calculated from the grade and recovery, and the grinding and flotation costs.

All the examples of plant-wide economic control given above use the same idea to create a relationship between the particle size from the grinding circuit and the recovery and grade from the flotation circuit (Matthews and Craig, 2013). This relationship is often empirical and specific to a certain plant or covers only a small operating region (le Roux and Craig, 2019). A mineral liberation model that predicts the particle composition as a function of the particle size to link the grinding and flotation is complex and difficult to handle in simulation studies (Sosa-Blanco et al., 2000).

2.5 CHAPTER SUMMARY

This chapter presented an overview of all the relevant flotation literature, including the process description, objectives, modelling and control. The PAR objective of a flotation cell is especially important for this study. Air recovery is an indicator that can be used to evaluate the efficiency and performance of a flotation cell, and there exists a peak air recovery operating point which is the optimal operating point for flotation performance. An optimization controller that utilizes PAR would be an ideal flotation controller, Chapter 3 discusses one such optimization controller that is used in this dissertation.

Phenomenological and empirical flotation models can be very effective in modelling the flotation dynamics and are useful for process control, Chapter 4 presents such a dynamic model that is used to create the simulation platform. Chapter 5 focuses on the implementation of the controller on the simulation platform to optimize air recovery.

CHAPTER 3 EXTREMUM SEEKING CONTROL

3.1 CHAPTER OVERVIEW

This chapter first gives an overview of the history and literature of ESC in Section 3.2. Thereafter three different ESC are discussed in Sections 3.3, 3.4 and 3.5. These sections serve as a methodology towards the implementation of the ESC controllers used in the optimization of a flotation circuit. The three different ESC approaches considered are the classic perturbation-based ESC (PESC), a time-varying parameter estimation ESC (TESC), and a simplex direct search ESC (SESC).

3.2 EXTREMUM SEEKING CONTROL BACKGROUND

Extremum seeking control (ESC) is an optimization technique that maximizes an objective function by exploring an unknown static map and steering the system towards the optimal operating condition (Krstić and Wang, 2000; Guay et al., 2015). ESC is a model-free adaptive controller and does not use any explicit knowledge of the process dynamics, but relies solely on online measurements collected directly from the system. This is an advantage for flotation control due to the challenges of accurately modelling the process. The adaptive nature of the controller means that it can adapt to uncertainties, disruptions or changes in the system. However, ESC has some drawbacks, a very common one being the slow convergence time to the optimum compared to model-based adaptive controllers (Benosman, 2016). ESC is best suited for the optimization layer of a control framework, operating on top of the supervisory and regulatory control layers to steer a process variable such as air recovery to the optimum.

A complete review of ESC history from 1922 to 2010 is given in Tan et al. (2010), but a short overview will be given here. The first use of ESC is in a 1922 paper by Leblanc (Leblanc,

1922) that used ESC to maximize the power delivery from an overhead transmission line to a tram car. ESC then received research attention in the 1950s and 1960s for automotive applications such as internal combustion engine ignition timing (Draper and Li, 1951). In the 1990s, stochastic rather than deterministic excitation became more popular and has been used since then. Deterministic excitation uses a periodic dither signal to perturb the system and extract the information, whereas stochastic excitation uses a random-noise perturbation signal with a zero mean. The advantage of the latter is that there is no unnatural predictable sinusoidal dither signal introduced to the system.

In 2000, Krstić and Wang (2000) published the first rigorous stability assessment of the classic ESC scheme sparking renewed research interest in ESC. Since then, many different attempts have been made to overcome the limitations of ESC and improve the performance of the controllers. Tan et al. (2006) considered several ESC schemes and formulated more precise statements on the dependency of tuning parameters on stability. A smaller tuning parameter slows down the convergence but enlarges the domain of attraction. Guay et al. (2004) presented an alternative ESC approach for continued stirred tank bioreactors that use explicit information about the objective function but assume that the objective function is not available for measurement. In Nešić et al. (2010), a systematic approach is presented for the design of ESC controllers for uncertain plants that are parameterized with unknown parameters. This paper also prescribes how the controller parameters should be tuned and propose a three-time scale approach where the plant dynamics are the fastest, followed by that of the estimator, with the optimization algorithm being the slowest.

Moase et al. (2010) developed a perturbation-based ESC scheme with a Newton-like step which is extended for a multivariable case by Ghaffari et al. (2012) with a dynamic estimator of the inverse Hessian matrix of the cost function. This proposed algorithm allows all the parameters to converge at the same speed, yielding straight trajectories to the extremum. Moase and Manzie (2012) presented a fast ESC for Wiener-Hammerstein plants that utilize a high-frequency dither signal and a direct estimation approach of the gradient. Zhang and Ordóñez (2009; 2012) presents a numerical optimization-based ESC method that makes use of numerical optimization algorithms and state regulation to solve the ESC problem, which does not assume the time scale separation between the plant dynamics and the ESC loop to improve the convergence. Fu and Özgüner (2011) developed a discrete-time sliding mode

gradient estimator for estimating the gradient of the performance profile. Lara-Cisneros et al. (2017) designed a robust sliding mode-based ESC for online optimization that does not make use of a dither signal or a gradient-based optimization algorithm.

Guay et al. (2015) presented an alternative ESC approach which is based on the estimation of the gradient as a time-varying parameter. This technique avoids the need to use the frequency of the dither signal as the only tuning parameter and provides more freedom in the tuning to achieve better transient performance. Hunnekens et al. (2014) presented a novel type of ESC that estimated the gradient of the performance map with a 1^{st}-order least-squares fit from past data of the performance map. This method is dither-free which allows for an exact convergence of the optimal parameter and also eliminates one of the time scales of the classical ESC scheme and results in potentially faster convergence. Another implementation by Chioua et al. (2016) uses recursive least squares estimation with a forgetting factor which eliminates a time scale and accelerates the convergence. Guay and Dochain (2017) proposes a solution that minimizes the impact of the time scale separation on the transient performance of an ESC by using a proportional-integral (PI) approach. The technique, first introduced by Guay and Dochain (2014), uses the integral mode to correspond to the standard ESC task and is used to identify the steady-state optimum conditions while the proportional mode is designed to ensure that the measured cost function is optimized instantaneously.

ESC has been successfully implemented in many different engineering systems, including brake system control, autonomous vehicles and robots, bio-processes, jet engine stability control, internal combustion engines, flow control, flocking and formation control, gyro control, neural network and fuzzy logic controllers, gain control in optical amplifiers, particle accelerators and plasma control, photovoltaic systems, and process control (Tan et al., 2010).

Applications of ESC in mineral processing and flotation remain relatively limited. Lu et al. (2021) used a perturbation-based ESC for the operational control of a grinding circuit, where both the regulation for setpoint tracking and throughput optimization were considered while dealing with input constraints. Pauw et al. (1985) used a multivariable peak-seeking controller for load and density control of pebble mills using the mill power as the input. Craig et al. (1992) describes the application of a throughput optimization strategy using a peak-seeking algorithm on a grinding circuit. The mill load is controlled to a point before the peak power

consumption, operating the mill close to the throughput peak. Ziolkowski et al. (2021; 2022) presented in simulation, the implementation of perturbation-based ESC, simplex ESC, and time-varying ESC methods to optimize a grinding mill by using grind curves. In the first application of flotation froth stability maximization, Shean et al. (2017) presented a direct search ESC method to optimize a single laboratory flotation cell using air recovery as the objective function. The direct search ESC algorithm is based on the generating set search methodology which makes increasingly smaller steps in the input (air rate) in the direction of the peak in the objective function until the controller converges to the extremum.

3.3 PERTURBATION-BASED EXTREMUM SEEKING CONTROL

When the reference-to-output map is unknown or contains uncertainty, it is necessary to use some sort of adaptation to find the extremum that maximizes the output (Krstić and Wang, 2000). A perturbation-based ESC uses a slow periodic signal added to the input of the system to perturb the plant and steer the plant through the map towards the extremum. The controller adjusts the input based on the gradient extracted from the measured objective function as it changes due to the perturbations added to the input. The continuous perturbations allow the ESC to track an unknown time-varying optimum over time, even in the presence of external disturbances. One advantage of ESC is that the controller is model-free. Therefore, as long as the objective function has a maximum and is convex, the controller does not require any knowledge of the process to steer the process to the optimal operating point (Wang et al., 1999).

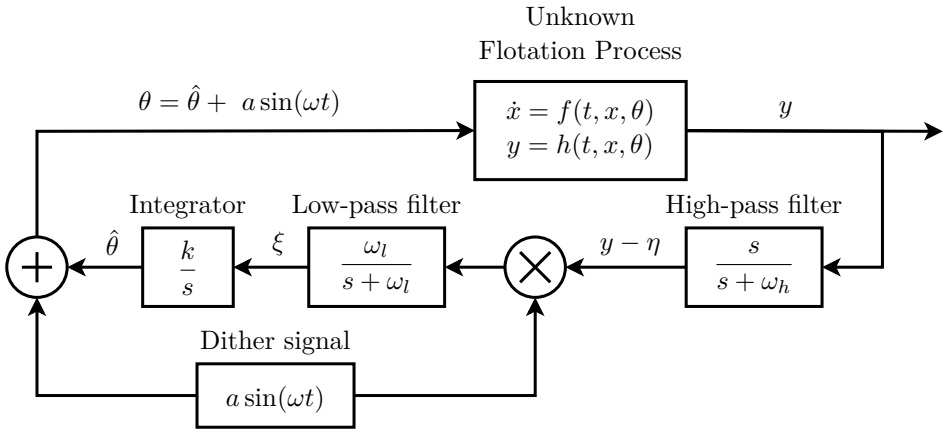

Figure 3.1. Extremum seeking control scheme. Adapted from Krstić and Wang (2000), with permission.

Figure 3.1 shows the peak-seeking feedback scheme of a perturbation-based ESC. In the diagram, the flotation process is represented by the functions $\dot{x} = f(t, x, \theta)$ and $y = h(t, x, \theta)$.

The process dynamics are unknown to the controller, and the functions f and h are considered as unknown black-box functions that take an input, θ, and provide an output, y, which is the measured objective function. The dither signal is a slow periodic perturbation, $a\sin(\omega t)$, where a is the amplitude, and ω is the perturbation frequency. The dither signal is added to $\hat{\theta}$, the best estimate of the optimal operating point (θ^*). The perturbations create a periodic response in the output which the high-pass filter isolates by removing the steady-state component from y, resulting in the filtered output, $y-\eta$. The periodic response in the output will either be in or out of phase with the dither signal depending on the location of $\hat{\theta}$ relative to θ^*. The product of $y-\eta$ and the dither signal contains the gradient, ξ, which is extracted with the low-pass filter. The sign of the gradient, ξ, provides the direction to the integrator for moving $\hat{\theta}$ towards θ^*. The integrator gain, k, controls how aggressive the ESC will be and has to be selected sufficiently small to ensure convergence (Krstić and Wang, 2000). The closed-loop system dynamics of Figure 3.1 are summarized as,

$$\dot{x} = f\left(t, x, \theta\right), \tag{3.1a}$$

$$y = h\left(t, x, \theta\right), \tag{3.1b}$$

$$\dot{\hat{\theta}} = k\xi, \tag{3.1c}$$

$$\dot{\xi} = -\omega_l \xi + \omega_l \left(y-\eta\right) a\sin\left(\omega t\right), \tag{3.1d}$$

$$\dot{\eta} = -\omega_h \eta + \omega_h y. \tag{3.1e}$$

For the ESC to operate effectively, the perturbation frequency has to be slow enough that the reference-to-output map of the plant appears as a static map. The static map ensures that the plant dynamics do not interfere with the ESC and that the controller can search along the static map for the optimum operating point. The system, therefore, has three time scales with sufficient separation between the scales. The fastest time scale is the process dynamics of the plant together with the stabilizing and regulatory controllers. The next time scale is the periodic perturbations which have to be slower than the process dynamics. The slowest time scale is the filters in the ESC scheme, as the cut-off frequencies have to be lower than the frequency of the perturbation signal. The amplitude of the dither signal should be selected to be larger than the expected input noise and large enough that the plant response to the dither signal is detectable in the measurement noise of the objective function. However, the dither signal should also be as small as possible to minimize the negative effect that the

perturbations can have on the quality of the objective function.

3.4 TIME-VARYING EXTREMUM SEEKING CONTROL

The time-varying ESC is based on the estimation of the gradient as a time-varying parameter which removes the need for averaging the results and minimizes the impact of the dither signal choice by providing more freedom in tuning the ESC to improve the transient performance (Guay and Dochain, 2015). The controller first estimates the time-varying parameter, θ, the gradient of the static map, which is defined as,

$$\theta = \frac{\partial \ell}{\partial u}, \tag{3.2}$$

where ℓ is the static map and u is the time-varying input. y is the objective function to be maximized,

$$y(t) = \ell(u(t)). \tag{3.3}$$

This estimate of the gradient, $\hat{\theta}$, is then used in the controller to achieve the extremum seeking task. The estimation error is given by,

$$e = y - \hat{y}. \tag{3.4}$$

The closed loop ESC system is shown in Figure 3.2, and the system equations are,

$$\dot{x} = f\left(t, x, u\right), \tag{3.5a}$$

$$y = h\left(t, x, u\right), \tag{3.5b}$$

$$\dot{u} = -k\hat{\theta} + d, \tag{3.5c}$$

$$\dot{\hat{\theta}} = \text{Proj}\left(\Sigma^{-1}(c(e - \hat{\eta}) - \sigma\hat{\theta}), \hat{\theta}\right), \tag{3.5d}$$

$$\dot{\hat{\eta}} = -K\hat{\eta}, \tag{3.5e}$$

$$\dot{c} = -Kc + \dot{u}, \tag{3.5f}$$

$$\dot{\hat{y}} = \dot{u}^T\hat{\theta} + Ke + c^T\dot{\hat{\theta}}, \tag{3.5g}$$

$$\dot{\Sigma}^{-1} = -\Sigma^{-1}(cc^T)\Sigma_{-1} + k_T\Sigma^{-1} - 2\sigma\Sigma^{-2}, \tag{3.5h}$$

where K and k_T are estimation gains. K is defined as,

$$K = k_{\eta_1} + k_{\eta_2}c^T c. \tag{3.6}$$

The positive gains k_{η_1}, k_{η_2}, σ, k_T, k and the dither signal $d = a\sin(\omega t)$ are all tuning parameters that can be selected such that the ESC system converges to the optimization

extremum of (3.3) (Guay et al., 2015). The projection in (3.5d) is given by,

$$\dot{\hat{\theta}} = \begin{cases} \phi & \text{if } \mathcal{P}(\hat{\theta}) > 0 \text{ or } \nabla_{\hat{\theta}}\mathcal{P}(\hat{\theta})\phi \leq 0 \\ \left(I - \dfrac{\nabla_{\hat{\theta}}\mathcal{P}(\hat{\theta})^T \nabla_{\hat{\theta}}\mathcal{P}(\hat{\theta})}{\|\nabla_{\hat{\theta}}\mathcal{P}(\hat{\theta})\|^2}\right)\phi & \text{otherwise,} \end{cases} \tag{3.7}$$

where $\phi = \Sigma^{-1}\left(c(e - \hat{\eta}) - \sigma\hat{\theta}\right)$ and the function $\mathcal{P}(\hat{\theta})$ is defined as,

$$\mathcal{P}(\hat{\theta}) = \|\hat{\theta}\|^2 - z_\theta^2, \tag{3.8}$$

with its gradient,

$$\nabla_{\hat{\theta}}\mathcal{P}(\hat{\theta}) = 2\hat{\theta}^T. \tag{3.9}$$

The constraint, z_θ is the upper limit on the size of the norm of the gradient estimate, $\hat{\theta}$.

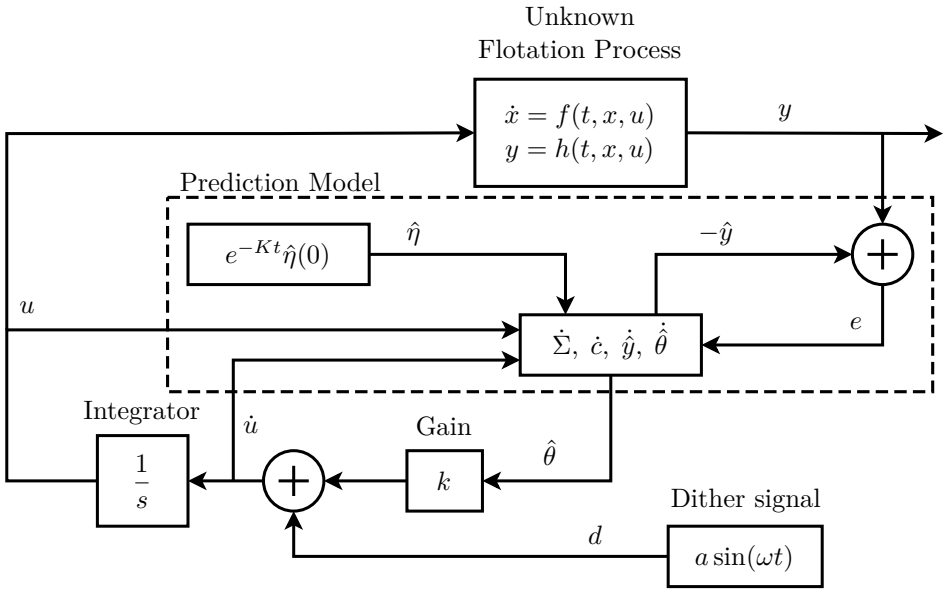

Figure 3.2. Time-varying extremum seeking control scheme. Adapted from Guay et al. (2015), with permission.

The diagram in Figure 3.2 shows the TESC control scheme implemented on the flotation process with unknown dynamics. The dashed block represents the prediction model given in (3.5d)–(3.5h). The optimization gain, k, controls the speed of the response, but an increase in k reduces the effect of the dither signal on u, which negatively affects the estimation routine. In general, there exists a maximum value of the gain k that can be achieved (Guay and Dochain, 2015). The parameter, σ, prevents that the value of Σ becomes too small, which could impede the estimation routine. Therefore, σ should be as small as possible, but for small values of σ, z_θ has to increase.

3.5 SIMPLEX EXTREMUM SEEKING CONTROL

The Simplex ESC is based on the Nelder-Mead algorithm (Nelder and Mead, 1965). The algorithm works by creating a simplex of function values with $n+1$ vertices, where n is the number of variables in the objective function. The simplex adapts to the static map and contracts to the extremum by replacing the lowest vertex with a new point for each iteration. Three operations are used to replace the point - *reflection*, *contraction* and *expansion*. This iterative direct search method can efficiently find the extremum of the objective function without using any gradient information.

The algorithm is shown in the flow diagram in Figure 3.3. In the initialization step, a simplex is created around the initial input value. The simplex consists of $n+1$ vertices, labelled as $v_1,\ \ldots,\ v_n,\ v_{n+1}$, and the objective function is evaluated at each of the vertices to find the function values,

$$f(v_1),\ \ldots,\ f(v_n),\ f(v_{n+1}). \tag{3.10}$$

The next step is to order the vertices from best to worst. Since the aim of the simplex method is to minimize the objective function[1], the minimum function value (best point) will be $f(v_1)$ and the maximum function value (worst point) will be $f(v_{n+1})$. The simplex is then ordered to be,

$$f(v_1) \leq \cdots \leq f(v_n) \leq f(v_{n+1}). \tag{3.11}$$

The flow diagram in Figure 3.3 is then followed, moving through the operations until a new point is accepted. The operation equations are given by,

$$v_r = \bar{v} + \rho(\bar{v} - v_{n+1}), \qquad (\textit{reflection}) \tag{3.12a}$$

$$v_e = v_r + \chi(v_r - \bar{v}), \qquad (\textit{expansion}) \tag{3.12b}$$

$$v_{co} = \bar{v} + \gamma(v_r - \bar{v}), \qquad (\textit{outside contraction}) \tag{3.12c}$$

$$v_{ci} = \bar{v} + \gamma(v_r - v_{n+1}), \qquad (\textit{inside contraction}) \tag{3.12d}$$

where $\bar{v}$ is the centroid of the simplex,

$$\bar{v} = \frac{\sum_{k=1}^{n} v_k}{n}. \tag{3.13}$$

The last operation is a *shrink* step where all the points in the simplex except for the best

[1]For the flotation circuit the objective function will be the negative of the air recovery as the aim is to maximize air recovery.

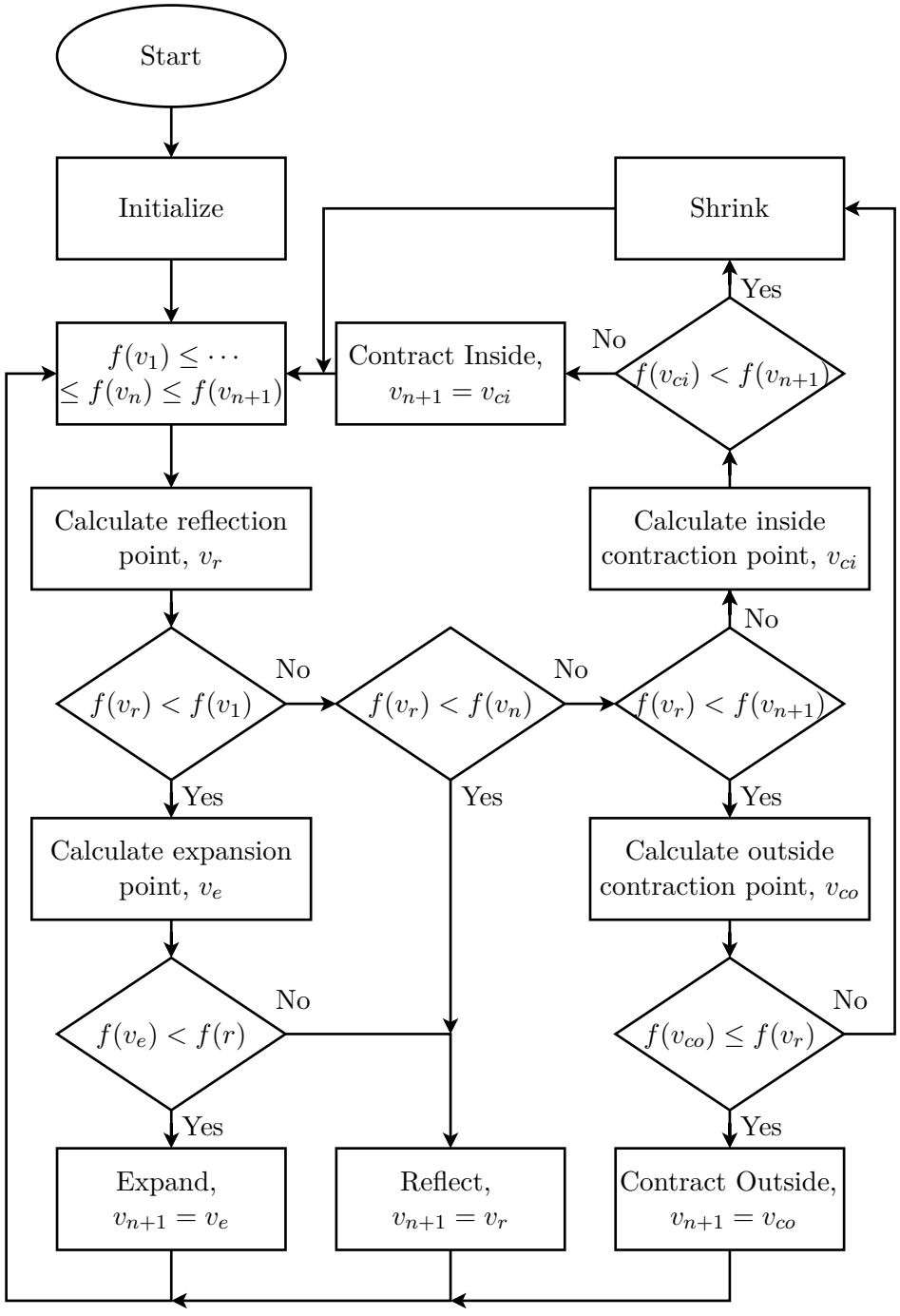

Figure 3.3. Simplex extremum seeking control scheme flow diagram.

point are shrunk according to,

$$v_i = v_1 + \sigma(v_i - v_1), \quad i = 2, \ \ldots, \ n+1. \tag{3.14}$$

The coefficients used in the operations should satisfy,

$$\rho > 0, \quad \chi > 1, \quad \chi > \rho, \quad 0 < \gamma < 1, \quad \text{and} \quad 0 < \sigma < 1. \tag{3.15}$$

When a non-shrink step occurs (reflect, expand, contact outside or contract inside), the worst vortex v_{n+1} is discarded and replaced by the new accepted point. When a shrinking step occurs, only the best point is kept, and the rest are all replaced. The new simplex is then sorted, and the process repeats with a new iteration.

When the simplex method is applied to a dynamic process, the function evaluations take place by assigning the calculated vertex value (v_r, v_e, v_{co} or v_{ci}) to the input of the process and allowing a sufficient time period (T_s) for the process to reach steady-state before measuring the output of the process and assigning it to the function value ($f(v_r)$, $f(v_e)$, $f(v_{co})$ or $f(v_{ci})$). To prevent undesired plant behaviour, such as overshoot and aggressive plant responses due to large step sizes, a ramp function can be used to linearly interpolate the operating point between step changes (Ziolkowski et al., 2022). The controller is set up to linearly ramp the process input value to the new vortex value in $T_s/2$ h and then keep the input constant for $T_s/2$ h.

The advantage of SESC is that the controller can make relatively large step changes and potentially reach the extremum quicker than, for example, the other two ESC approaches discussed previously. The controller evaluates the objective function itself and not the gradient. As a result, the method is much more resistant to noise and variations in the objective function. The size of the simplex decreases as the process approaches the extremum, which results in increasingly smaller perturbations. However, this also means that the controller loses the ability to track a time-varying extremum. If the optimum changes after the controller converged to a point, the algorithm would not be able to adapt and track the new optimum unless the method is reinitialized with a new simplex so that the optimization can start again. The frequency of reinitialization needs to be selected carefully to prevent unnecessary disturbances or reduced tracking performance. An alternative solution is to limit the minimum simplex size to allow the method to continue to perturb the process and track any changes in the optimum (Xiong and Jutan, 2003).

3.6 CHAPTER SUMMARY

In this chapter, an overview of the history and relevant literature of ESC is discussed, and three different ESC approaches are presented to be used in the optimization of a flotation circuit. The three ESCs chosen to implement in this dissertation are two gradient-based ESCs, a classical perturbation-based ESC and a time-varying ESC, as well as a non-gradient-based direct search Nelder-Mead simplex ESC. In Chapter 5, the ESC controllers are implemented in simulation and used to optimize a flotation circuit.

CHAPTER 4 FLOTATION MODELING AND SIMULATION

4.1 CHAPTER OVERVIEW

In this chapter, the flotation circuit model that is used throughout the study is presented and described. Section 4.2 gives an overview of the dynamic model of a four-cell flotation circuit presented by Oosthuizen et al. (2021). The most important model equations are given along with tables containing a description of the model variables. In Section 4.3, the steady-state model simulations are presented, showing the effect of the input variables, aeration rate and froth height on air recovery, grade, and mineral recovery, respectively.

4.2 FLOTATION CIRCUIT MODEL

The flotation circuit used in this simulation study includes four flotation cells in the rougher section. The four cells are connected in series as shown in Figure 4.1.

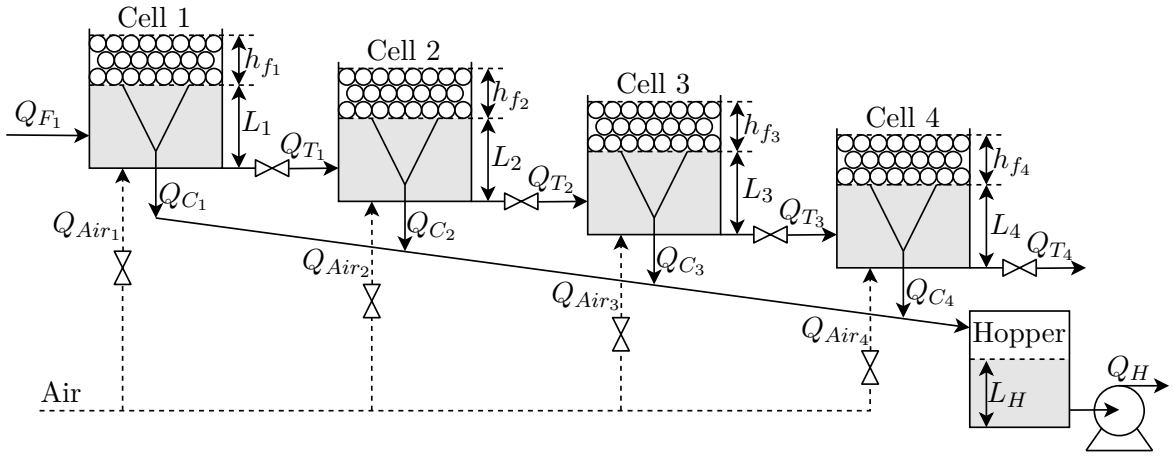

Figure 4.1. Flotation circuit configuration. Adapted from Oosthuizen et al. (2021), with permission.

The slurry from the comminution stage flows into the first flotation cell with a flow rate, Q_{F_1}. The tailings flow rates of the slurry flowing out of the cells are given by Q_{T_k}, where k is the cell number. The aeration rate to each cell, Q_{Air_k}, gives the flow rate of air flowing into the cell that forms bubbles that rise through the slurry. The measurement of the aeration rate is the superficial gas velocity. As the air bubbles rise, the valuable mineral particles attach to the bubbles because of their hydrophobicity and collect in the froth layer at the top of the cell. The froth height is denoted by h_{f_k} while L_k is the pulp level in each cell. The air bubbles in the froth layer flow over the cell lip into the concentrate launder with flow rates, Q_{C_k}, and collect in the concentrate hopper. The slurry level in the hopper is given by L_H. From the hopper, the concentrate is pumped away for further processing with a flow rate of Q_H.

The dynamic model of a four-cell flotation circuit as shown in Figure 4.1 and given in Oosthuizen et al. (2021) is used to simulate the performance of the proposed controller. Each of the flotation cells has the following states, the cell pulp level (L_k), the mineral masses in the cell ($M_k^{i,j}$), the air recovery (α_k) and the top of froth bubble size (D_{BF_k}). The superscript, i, represents the different mineral species in the cell (gangue or valuable minerals), and j represents the different sub-classes within the mineral class for minerals with different flotabilities or sizes. In this study, the model is simplified to include only two mineral species, valuable minerals ($i = 0$) and gangue ($i = 1$). It is also assumed that there are no sub-classes, and j will therefore be omitted. A comprehensive model description can be found in Oosthuizen et al. (2021). The change in the pulp level of each cell is modelled using the volume balance in the cell,

$$\frac{d}{dt}L_k = \frac{Q_{F_k} - Q_{T_k} - Q_{C_k}}{A_k}, \tag{4.1}$$

where A_k is the surface area of cell k. The effect of a change in gas holdup on the change in level is not included in the model as it is relatively small compared to the effect of the flow rates and it changes on a much slower time scale. The tailings flow rate from the cell (Q_{T_k}) is the feed flow rate into the next cell ($Q_{F_{k+1}}$) and is modelled according to (Jämsä-Jounela et al., 2003),

$$Q_{T_k} = C_{v_k} v_k \sqrt{L_k - L_{k+1} + h_k}, \tag{4.2}$$

where C_{v_k} is the valve constant for valve position, v_k, and h_k is the physical difference in height between the two cells. A mass balance is used to model the change in mass in each cell,

$$\frac{d}{dt}M_k^i = \dot{M}_{F_k}^i - \dot{M}_{T_k}^i - \dot{M}_{C_k}^i, \tag{4.3}$$

where $\dot{M}^i_{\square_k}$ is the mass flow rate associated with the feed ($\square = F$), tailings ($\square = T$) or concentrate ($\square = C$) of cell k. The tailings mass flow rate of cell k is the feed flow rate of the next cell, $\dot{M}^i_{F_{k+1}} = \dot{M}^i_{T_k}$, and is calculated by,

$$\dot{M}^i_{T_k} = \frac{M^i_k}{L_k A_k} Q_{T_k}. \tag{4.4}$$

The concentrate mass flow rate includes true flotation and entrainment components. True flotation occurs when a particle collides with a bubble, attaches to its surface and rises to the froth. Entrainment occurs when the particle is dragged to the froth by the liquid between the bubbles. The concentrate mass flow rate is given by,

$$\dot{M}^i_{C_k} = K^i M^i_k S_{b_k} \alpha_k + Ent^i_{Frac} \frac{M^i_k}{A_k L_k} Q_{C_k}, \tag{4.5}$$

where K^i is a pseudo rate-constant, M^i_k is the mass of mineral i in cell k, S_{b_k} is the bubble surface area flux, α_k is the air recovery (see (4.8)), and Ent^i_{Frac} is the entrainment factor. The concentrate flow rate is calculated from water recovery and true flotation models,

$$\frac{Q_{C_k}}{A_k} = \begin{cases} \dfrac{J^2_{g_k} \lambda_{out}}{\kappa}(1-\alpha_k)\alpha_k + \dfrac{d}{dt} M^i_{TF_k}/\rho^i_s & 0 < \alpha_k < 0.5 \\ \dfrac{J^2_{g_k} \lambda_{out}}{4\kappa} + \dfrac{d}{dt} M^i_{TF_k}/\rho^i_s & \alpha_k \geq 0.5 \end{cases}, \tag{4.6}$$

where $\frac{d}{dt} M^i_{TF_k} = K^i M^i_k S_{b_k} \alpha_k$ is the mass flow rate of mineral i to the froth phase in cell k due to true flotation, and ρ^i_s is the density of the mineral. J_{g_k} is the superficial gas velocity for cell k, and κ is a constant. The Plateau border length (λ_{out}) per volume of froth is inversely proportional to the square of the top of froth bubble diameter (D_{BF_k}),

$$\lambda_{out} \approx \frac{6.81}{D^2_{BF_k}}. \tag{4.7}$$

The models for air recovery and the bubble size are empirical models derived by Oosthuizen et al. (2021) using industrial data. The change in air recovery is,

$$\frac{d}{dt}\alpha_k = \frac{\alpha_{SS_k} - \alpha_k}{\lambda_{air_k}}, \tag{4.8}$$

where λ_{air_k} is the average froth residence time,

$$\lambda_{air_k} = \frac{h_{f_k}}{J_{g_k}}. \tag{4.9}$$

The steady-state model of air recovery, α_{SS_k}, is given by,

$$\alpha_{SS_k} = K_{\alpha_{J_g}} \left(J_{g_k} - K_{\alpha_{J_{gk}}} - K_{\alpha_{h_f}} h_{f_k} \right)^2 + \alpha_{OS_k}. \tag{4.10}$$

The parameters, $K_{\alpha_{J_g}}$, $K_{\alpha_{J_{gk}}}$, $K_{\alpha_{h_f}}$ and α_{OS_k} are empirically fitted. $K_{\alpha_{J_g}}$ is a negative constant to create a parabolic shape in the air recovery as a function of the aeration rate. The

Table 4.1. Description of flotation model variables.

Variable	Unit	Description
i	–	Superscript for mineral species: valuable mineral ($i = 0$) and gangue ($i = 1$)
k, H	–	Subscript for unit (flotation cell k, or hopper, H)
$\square$	–	Subscripts for feed ($\square = F$), tails ($\square = T$), concentrate ($\square = C$)
A_k, A_H	m^2	Surface area of cell k or hopper H
h_k	m	Difference in height between cell k and $k+1$
ρ_s^i	kg/m^3	Density of mineral species i
λ_{out}	–	Plateau border length per volume of froth
K^i	–	Pseudo rate-constant of mineral species i
λ_{air_k}	s	Average froth residence time in cell k
S_{b_k}	s^{-1}	Bubble surface area flux in cell k
Ent^i_{Frac}	–	Entrainment factor of mineral species i
$Q_{\square_k}$, Q_H	m^3/h	Volumetric flow rate associated with cell k or hopper H
Q_{air_k}	m^3/h	Volumetric airflow rate to cell k
$\dot{M}^i_{\square_k}$	kg/h	Mass flow rate of mineral species i associated with cell k
C_{v_k}	$m^{5/2}/h$	Valve constant for cell k
v_k	–	Valve position for cell k
h_{f_k}	mm	Froth depth of cell k
J_{g_k}	mm/s	Superficial gas velocity for cell k
J_{gSP_k}	mm/s	Superficial gas velocity setpoint for cell k
τ_{Jg_k}	s	First order time constant of the air valve response of cell k

Table 4.2. Description of flotation model states.

Variable	Unit	Description
L_k, L_H	m	Pulp level in cell k or hopper H
M^i_k, M^i_H	kg	Masses of mineral species i in cell k or hopper H
α_k	–	Air recovery in cell k
D_{BF_k}	mm	Top of froth bubble diameter in cell k

parabola has a peak in air recovery where $J_{g_k} = K_{\alpha_{J_{gk}}} + K_{\alpha_{h_f}} K_{\alpha_{h_f}}$.

The rate of change in bubble size is,

$$\frac{d}{dt} D_{BF_k} = \frac{K_{BF_{J_g}} J_{g_k} + K_{BF_\lambda} \lambda_{air_k} - D_{OS_k}}{\lambda_{air_k}}, \tag{4.11}$$

where $K_{BF_{J_g}}$, K_{BF_λ} and D_{OS_k} are empirically fitted parameters. The dynamic responses of superficial gas velocities (J_{g_k}) to setpoint changes (J_{gSP_k}) are defined with first-order models

Table 4.3. Description of flotation model empirical parameters.

Variable	Description
α_{SS_k}	Steady-state value of air recovery in cell k
$K_{\alpha_{J_{gk}}}$	Value of the superficial gas velocity in cell k where air recovery is maximized when $h_{f_k} = 0$
$K_{\alpha_{J_g}}$	Effect of the difference between J_{g_k} and $K_{\alpha_{J_{gk}}}$ squared on air recovery
$K_{\alpha_{h_f}}$	Effect of a change in h_{f_k} on the superficial gas velocity where air recovery is maximized
α_{OS_k}	Offset included in steady-state air recovery in cell k
$K_{BF_{J_g}}$	Effect of the superficial gas velocity on the mean top-of-froth bubble diameter
K_{BF_λ}	Effect of the average froth residence time on the mean top-of-froth bubble diameter
D_{OS_k}	Offset included in steady-state top-of-froth bubble diameter in cell k

with unity gains,

$$\frac{d}{dt}J_{g_k} = \frac{J_{gSP_k} - J_{g_k}}{\tau_{J_{g_k}}}, \tag{4.12}$$

where $\tau_{J_{g_k}}$ is the first-order time constant of the air valve response of cell k. The concentrate hopper has two states, the hopper level (L_H) and the masses of mineral species i in the hopper (M_H^i). The state equations are,

$$\frac{d}{dt}L_H = \frac{Q_{C_1} + Q_{C_2} + Q_{C_3} + Q_{C_4} - Q_H}{A_k}, \tag{4.13}$$

$$\frac{d}{dt}M_H^i = \sum_{k=1}^{4} \dot{M}_{C_k}^i - \frac{M_H^i}{L_H A_H} Q_H. \tag{4.14}$$

The total mass pull rate of the hopper is given by,

$$\dot{M}_H^{Tot} = \left(\dot{M}_H^0 + \dot{M}_H^1\right) \frac{Q_H}{L_H A_H}. \tag{4.15}$$

The concentrate grade in the hopper is the ratio of the mass of the desired mineral to the total mass in the hopper,

$$\text{Grade} = \frac{M_H^0}{M_H^0 + M_H^1}. \tag{4.16}$$

An *instantaneous* mineral recovery is given by,

$$\text{Recovery} = \frac{\sum_{k=1}^{4} \dot{M}_{C_k}^0}{\dot{M}_{F_1}^0}, \tag{4.17}$$

where $\dot{M}_{C_k}^0$ is the desired element mass flow rate in the concentrate stream of cell k and $\dot{M}_{F_1}^0$ is the desired element mass flow rate in the feed stream. Although recovery is generally calculated at steady-state, the *instantaneous* recovery is a useful real-time approximation. The variables used in the flotation model are summarized in Table 4.1 and the model states

are given in Table 4.2. Table 4.3 shows all the empirical parameters to be estimated. The nominal values of the variables, states and estimated empirical parameters are taken from Oosthuizen et al. (2021).

4.3 MODEL SIMULATION

This section presents the simulation results of the flotation model in Section 4.2 under steady-state conditions. To create the simulations, small step changes in the inputs aeration rate (J_{g_k}) and froth height (h_{f_k}) were made while keeping all the other inputs constant and removing all noise and disturbances. The plant model was allowed to settle after each input change before the outputs were recorded and the next input step change was made. The air recovery (α), grade and recovery were determined by the model (Oosthuizen et al., 2021) and then plotted.

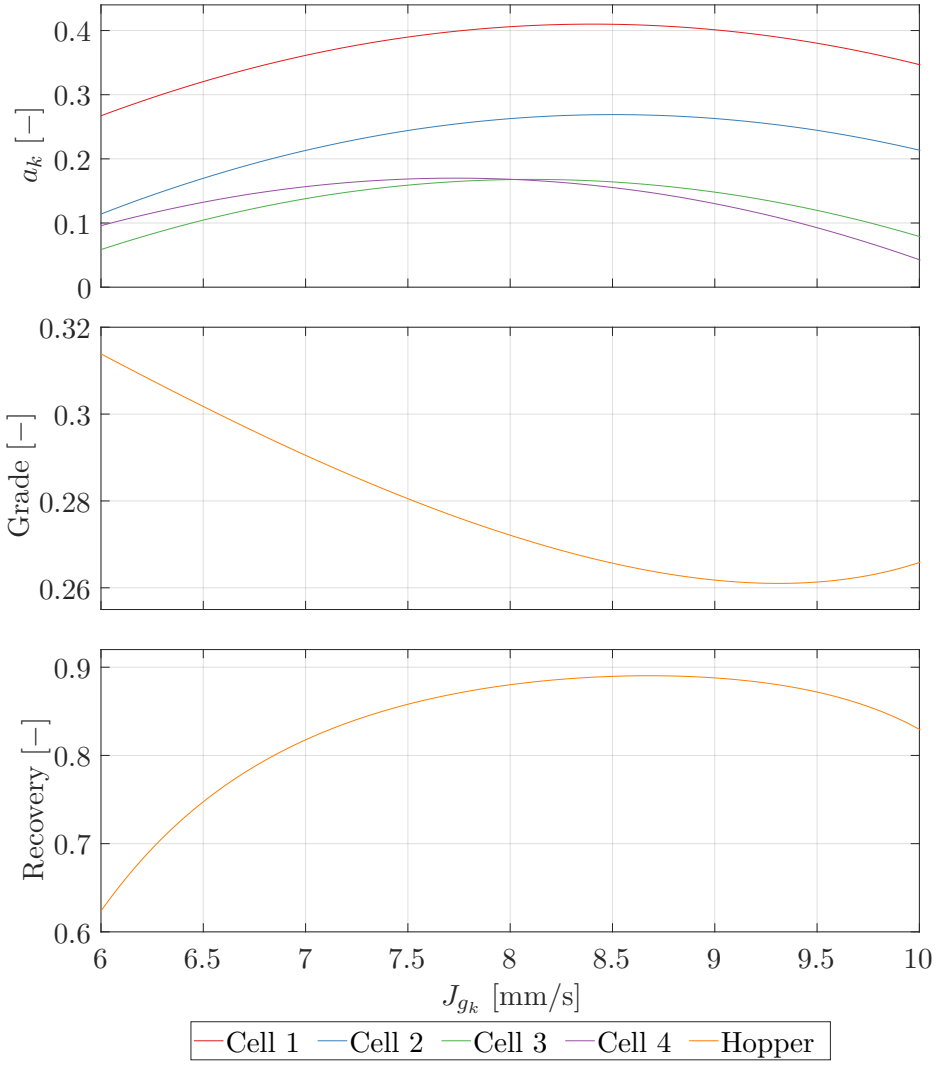

Figure 4.2. Steady-state model simulation showing the effect of the aeration rate on air recovery, hopper grade and hopper mineral recovery respectively at a constant froth height.

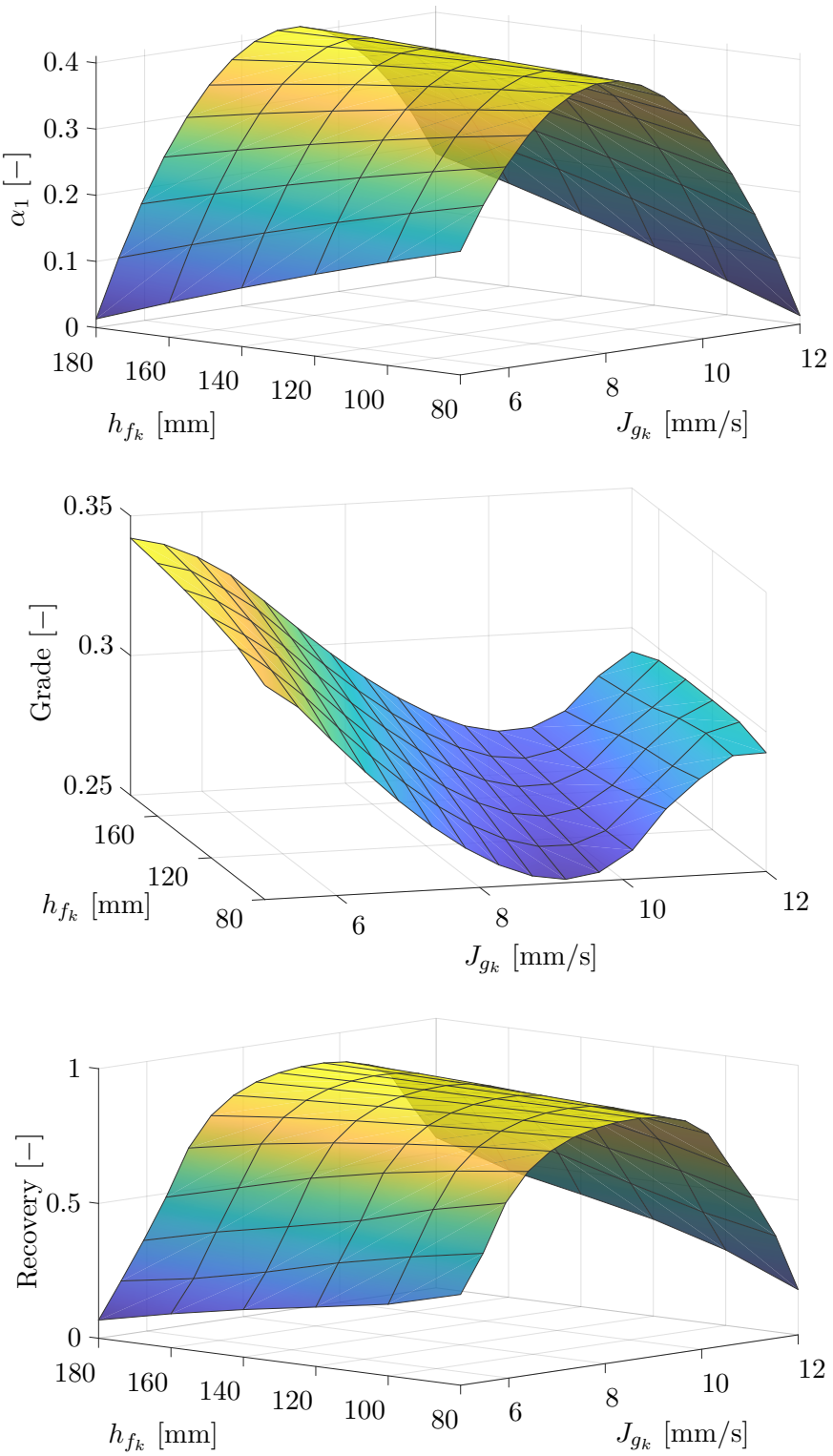

Figure 4.3. 3D surface map of the steady-state model simulation showing the effect of the aeration rate and froth height on air recovery, grade and recovery respectively. Only the air recovery for cell 1 is shown, but the shape is representative of all of the cells.

Figure 4.2 shows the effect of only the aeration rate on the air recovery, grade and recovery while the froth height is kept constant at a setpoint. Figure 4.3 shows the 3D surface map highlighting the effect of both the aeration rate and froth height.

Air recovery initially increases with an increase in the aeration rate, but it reaches a peak after which a further increase in the aeration rate lowers the air recovery. As explained in Section 2.2.4, the low aeration rate results in a high grade and low recovery, whereas a high aeration rate results in a lower grade at high recovery. These relationships are confirmed in Figure 4.2 as the aeration rate is linearly varied. The shape of the air recovery plots is similar to the air recovery measured on industrial plants as shown in Hadler et al. (2010), confirming that the air recovery model can accurately represent the air recovery measurements of an industrial plant. The steady-state model simulations of the mineral recovery and grade, measured in the concentrate hopper and shown in Figure 4.3, show the inverse relationship between grade and recovery. The aeration rates that create the peaks on the recovery curve also correspond approximately to the low points on the grade curve.

The froth height (h_{f_k}) has a much smaller effect on the air recovery than the aeration rate and the plant is able to reach the peak air recovery operating point at any froth height by changing only the aeration rate. When controlling for air recovery only, the benefits of controlling the froth height as well as the aeration rate might not outweigh the disadvantages that come with the added complexity of implementing a multiple-input controller and the possibility of reduced grade and recovery performance or a slower convergence time. Therefore, two different optimization strategies are evaluated and compared in Chapter 5: Varying only the aeration rate while keeping the froth height constant and varying both the aeration rate and froth height. Figure 4.2 shows the effect of the aeration rate on the air recovery, grade and recovery while the froth height is kept constant at a setpoint. The updated version of the model in Oosthuizen et al. (2021) is used, which allows for different air recoveries in each cell.

4.4 CHAPTER SUMMARY

In this chapter, the flotation circuit model was presented, described and simulated. The dynamic model developed by Oosthuizen et al. (2021) is implemented on a simulation platform where it is used in Chapter 5 to evaluate the ESC optimization strategies. A simulation of

the dynamic model under steady-state conditions shows the effect of the aeration rate and froth height on the air recovery, grade and mineral recovery. This simulation highlights the PAR operating point and how it corresponds to increased mineral recovery.

CHAPTER 5 OPTIMIZING A FLOTATION CIRCUIT WITH ESC

5.1 CHAPTER OVERVIEW

In this chapter, the setup for the simulation study is described, and then the results are presented and discussed. Section 5.2 shows how the dynamic flotation model described in Section 4.2 is used in the simulation study to test the controllers. The setup of the regulatory controllers and the ESC controllers are shown, and the addition of noise to the simulation is explained.

Two optimization strategies are simulated to control the air recovery. For the first strategy, in Section 5.3, only the aeration rate (J_{g_k}) is varied while the froth height (h_{f_k}) is kept constant at a setpoint. For the second strategy, in Section 5.4, both the aeration rate and the froth height are varied. The strategies are referred to as SISO and MISO, respectively.

For each strategy, two simulation scenarios are considered: Firstly, the optimization ability of the ESC controllers is evaluated by starting the flotation circuit at a suboptimal operating point and letting the controllers optimize the plant. Secondly, the disturbance rejection ability of the ESC controllers is evaluated by subjecting the plant to a large disturbance and seeing if the controllers can find the optimal operating point again. The ESC controllers are compared, and their differences are discussed in Section 5.5.

5.2 SIMULATION SETUP

The purpose of the simulations is to demonstrate how well each of the different ESCs works as optimization controllers on a flotation circuit and to compare the relative performances. Figure 5.1 shows a diagram of the flotation cells and controllers implemented. The flotation

cells are modelled with the dynamic flotation model given in Section 4.2. On the tailings stream of each of the cells, as well as the outflow of the hopper, PI-controllers are implemented to stabilize the pulp levels, L_k. These regulatory controllers keep the cell and hopper levels constant in the presence of plant disturbances. The froth height of each cell, h_{f_k}, can be controlled by changing the pulp level setpoint of the cell. The top of the froth level is assumed to always be equal to the cell height, so when the pulp level decreases, the froth height will increase by an equal amount. In the SISO optimization strategy, the froth height remains constant, while in the MISO strategy, the pulp level setpoints are determined by the ESC controllers to vary the froth height.

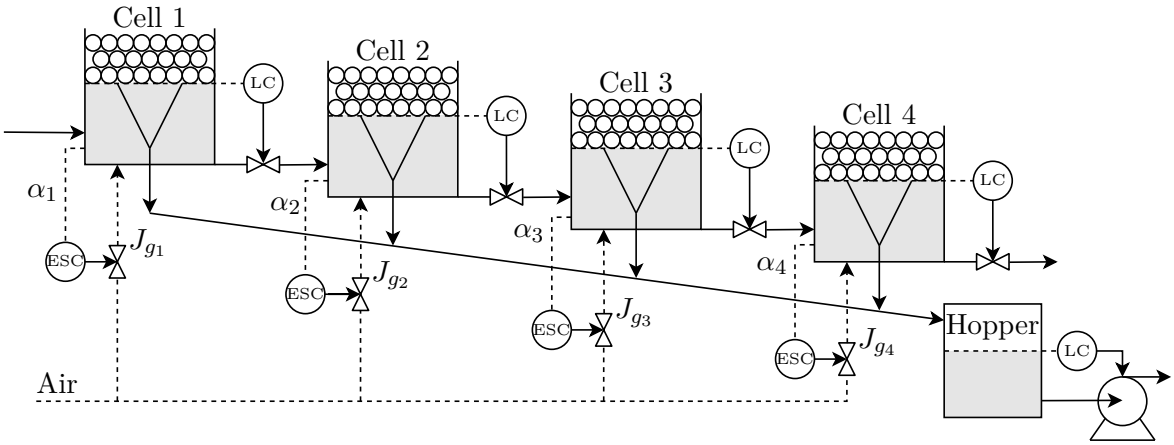

Figure 5.1. The control architecture for the flotation circuit used in the simulation study.

A separate ESC is implemented on each of the cells to maximize the air recovery, α_k, by manipulating the aeration rate of the cells. Since the TESC and SESC controllers both minimize an objective function, the negative of the air recovery is used in these objective functions. The local optimization problem of finding the aeration rate that produces the maximum air recovery can be solved in each of the cells independently of how the other cells are being operated. The ESCs are all tuned with the same tuning parameters. Each controller is tuned through trial and error to find a good balance between the transient response and robustness while adhering to the parameter constraints and tuning guidelines described in Chapter 3. The ESC controllers in the simulation are not constrained by limiting the range of inputs that can be provided to the plant. Input constraints are easy to add to the controllers and should be included when the controllers are implemented on a real plant where the constraints are important to ensure that the plant remains within safe operating ranges. The model simulation results in Figure 4.2 show that the PAR operating point that the controllers

aim to track is within the allowed plant input range. Therefore, the controller should never reach a constraint in normal operation.

The process is simulated with a 4^{th} order *Runge-Kutta* numerical integration method using a fixed time-step of 10 s. White Gaussian noise with a noise level of -50 dB is added to J_{g_k} and -30 dB is added to the level control valve signals, v_k, as input noise. White Gaussian noise with a noise level of -70 dB is added to α_k, L_k and L_H to evaluate the performance of the controllers in the presence of measurement noise.

Two simulation scenarios are considered:

1. The optimization ability of ESC ($t = 0$ h to $t = 120$ h).

In this scenario, only the ability of the ESC to find the optimum is evaluated. The simulation starts at a sub-optimal operating point, and the ESCs optimize the flotation circuit over a period of 5 days (120 h). During this time period, there are no external disturbances or changes to the process. For the first 20 h, the plant is still operating under normal operating conditions, and the ESC controllers are only switched on at $t = 20$ h and start optimizing the plant.

2. The disturbance rejection ability of ESC ($t = 120$ h to $t = 240$ h).

In this scenario, the ability of the ESC to reject disturbances is evaluated. Continuing from the previous scenario, at $t = 140$ h the plant is subjected to a large disturbance that changes the peak air recovery operating point significantly. In reality, the disturbances in industrial plants are usually much smaller and more gradual. The disturbance was made by decreasing $K_{\alpha_{J_{gk}}}$ by 1.3 and decreasing α_{OS_k} by 0.00864 in (4.10) over a 3 h period. Since the effect of individual specific disturbances such as changes in mineral grade and percentage solids are not modelled, the step-changes in $K_{\alpha_{J_{gk}}}$ and α_{OS_k} aim to simulate any combination of disturbances that influence the optimal peak air recovery operating point. These parameter changes cause the curves in Figure 4.3 to shift, and the operating point essentially moves to a different place on the curve for which the controller needs to find the peak again.

One of the main performance metrics used to compare the different ESC controllers is the convergence time. This is the time that it takes the controller to converge to the peak air recovery operating condition from the moment the controller is switched on. The criteria used for convergence is chosen as the time it takes the air recovery of all the cells to settle within

1 % of the peak air recovery point. For the simulations, the theoretical PAR value is used, as defined by α_{OS_k} in (4.10). To ensure that the noise does not affect the convergence time, a 5 min moving average is used for the calculation.

5.3 SINGLE INPUT PERTURBATION (SISO) AIR RECOVERY OPTIMIZATION

The tuning parameters for the different controllers are given in Table 5.1. These parameters are not necessarily the optimal choices in terms of conversion time or robustness but are selected to result in a balanced response and should enable a fair comparison between the controllers.

Table 5.1. SISO air recovery optimization ESC parameters.

Method	Tuning Parameter	Description
PESC	$a = 0.002$	Dither amplitude
	$\omega = 75.3982\,\text{rad/h}$	Dither frequency
	$\omega_h = 72.0000\,\text{rad/h}$	High-pass cutoff frequency
	$\omega_l = 0.3600\,\text{rad/h}$	Low-pass cutoff frequency
	$k = 250$	Integrator gain
TESC	$a = 0.00026$	Dither amplitude
	$\omega = 75.3982\,\text{rad/h}$	Dither frequency
	$k_T = 0.01$	Estimation gain
	$k_{\eta_1} = 0.23$	Estimation gain constant
	$k_{\eta_2} = 0.23$	Estimation gain constant
	$k = 0.05$	Optimization gain
	$\sigma = 0.0001$	Positive constant
	$z_\theta = 1$	Uncertainty set radius
SESC	$\rho = 0.5$	Reflection coefficient
	$\chi = 2$	Expansion coefficient
	$\gamma = 0.5$	Contraction coefficient
	$\sigma = 0.5$	Shrinking coefficient
	$T_s = 0.5\,\text{h}$	Time to reach steady-state

5.3.1 The optimization ability of ESC ($t = 0\,\text{h}$ to $t = 120\,\text{h}$).

The simulation results for the first 120 h are first shown in Figure 5.2 for each of the three different controllers. The first row shows the air recovery (α_k) that has to be maximized. The second row shows the aeration rate (J_{g_k}), i.e. the control inputs that the controllers use to steer the plant to the optimum. On the third and fourth rows, the hopper grade (4.16) and mineral recovery (4.17) is plotted against time. The convergence times of the ESC controllers are summarized in Table 5.2.

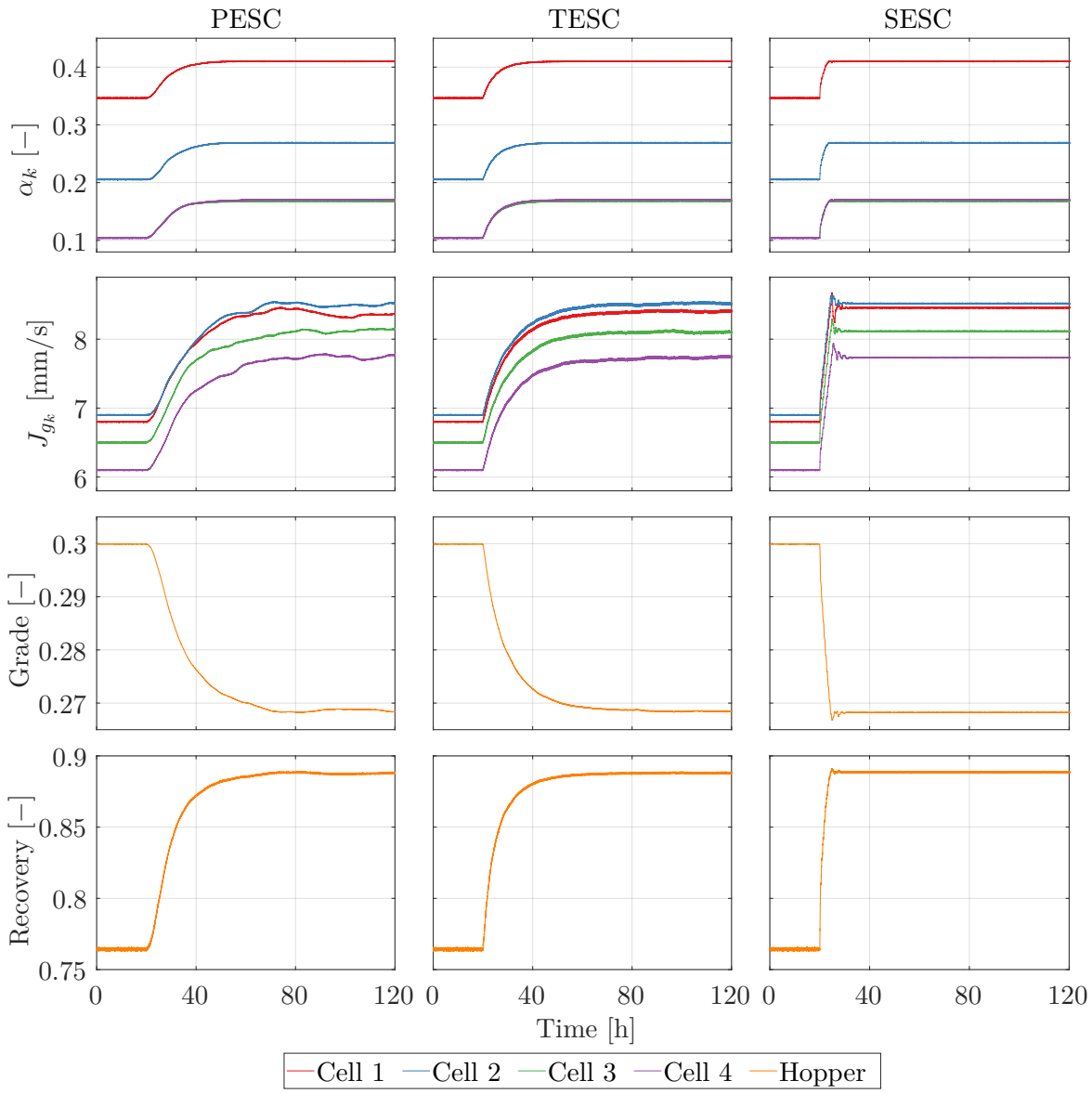

Figure 5.2. Optimization simulation results for SISO air recovery optimization.

Figure 5.3 shows the grade-recovery curve that can be used to evaluate the overall performance of the flotation plant. Since the simulation allows the plant to reach steady-state over a long time period, the instantaneous recovery shown is not expected to differ significantly from the true recovery. Figure 5.4 is a projection of the air recovery for cell 1 on the 3D surface plot showing the effect of the entire range of input values. The air recovery projections of cells 2–4 are shown in Figures A.1, A.2, and A.3. Since the froth height is controlled to a set point, the path that the controller takes will not vary much in the $h_{f_k}-$dimension. Figures 5.5 and 5.6 show the projections of the grade and recovery of all the controllers on the 3D surface plots from Figure 4.3.

Table 5.2. Convergence time of the SISO air recovery optimization ESC controllers.

Controller	Convergence Time
PESC	31.9167 h
TESC	20.8861 h
SESC	3.8250 h

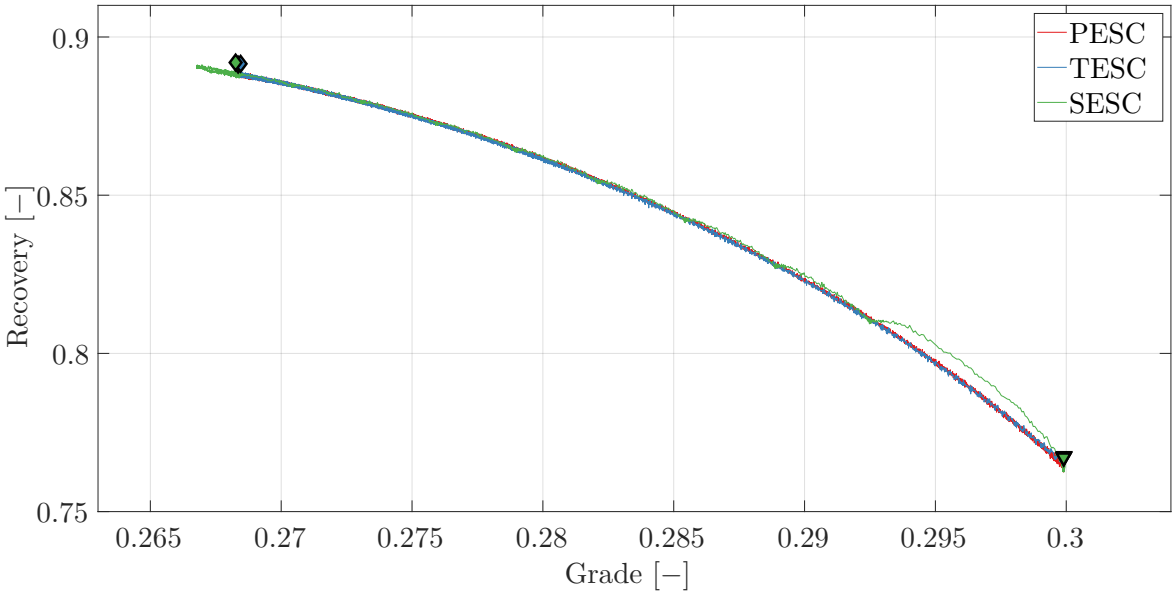

Figure 5.3. Grade-recovery curve for SISO air recovery optimization. The initial conditions are indicated by ∇ and the final optimized operating points by ◊.

Figures 5.2 and 5.4 show that the process starts at a sub-optimal operating point, and for the first 20 h the controllers are deactivated while the plant operates under regulatory level controller only. At $t = 20$ h, the ESC controllers are activated and start to optimize the flotation plant by maximizing the air recovery. The PESC and TESC controllers take very similar paths towards the peak air recovery point. The main difference is the speed of the convergence. As shown in Table 5.2, the TESC is able to react quicker than the PESC and is able to reach the peak air recovery more than 11 h faster than the PESC. Once the peak air recovery is reached in each of the cells, the perturbations continue to keep the process at the optimal operating point.

The SESC controller, shown in Figure 5.2 in the right column, is quite different from the PESC and TESC controllers, resulting in a much more aggressive transient response due to larger step sizes. The ESC converges to the peak air recovery point more than 17 h and

28 h faster than the TESC and PESC, respectively. As a result of the relatively aggressive control action, the SESC controller can be seen to overshoot the optimal J_{g_k} operating point, and it also oscillates around the optimal point before settling. The larger step sizes of the SESC algorithm can be seen on the grade-recovery curve of Figure 5.3, especially at the start of the optimization routine when the simplex is still relatively large. Since the simplex becomes increasingly smaller after the extremum has been reached, the SESC control input, J_{g_k}, has very small perturbations, if any, unlike the more noisy signals of the PESC and TESC controllers.

There is very little difference in the final optimized air recovery, hopper grade and recovery operating point where the controllers settle as all the ESCs are successful in finding the peak air recovery point in each of the cells. The ESCs increase the recovery up to 88.8 % where it stabilizes close to the theoretical maximum mineral recovery of 89 % as shown in Figure 4.2. This increase in hopper mineral recovery comes at a cost of a reduced hopper grade which drops to below 26.9 %. On the grade-recovery curves, the operating point moves from the bottom right at a high grade and low recovery towards the top left, where the recovery is maximized at a reduced grade. This relationship is also demonstrated in Figures 5.5 and 5.6 where the grade is steered towards the valley while the recovery is being maximized.

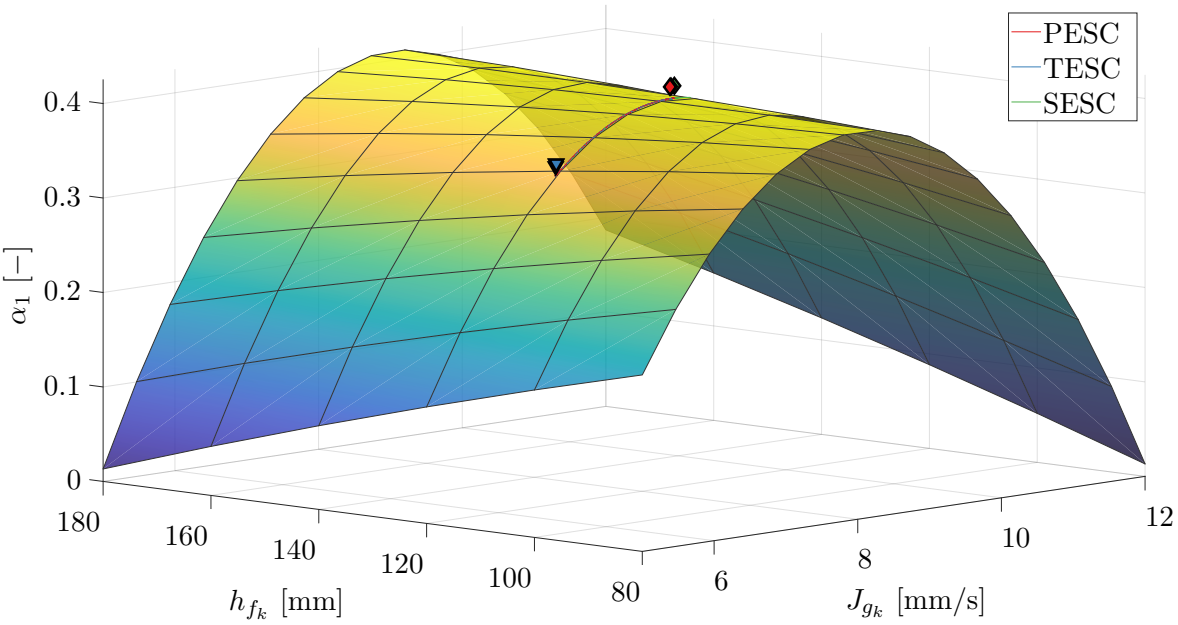

Figure 5.4. Air recovery surface plot for cell 1 showing SISO air recovery optimization. The initial conditions are indicated by ∇ and the final optimized operating points by ◊.

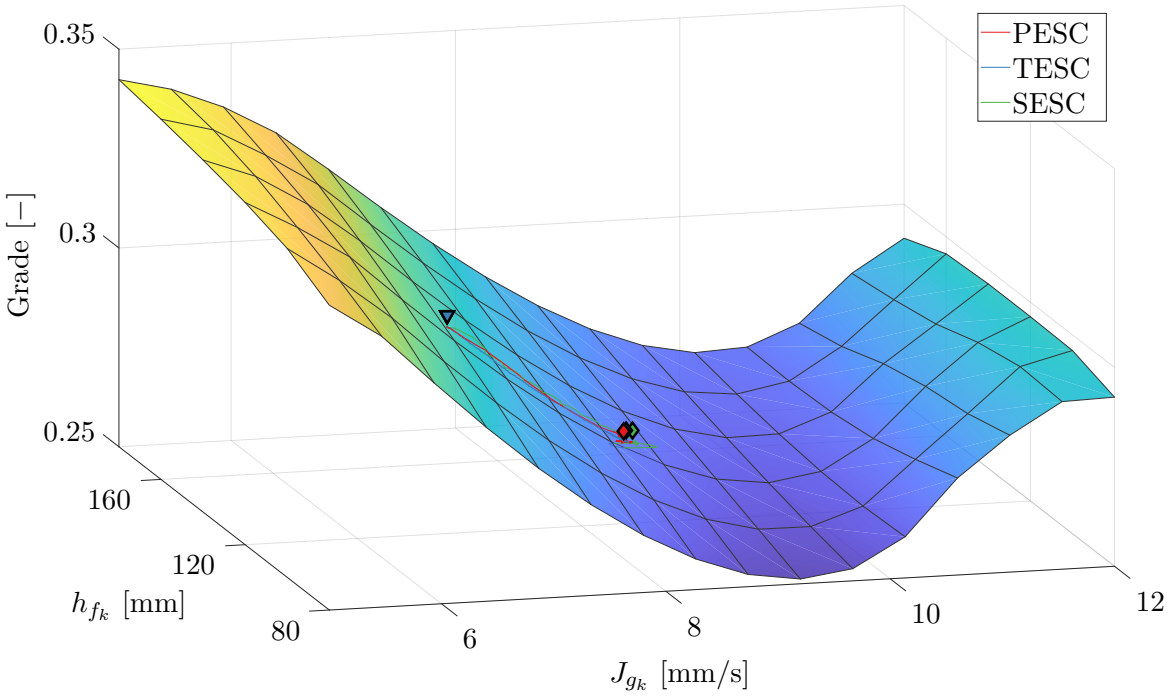

Figure 5.5. Grade surface plot showing SISO air recovery optimization. The initial conditions are indicated by ∇ and the final optimized operating points by ◊.

From the results in Figure 5.3, it is clear when looking at the SESC path that although the final mineral recovery is close to the optimum mineral recovery, it is not maximized, and a higher

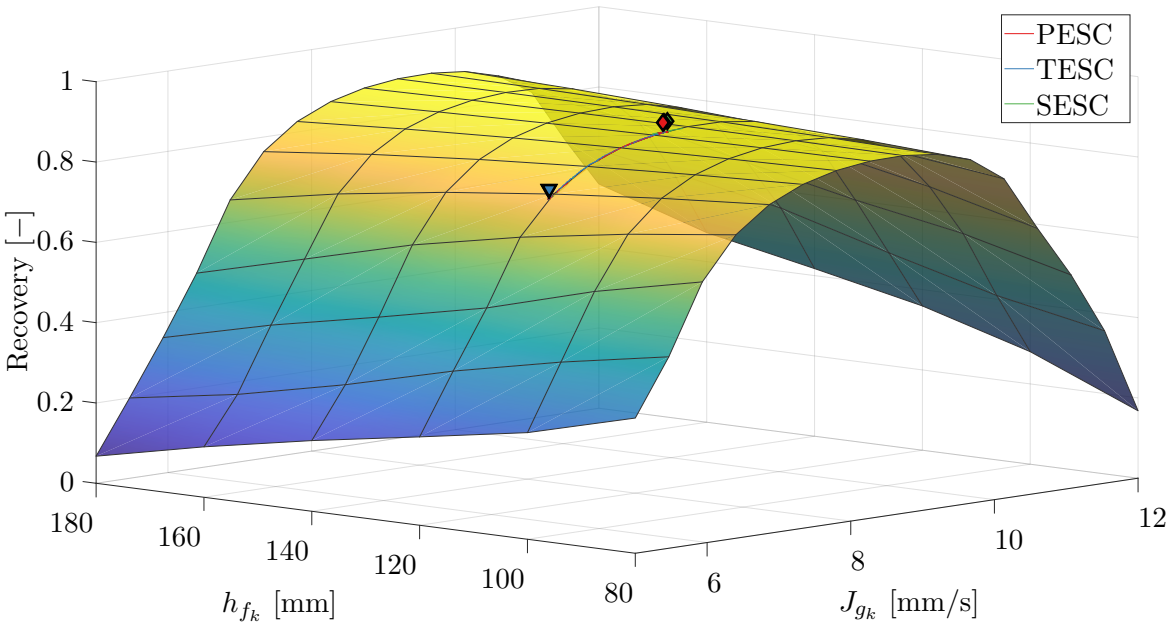

Figure 5.6. Recovery surface plot showing SISO air recovery optimization. The initial conditions are indicated by ∇ and the final optimized operating points by ◊.

mineral recovery would be possible further to the left on the curve. Therefore, the conclusion can be made that air recovery optimization is not equal to mineral recovery optimization. Instead, air recovery optimization increases the mineral recovery until it reaches a point where any further increase in recovery comes at a much greater reduction in grade.

5.3.2 The disturbance rejection ability of ESC ($t = 120\,\text{h}$ to $t = 240\,\text{h}$).

The simulation results from the second 120 h are summarized in Figure 5.7, showing how the different controllers react to the large disturbance introduced at $t = 140\,\text{h}$ in Figure 5.7. When the disturbance takes place, the operating conditions change, and the peak air recovery

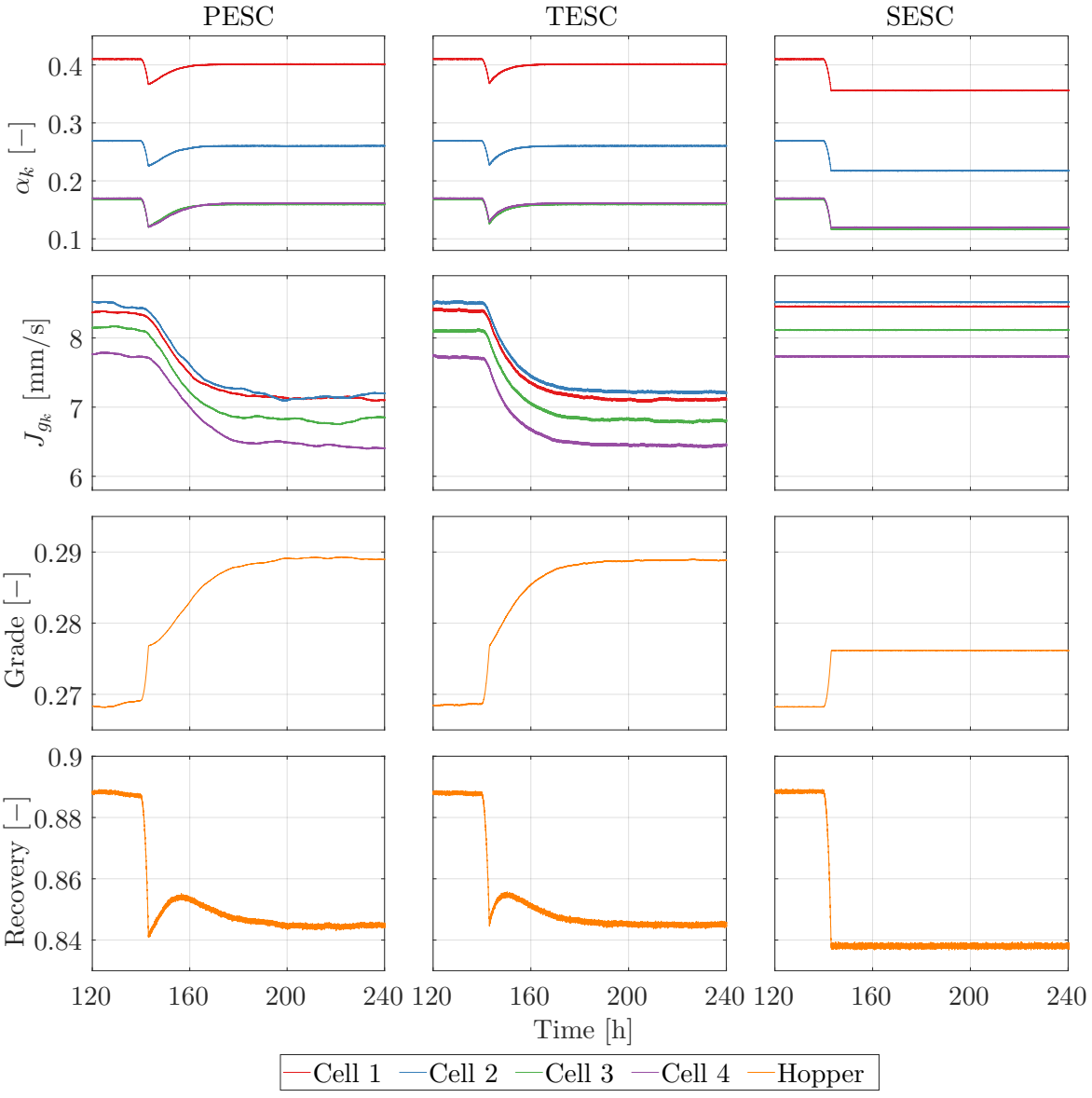

Figure 5.7. Disturbance simulation results for SISO air recovery optimization.

point is no longer at the same aeration rate as before, which causes the air recoveries of all the cells to drop significantly. The PESC and TESC controllers react to the disturbance by optimizing the air recovery again until the new peak air recovery operating point has been reached. The convergence times of the ESC controllers to reach the peak air recovery again after the disturbance are summarized in Table 5.3.

Table 5.3. Convergence time of the SISO air recovery optimization ESC controllers after the disturbance.

Controller	Convergence Time
PESC	29.9139 h
TESC	20.0611 h
SESC	∞

The TESC controller is once again faster to react and reaches the optimum faster than the PESC controller. The PESC and TESC controllers decrease the aeration rate to steer the process to the peak air recovery operating point as the disturbance shifted the operating point to the other side of the parabola peak in Figures 4.3 and 4.2. This is confirmed by the different shape of the grade-recovery curve in Figure 5.8 and both the hopper grade and recovery that increases as the optimization continues. At the new peak air recovery operating point, the

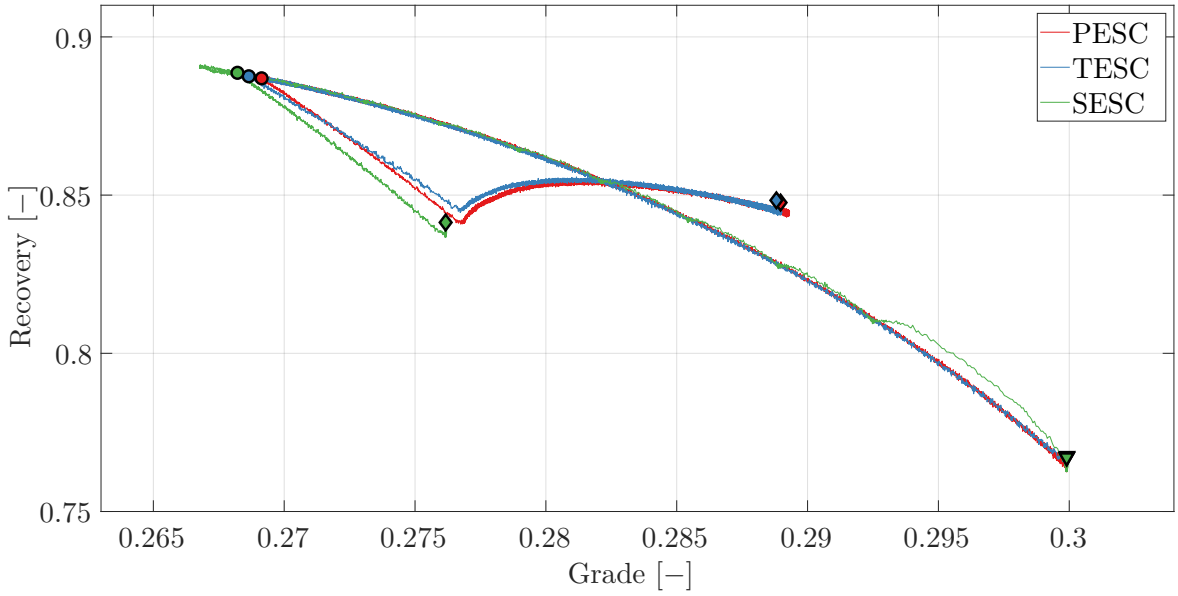

Figure 5.8. Grade-recovery curve for SISO air recovery optimization with disturbance. The initial conditions are indicated by ∇, ○ is when the disturbance takes place and ◊ are the final optimized operating points.

recovery is lower at 84.5 %, but the grade is better at 28.9 %. The theoretical maximum mineral recovery under these new operating conditions is 85 %. The SESC controller is not able to adjust to the disturbance because the simplex is already much too small to provide a perturbation to steer the plant to the new optimum. Therefore, the SESC controller will keep operating at the sub-optimal operating point until the controller is reinitialized with a new simplex and the optimization can start over.

Once again, it is clear from Figure 5.8 that although the final operating point is close to the maximum recovery, the PAR points do not correspond exactly to the peak in mineral recovery. The air recovery optimization controllers search past the recovery maxima to settle at a slightly reduced mineral recovery at a higher grade.

5.4 MULTIPLE INPUT PERTURBATION (MISO) AIR RECOVERY OPTIMIZATION

The tuning parameters for the different controllers are given in Table 5.4. These parameters are not necessarily the optimal choices in terms of conversion time or robustness but are selected to result in a balanced response and should enable a fair comparison between the controllers.

5.4.1 The optimization ability of ESC ($t = 0\,\text{h}$ to $t = 120\,\text{h}$).

The simulation results for the first 120 h are first shown in Figure 5.9 for each of the three different controllers. The first row shows the air recovery (α_k) that has to be maximized. The second and third rows show the aeration rate (J_{g_k}) and the froth height (h_{f_k}), i.e. the control inputs that the controllers use to steer the plant to the optimum. On the fourth and fifth rows, the hopper grade (4.16) and mineral recovery (4.17) is plotted against time. The convergence times of the ESC controllers are summarized in Table 5.5.

Table 5.5. Convergence time of the MISO air recovery optimization ESC controllers.

Controller	Convergence Time
PESC	28.1750 h
TESC	19.9472 h
SESC	7.6500 h

Figure 5.10 shows the grade-recovery curve that can be used to evaluate the overall performance

Table 5.4. MISO air recovery optimization ESC parameters.

Method	J_g Tuning Parameter	h_f Tuning Parameter	Description
PESC	$a = 0.002$	$a = 0.2$	Dither amplitude
	$\omega = 75.3982\,\text{rad/h}$	$\omega = 13.4640\,\text{rad/h}$	Dither frequency
	$\omega_h = 72.0000\,\text{rad/h}$	$\omega_h = 10.8000\,\text{rad/h}$	High-pass cutoff frequency
	$\omega_l = 0.3600\,\text{rad/h}$	$\omega_l = 0.3600\,\text{rad/h}$	Low-pass cutoff frequency
	$k = 250$	$k = 15$	Integrator gain
TESC	$a = 0.00026$	$a = 0.001$	Dither amplitude
	$\omega = 75.3982\,\text{rad/h}$	$\omega = 13.4640\,\text{rad/h}$	Dither frequency
	$k_T = 0.01$	$k_T = 0.01$	Estimation gain
	$k_{\eta_1} = 0.23$	$k_{\eta_1} = 0.01$	Estimation gain constant
	$k_{\eta_2} = 0.23$	$k_{\eta_2} = 0.01$	Estimation gain constant
	$k = 0.05$	$k = 0.25$	Optimization gain
	$\sigma = 0.0001$	$\sigma = 0.0001$	Positive constant
	$z_\theta = 1$	$z_\theta = 40$	Uncertainty set radius
SESC	$\rho = 0.65$	$\rho = 0.65$	Reflection coefficient
	$\chi = 2$	$\chi = 2$	Expansion coefficient
	$\gamma = 0.65$	$\gamma = 0.65$	Contraction coefficient
	$\sigma = 0.65$	$\sigma = 0.65$	Shrinking coefficient
	$T_s = 0.5\,\text{h}$	$T_s = 0.5\,\text{h}$	Time to reach steady-state

of the flotation plant. Since the simulation allows the plant to reach steady-state over a long time period, the instantaneous recovery shown is not expected to differ significantly from the true recovery. Figure 5.11 is a projection of the air recovery on the 3D surface plot showing the effect of the entire range of input values. The air recovery projections of cells 2–4 are shown in Figures A.4, A.5, and A.6. Figures 5.12 and 5.13 show the projections of the grade and recovery of all the controllers on the 3D surface plots from Figure 4.3. The convergence times of the PESC and TESC controllers in Table 5.5 are faster than the convergence times of the SISO controllers given in Table 5.2. The reason for these faster times is that the distance the controllers have to search in the J_{g_k}-dimension to find the PAR is smaller when the controller search in the h_{f_k}-dimension as well. The same optimal air recovery value is found in both cases, but in the MISO case, it is found at an aeration rate of $J_{g_1} \approx 8.3$ instead of at an aeration rate of $J_{g_1} \approx 8.4$ in the SISO case. This is not a large difference, but it is enough to allow for a slightly faster convergence time. In contrast, the SESC controller takes much longer to reach the PAR point when using both the aeration rate and froth height as inputs. The extra input increases the size of the simplex used in the algorithm, which makes the optimization less efficient as a larger region has to be searched. The controller also

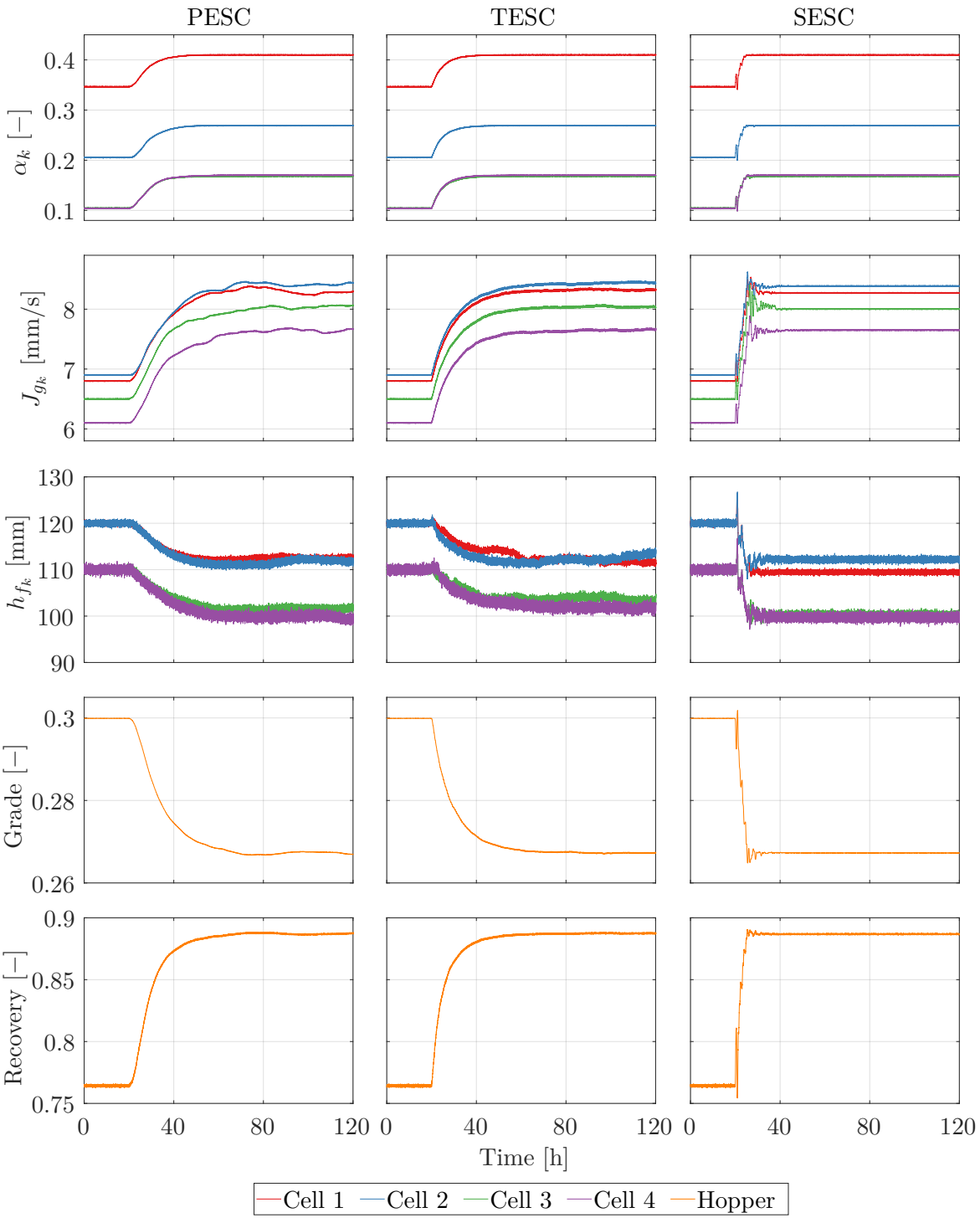

Figure 5.9. Optimization simulation results for MISO air recovery optimization.

takes longer initially to find the correct optimization direction, as seen in the loop being made around the starting position in Figure 5.10.

The three MISO ESC controllers all settled on approximately the same final operating points, and all the controllers found the same final optimal PAR points in each of the cells as the SISO controllers did. However, these points are achieved at different aeration rates and froth height setpoints, which correspond to different mineral grades and recoveries. The SISO controllers achieved a recovery of 88.8 % at a grade of 26.8 % and the MISO controllers achieved a recovery of 88.7 % at a grade of 26.7 %. The differences are not very large, but the plant performance will be slightly worse under the MISO controllers. The reason for the reduced recovery is that the optimization stopped at a slightly smaller aeration rate. A further increase in the aeration rate will result in a larger recovery, as shown in Figure 5.13. The reduced grade can be explained by the froth height changes; a decrease in froth height results in a lower grade, as shown in Figure 5.12.

5.4.2 The disturbance rejection ability of ESC ($t = 120\,\text{h}$ to $t = 240\,\text{h}$).

The simulation results from the second 120 h are summarized in Figure 5.14, showing how the different controllers react to the large disturbance introduced at $t = 140\,\text{h}$ in Figure 5.14. Figure 5.15 shows the grade-recovery relationships of the three controllers throughout the simulation.

When the disturbance takes place, the operating conditions change, and the peak air recovery

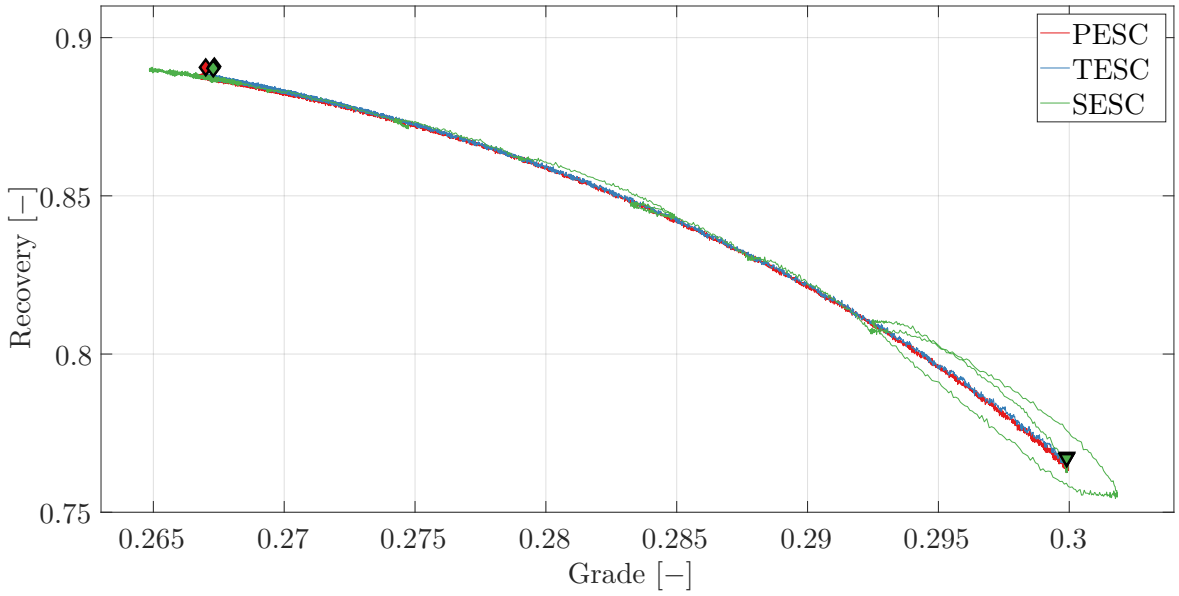

Figure 5.10. Grade-recovery curve for MISO air recovery optimization. The initial conditions are indicated by ∇ and the final optimized operating points by ◊.

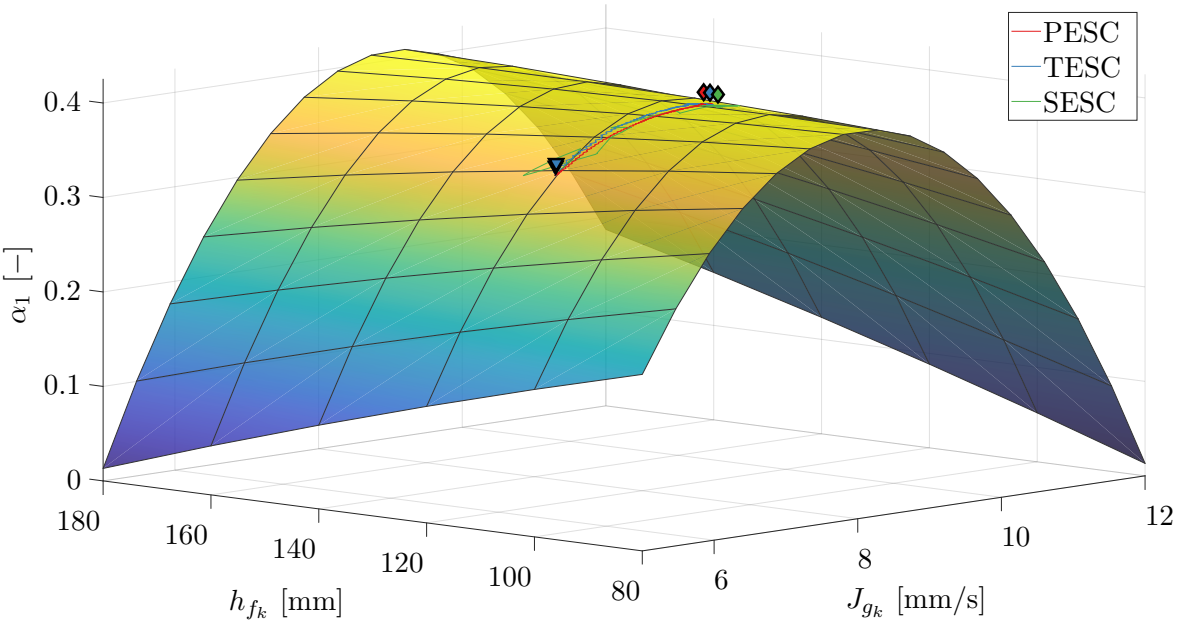

Figure 5.11. Air recovery surface plot for cell 1 showing MISO air recovery optimization. The initial conditions are indicated by ∇ and the final optimized operating points by ◊.

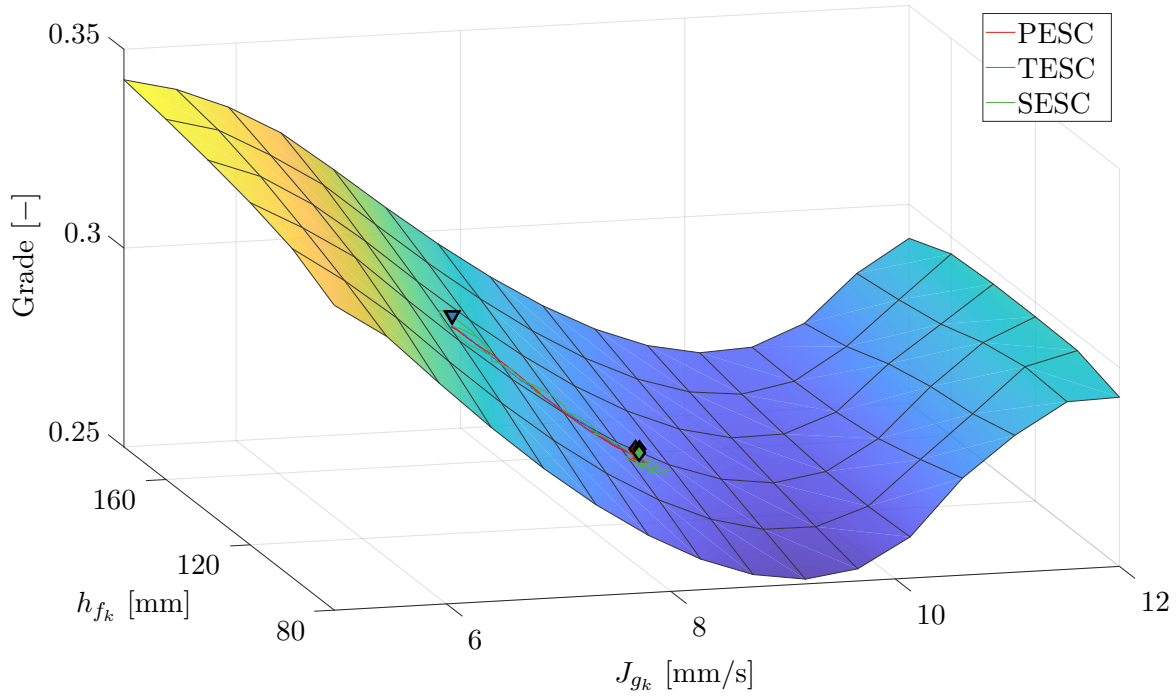

Figure 5.12. Grade surface plot showing MISO air recovery optimization. The initial conditions are indicated by ∇ and the final optimized operating points by ◊.

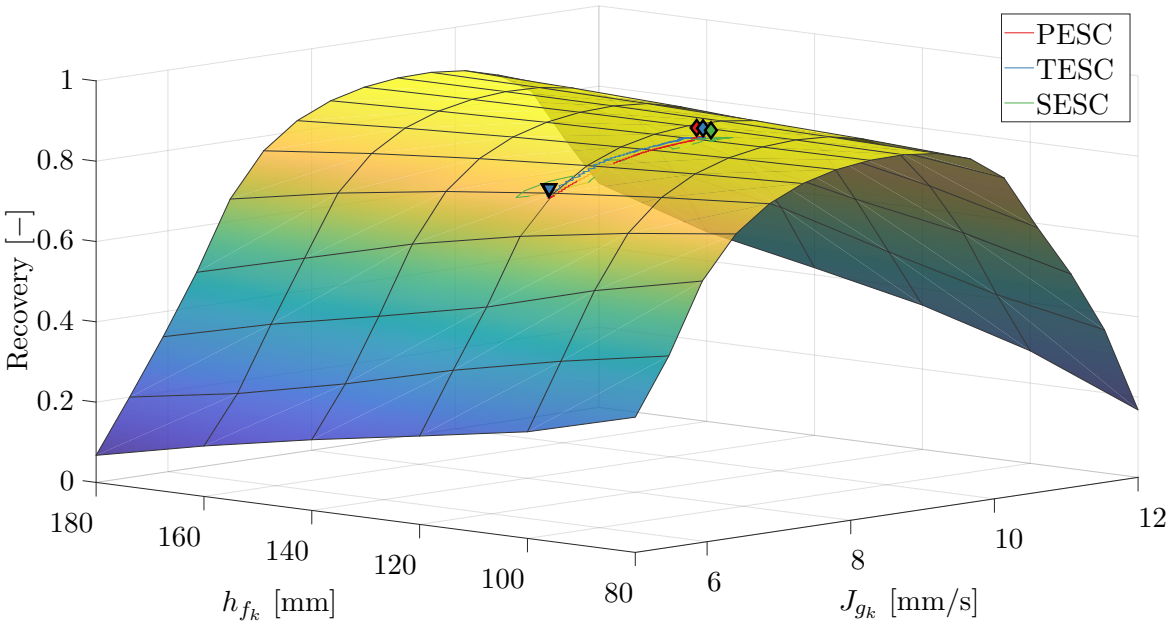

Figure 5.13. Recovery surface plot showing MISO air recovery optimization. The initial conditions are indicated by ∇ and the final optimized operating points by ◊.

point is no longer at the same aeration rate as before, which causes the air recoveries of all the cells to drop significantly. The PESC and TESC controllers react to the disturbance by optimizing the air recovery again until the new peak air recovery operating point has been reached. The convergence times of the ESC controllers to reach the peak air recovery again after the disturbance are summarized in Table 5.6.

Table 5.6. Convergence time of the MISO air recovery optimization ESC controllers after the disturbance.

Controller	Convergence Time
PESC	28.6694 h
TESC	18.8917 h
SESC	∞

The PESC and TESC controllers increase the froth height while decreasing the aeration rate to steer the process to the peak air recovery operating point as the disturbance shifted the operating point to the other side of the parabola peak in Figures 4.3 and 4.2. The change in the direction of optimization in Figure 5.15 confirms that the operating point shifted to the opposite side of the parabola as where the initial operating point was. The PESC and TESC MISO controllers are once again slightly faster to react and reach the optimum faster than

the SISO controllers, but the difference is just about an hour for the PESC controller and less than an hour for the TESC controller. Since the MISO controllers did not search as far in the J_{g_k}-dimension during the optimization scenario, the faster convergence after the disturbance

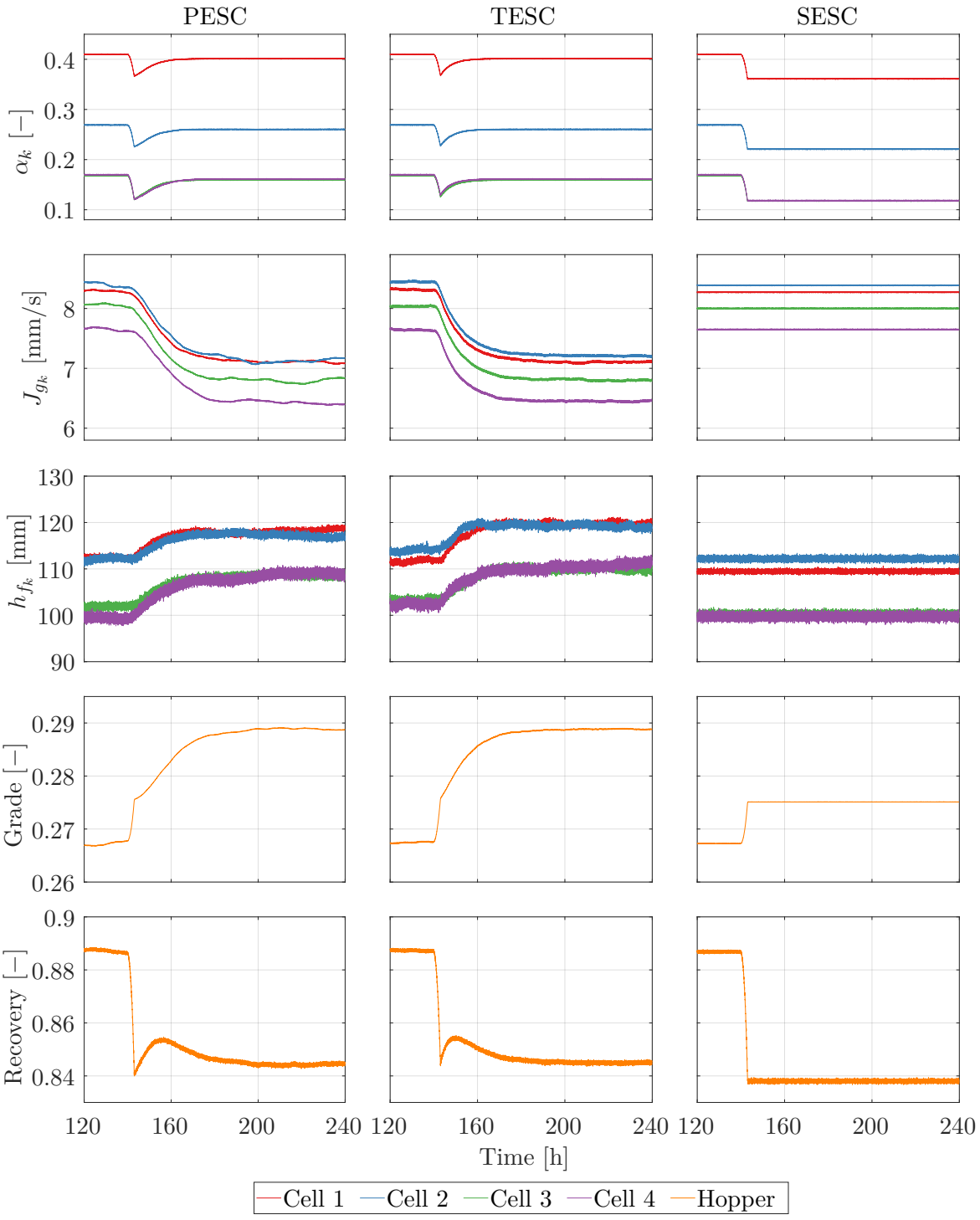

Figure 5.14. Disturbance simulation results for MISO air recovery optimization.

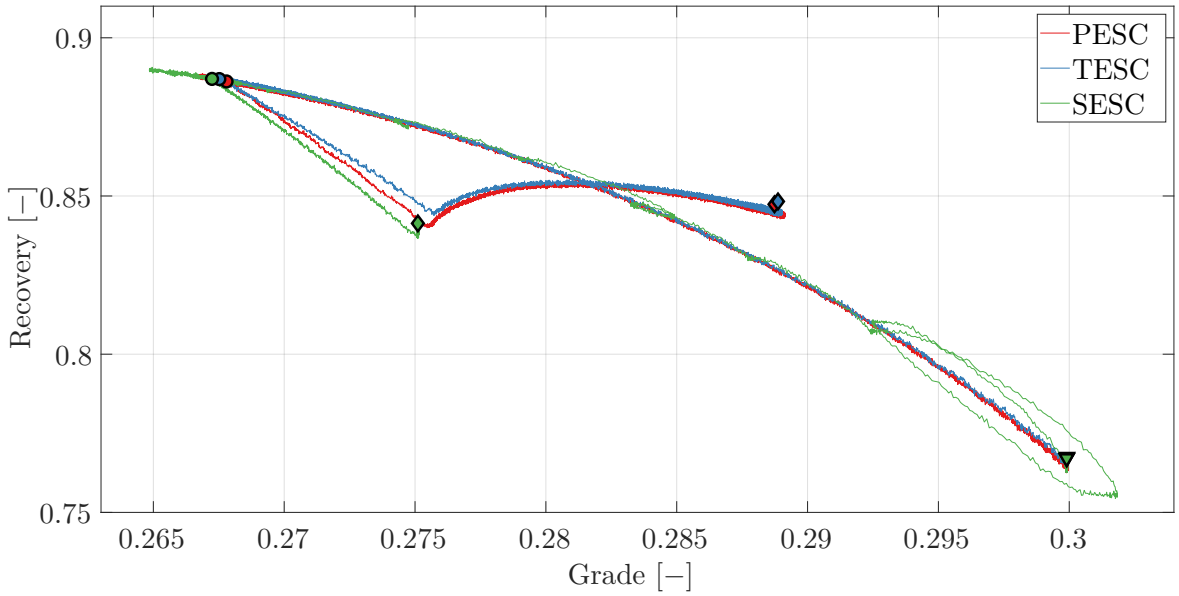

Figure 5.15. Grade-recovery curve for MISO air recovery optimization with disturbance. The initial conditions are indicated by ∇, ○ is when the disturbance takes place and ◊ are the final optimized operating points.

could be due to the smaller search distance to the new optimum. The final operating points after the disturbance are the same operating points that the SISO controllers achieved, with the final mineral grade and recovery being 28.9 % and 84.5 % respectively for the PESC and TESC controllers. Once again, the SESC controller is not able to adjust to the disturbance because the simplex is already much too small to provide a perturbation to steer the plant to the new optimum. Therefore, the SESC controller keeps the aeration rate and froth height at the previous (now sub-optimal) operating points.

5.5 CONTROLLER COMPARISONS

Comparing the three ESCs, there are some clear advantages and disadvantages of each. All the controllers are successful in optimizing the flotation circuit from a sub-optimal operating point to the peak air recovery operating point by either adjusting only the aeration rate or the aeration rate and froth height.

The PESC is simple to tune, but the performance can be limited by the choice of dither signal and the dynamics of the plant. The three frequency tuning parameters (ω, ω_l, and ω_h), are dependent on the plant dynamics. Therefore, the frequencies should be selected to create the required time-scale separation between the plant, dither, and optimization. The dither amplitude and the integration gain are the two important tuning parameters that determine

the performance of the controller. The amplitude must be large enough for the controller to detect the plant response to the perturbation in the presence of noise, but not too large that the perturbations reduce the performance of the plant. The integration gain, k, should be as large as possible to improve the transient performance of the controller, but still small enough to minimize oscillations in the plant output and ensure convergence.

The TESC provides more freedom to tune the controller to improve the performance beyond the choice of dither signal. However, the many tuning parameters make the controller more difficult to tune well. The dither signal and optimization gain can be tuned similarly to the PESC controller, but the rest of the tuning parameters are less intuitive to select. The tuning parameters are interconnected and dependent on each other, which makes it challenging to find the optimal parameter choices. The TESC can also perform well with a much smaller dither signal than the PESC, i.e., in this example, the chosen TESC dither amplitude for J_{g_k} is more than 7 times smaller than the PESC dither amplitude (Tables 5.1 and 5.4). The PESC and TESC controllers both worked well in the SISO and MISO configurations, and the additional input did not reduce the optimization efficiency. The convergence times of the different controllers are summarized in Table 5.7.

Table 5.7. Comparison of convergence times of the ESC controllers.

Controller	Optimization		Disturbance Rejection	
	SISO	MISO	SISO	MISO
PESC	31.9167 h	28.1750 h	29.9139 h	28.6694 h
TESC	20.8861 h	19.9472 h	20.0611 h	18.8917 h
SESC	3.8250 h	∞	7.6500 h	∞

The TESC controller performed better than the PESC controller in terms of convergence times and produced a more stable input and output in the presence of the environment noise. SESC has the fastest convergence time and is also dither-free with no perturbations visible in the output that can reduce the plant performance at the optimum. However, the faster convergence time comes at the cost of more aggressive control moves and significant overshoots before settling at the optimal operating point. The SESC controller can also tolerate higher noise levels because of the lack of dependence on gradient information. The SESC controller is easy to tune, and the standard values for the coefficients often lead to optimal performance. The setting time parameter, T_s, should be selected based on the plant dynamics. The time

should be chosen as small as possible to improve the transient performance of the controller, but still large enough to allow the plant to reach a steady state before making the next control move. The convergence time of the SESC controller increased when both inputs were used in the optimization due to the larger, less efficient simplex. Therefore, in the case of flotation where a single input is sufficient for optimization, the simpler SESC controller works better. The SESC controller is not suitable for tracking a time-varying extremum as a result of changes in the operating conditions. An operator will need to reinitialize the SESC to track a new extremum when they are aware of significant changes in the operating conditions. A big advantage of all the controllers is that they are not dependent on a plant model to optimize the process. The ESCs can operate effectively with only basic knowledge of the response time and dynamics of the plant.

5.6 CHAPTER SUMMARY

This chapter presented the simulation setup for the simulation study and the simulation results. The dynamic flotation model from Oosthuizen et al. (2021) is used as the simulation model and consists of four rougher flotation cells connected in series. The simulation setup includes regulatory controllers, separate ESC controllers on each of the flotation cells and the inclusion of input and measurement noise to simulate real-world plant conditions. MISO and SISO optimization strategies are evaluated in two simulation scenarios, optimization from a suboptimal operating point and disturbance rejection.

The ESCs move the flotation circuit from a suboptimal operating point to the peak air recovery operating point. The gradient-based PESC and TESC are successful in continuously tracking the optimum, and after the introduction of a simulated disturbance, the ESCs can adapt to the time-varying extremum and once again reach the new peak air recovery operating point. The SESC is able to reach the extremum relatively quickly, but then maintains the same operating point and does not adapt after the introduction of the disturbance.

The MISO strategy resulted in faster convergence in the gradient-based controllers, but with slightly worse performance compared to the SISO strategy. The convergence time of MISO SESC optimization is much slower than SISO optimization due to the added complexity of the larger simplex.

CHAPTER 6 CONCLUSION

This dissertation demonstrates in simulation how extremum seeking control (ESC) can be used to optimize flotation circuit performance using peak air recovery. A perturbation-based ESC (PESC), time-varying ESC (TESC), and simplex ESC (SESC) are investigated, and all the controllers are able to manipulate the aeration rate of a flotation circuit to maximize the air recovery. Both the optimization ability and the disturbance rejection ability of the controllers are evaluated for two optimization strategies, single-input perturbation and multiple-input perturbation.

In Chapter 2, the relevant literature on flotation is reviewed including the process description, modelling and control of flotation circuits, and the objectives of the process. Maximizing the air recovery in a flotation cell and operating at the PAR operating point is a very useful objective that results in optimal flotation performance. At this operating point, the froth is stable, and the mineral recovery is close to the maximum possible recovery while the grade is acceptable. Phenomenological and empirical flotation models can be very effective in modelling the flotation dynamics and are useful for process control, Chapter 4 presents such a dynamic model that is used to create the simulation platform. The model presents the relationships between the inputs, aeration rate and froth height and the outputs, air recovery, grade and mineral recovery. A simulation of the model under steady-state conditions highlights the PAR operating point and how it corresponds to increased mineral recovery.

In Chapter 3, three different ESC approaches are presented. The perturbation-based ESC is a classic ESC method that is easy to implement. An important requirement for the ESC to work is a time scale separation between the plant dynamics (fastest), dither signal (medium time scale) and the optimization (slowest). This time scale separation results in the convergence

of the controller being quite slow. The time-varying ESC is an adaption of the classic ESC and uses the estimation of the gradient as a time-varying parameter to remove the need for averaging the results. This approach minimizes the impact of the dither signal choice by providing more freedom in tuning the ESC and improving the transient performance. Unlike perturbation-based ESC and time-varying ESC, the simplex ESC is not a gradient-based ESC, but a direct search ESC that uses the Nelder-Mead algorithm to optimize the objective function. The SESC controller can have very good transient performance but is not ideally suited to adapt to disturbances and changes in operating conditions.

Chapter 5 focuses on the implementation of the controller on the simulation platform to optimize air recovery. Two different optimization strategies are evaluated; in the SISO strategy, only the aeration rate (J_{g_k}) is varied while the froth height (h_{f_k}) is kept constant at a setpoint and in the MISO strategy both the aeration rate and the froth height are varied. To test the optimization ability of the ESC controllers, the flotation plant is initialized at a suboptimal operating point, and the controllers are required to optimize the flotation performance from this point. The disturbance rejection ability of the ESC controllers is also evaluated by simulating a large disturbance in the air recovery model. This disturbance changes the aeration rate that corresponds to the peak in air recovery and also changes the magnitude of the air recovery peak.

6.1 SUMMARY OF RESULTS

All of the ESC controllers are able to optimize the plant by maximizing the air recovery and operating at the PAR operating point in both the SISO and MISO optimization strategies. The PESC and TESC controllers react similarly, and the main difference between the two is the convergence time. Both of the controllers have relatively long convergence times, but TESC reaches the PAR point more than 11 h faster than the PESC controller. Once the peak air recovery is reached in each of the cells, the perturbations continue to keep the process at the optimal operating point. The SESC controller is not gradient-based and reacts quite differently. The convergence of the SESC controller is much faster than the other controllers, reaching the peak more than 17 h and 28 h faster than TESC and PESC respectively. The more aggressive behaviour of the SESC controller results in larger steps in the manipulated variable and some overshoot and oscillations before setting at the optimum. In terms of the final operating point, the three controllers reach the same point at the optimal air recovery

and mineral recovery, but at a reduced grade.

In the MISO case where both inputs are used in the optimization, the convergence times are slightly faster for the gradient-based controllers, this is because the controllers do not have to search as far to find the PAR point when using both inputs. The convergence time of MISO SESC optimization is much slower than SISO optimization due to the added complexity of the larger simplex. The final operating point reached in the MISO strategy corresponds to a slightly worse performance in terms of grade and recovery compared to the SISO strategy, even though the same optimum air recovery is achieved. Therefore, using froth height as an input to optimize air recovery along with aeration rate is not the optimal strategy in terms of performance and only results in a faster convergence time when using the gradient-based ESCs. It might be better to use the froth height to optimize the grade while the aeration rate is used to optimize the air recovery instead of using both inputs to optimize the air recovery.

After the disturbance takes place, the gradient-based controllers, PESC and TESC, are able to detect that the plant is no longer operating at PAR and start to steer the system to the new peak. Both of the controllers are able to find the new PAR operating point and keep the flotation circuit operating at that point. The TESC controller is once again faster to converge to the optimum operating point, reaching the point almost 10 h before the PESC controller. The SISO and MISO strategies of the PESC and TESC controllers perform similarly after the disturbance, with the MISO controllers converging at the new optimum about an hour faster than the SISO controllers. The SESC controller is not able to adjust to the disturbance because the simplex is already much too small to provide a perturbation to steer the plant to the new optimum. As a result, the SESC controller does not do anything when the disturbance happens and keeps the circuit operating at the suboptimal operating point. For the SESC controller to optimize the plant again, it would have to be reinitialized with a new simplex. Regular reinitialization can be added to the controller, but this would negatively affect the performance if the circuit is already operating at PAR when the reinitialization happens.

From the results shown in the grade-recovery curves, especially Figures 5.8 and 5.15, it is clear that although the final mineral recovery is close to the optimum mineral recovery, it is not maximized and a higher mineral recovery would be possible. The air recovery optimization controllers search past the recovery maxima to settle at a slightly reduced mineral recovery

at a higher grade. Therefore, the conclusion can be made that air recovery optimization is not equal to mineral recovery optimization. Instead, air recovery optimization increases the mineral recovery until it reaches a point where the recovery is close to the maximum recovery, and the grade is not reduced too much. Therefore, air recovery optimization results in better performance compared to mineral recovery optimization, as the increase in grade outweighs the slightly reduced recovery.

In summary, when comparing the ESC controllers, PESC is simple to tune but is quite slow, and the performance can be limited by the choice of dither signal and the dynamics of the plant. TESC provides more freedom for tuning to improve the transient performance and can use a smaller dither signal but can be more challenging to tune well. SESC has the fastest convergence time and is dither free, but is not ideally suitable to track a constantly varying extremum. All three ESCs can optimize the flotation circuit using peak air recovery and are not dependent on a plant model. The MISO strategy can improve the convergence times of the PESC and TESC controllers at the cost of a slight reduction in grade and recovery performance when compared to the SISO strategy. The MISO strategy reduces the efficiency of the SESC controller as it adds complexity with a larger simplex which results in a longer convergence time.

6.2 CONCLUDING REMARKS

The ESCs take a relatively long time to converge to an optimum, and if the peak air recovery operating point changes too rapidly, as shown in Phillpotts et al. (2020), ESCs would not be able to effectively track the changing optimum. The convergence time can be decreased by selecting the initial operating conditions closer to the optimum so that the ESC does not have to explore far to reach the extremum. The ESCs are ideally suited for long-term automated optimization with slow-changing optimal operating conditions that the ESCs can track. PESC and TESC use continuous perturbations that can be visible in the output, and the process is never at a steady-state, but operates within the neighbourhood of the steady-state optimum. SESC is dither-free, and once the controller converges, the output is approximately constant.

The ESC controllers are model-free and do not need a plant model to optimize the plant. This is an important advantage since flotation models are often very complicated and difficult to fit

to industrial data. Air recovery measurements can sometimes be unreliable and can cause the ESCs to operate the flotation circuit at a different point from where true peak air recovery occurs, resulting in sub-optimal performance. However, Phillpotts et al. (2020) demonstrated that air recovery measurements can successfully be used for control.

The peak air recovery strategy optimizes the mineral recovery over the grade, which might not always be the optimal strategy for all flotation plants. For some plants, it might be beneficial to adjust the objective function to align with the operational objectives of the wider plant-wide process (Muñoz and Cipriano, 1999).

6.3 FUTURE WORK

In future work, the controllers can be adjusted to different optimization strategies. The results have shown that using the froth height in addition to the aeration rate to optimize air recovery does not contribute much to the performance of the controller. The froth height can rather be used to maximize grade while the aeration rate optimizes the air recovery. Another strategy can be to use a different objective function instead of air recovery. The ESC controllers can be used to optimize mineral recovery while keeping the grade at a setpoint or to use a weighted objective function that includes both grade and recovery.

Another possible direction for future work is to combine two different ESC controllers to form a hybrid controller that can benefit from the advantages of both controllers. Such a hybrid controller can use SESC to find the initial optimum and then switch over to TESC to track the optimum. The controller can switch back to a reinitialized SESC again when a certain criterion is met, such as a gradient above a predefined threshold.

REFERENCES

Aldrich, C., Avelar, E. and Liu, X. (2022). Recent advances in flotation froth image analysis, *Minerals Engineering* **188**(May): 107823.

Aldrich, C., Marais, C., Shean, B. J. and Cilliers, J. J. (2010). Online monitoring and control of froth flotation systems with machine vision: A review, *International Journal of Mineral Processing* **96**(1-4): 1–13.

Barbian, N., Hadler, K. and Cilliers, J. J. (2006). The froth stability column: Measuring froth stability at an industrial scale, *Minerals Engineering* **19**(6-8): 713–718.

Barbian, N., Hadler, K., Ventura-Medina, E. and Cilliers, J. J. (2005). The froth stability column: Linking froth stability and flotation performance, *Minerals Engineering* **18**(3): 317–324.

Barbian, N., Ventura-Medina, E. and Cilliers, J. J. (2003). Dynamic froth stability in froth flotation, *Minerals Engineering* **16**(11): 1111–1116.

Bascur, O. A. (1982). *Modelling and computer control of a flotation cell*, PhD thesis, University of Utah.

Bauer, M. and Craig, I. K. (2008). Economic assessment of advanced process control - A survey and framework, *Journal of Process Control* **18**(1): 2–18.

Benosman, M. (2016). *Learning-Based Adaptive Control: An Extremum Seeking Approach – Theory and Applications*, 1st edn, Butterworth-Heinemann, Oxford, UK.

Bergh, L. and Yianatos, J. (2013). Control of rougher flotation circuits aided by industrial simulator, *Journal of Process Control* **23**(2): 140–147.

Bergh, L. G. and Yianatos, J. B. (2011). The long way toward multivariate predictive control of flotation processes, *Journal of Process Control* **21**(2): 226–234.

Bouchard, J., Desbiens, A., del Villar, R. and Nunez, E. (2009). Column flotation simulation and control: An overview, *Minerals Engineering* **22**(6): 519–529.

Brogan, W. L. (1991). *Modern Control Theory*, 3rd edn, Prentice-Hall, Upper Saddle River, New Jersey, USA.

Brooks, K. and Munalula, W. (2017). Flotation velocity and grade control using cascaded model predictive controllers, *IFAC-PapersOnLine* **50**(2): 25–30.

Brożek, M. and Młynarczykowska, A. (2007). Analysis of Kinetics Models of Batch, *Physicochemical Problems of Mineral Processing* **41**: 51–65.

Camacho, E. F. and Bordons, C. (2013). *Model Predictive Control*, 2nd edn, Springer science & business media, London, UK.

Casali, A., Gonzalez, G., Agusto, H. and Vallebuona, G. (2002). Dynamic simulator of a rougher flotation circuit for a copper sulphide ore, *Minerals Engineering* **15**(4): 253–262.

Chioua, M., Srinivasan, B., Guay, M. and Perrier, M. (2016). Performance improvement of extremum seeking control using recursive least square estimation with forgetting factor, *IFAC-PapersOnLine* **49**(7): 424–429.

Craig, I. K. and Koch, I. (2003). Experimental design for the economic performance evaluation of industrial controllers, *Control Engineering Practice* **11**: 57–66.

Craig, I. K., Hulbert, D. G., Metzner, G. and Moult, S. P. (1992). Optimized multivariable control ot an industrial run-of-mine milling circuit, *Journal of the Southern African Institute of Mining and Metallurgy* **92**(6): 169–176.

Desbiens, A., Hodouin, D., Najim, K. and Flament, F. (1994). Long-range predictive control of a rougher flotation unit, *Minerals Engineering* **7**(1): 21–37.

Draper, C. S. and Li, Y. T. (1951). *Principles of optimalizing control systems and an application to the internal combustion engine*, American Society of Mechanical Engineers, New York, USA.

Fu, L. and Özgüner, Ü. (2011). Extremum seeking with sliding mode gradient estimation and asymptotic regulation for a class of nonlinear systems, *Automatica* **47**(12): 2595–2603.

Ghaffari, A., Krstić, M. and Nešić, D. (2012). Multivariable Newton-based extremum seeking, *Automatica* **48**(8): 1759–1767.

Gharai, M. and Venugopal, R. (2016). Modeling of flotation process - An overview of different approaches, *Mineral Processing and Extractive Metallurgy Review* **37**(2): 120–133.

Gomez, C. O. and Finch, J. A. (2007). Gas dispersion measurements in flotation cells, *International Journal of Mineral Processing* **84**(1-4): 51–58.

Guay, M. and Dochain, D. (2014). A proportional integral extremum-seeking control approach, *IFAC Proceedings Volumes* **47**(3): 377–382.

Guay, M. and Dochain, D. (2015). A time-varying extremum-seeking control approach, *Automatica* **51**: 356–363.

Guay, M. and Dochain, D. (2017). A proportional-integral extremum-seeking controller design technique, *Automatica* **77**: 61–67.

Guay, M., Dochain, D. and Perrier, M. (2004). Adaptive extremum seeking control of continuous stirred tank bioreactors with unknown growth kinetics, *Automatica* **40**(5): 881–888.

Guay, M., Moshksar, E. and Dochain, D. (2015). A constrained extremum-seeking control approach, *International Journal of Robust and Nonlinear Control* **25**(16): 3132–3153.

Gupta, A. and Yan, D. (2016). *Mineral processing design and operations: an introduction*, 2nd edn, Elsevier, Amsterdam, Netherlands.

Hadler, K. and Cilliers, J. J. (2009). The relationship between the peak in air recovery and flotation bank performance, *Minerals Engineering* **22**(5): 451–455.

Hadler, K., Greyling, M., Plint, N. and Cilliers, J. J. (2012). The effect of froth depth on air recovery and flotation performance, *Minerals Engineering* **36-38**: 248–253.

Hadler, K., Smith, C. D. and Cilliers, J. J. (2010). Recovery vs. mass pull: The link to air recovery, *Minerals Engineering* **23**(11-13): 994–1002.

Hernáinz, F. and Calero, M. (2001). Froth flotation: Kinetic models based on chemical analogy, *Chemical Engineering and Processing* **40**(3): 269–275.

Hodouin, D. (2011). Methods for automatic control, observation, and optimization in mineral processing plants, *Journal of Process Control* **21**(2): 211–225.

Hodouin, D., Jämsä-Jounela, S. L., Carvalho, M. T. and Bergh, L. (2001). State of the art and challenges in mineral processing control, *Control Engineering Practice* **9**(9): 995–1005.

Hunnekens, B. G., Haring, M. A., Van De Wouw, N. and Nijmeijer, H. (2014). A dither-free extremum-seeking control approach using 1st-order least-squares fits for gradient estimation, *53rd IEEE Conference on Decision and Control, 15–17 Dec 2014*, IEEE, Los Angeles, CA, USA, pp. 2679–2684.

ISA-75.01.01-2007 (2007). Flow Equations for Sizing Control Valves, *Technical report*, International Society for Automation, North Carolina, USA.

Jameson, G. J. (1998). New technology and science in flotation separations, *Current Opinion in Colloid and Interface Science* **3**(4): 351–359.

Jämsä-Jounela, S. L. (1992). Simulation study of self-tuning adaptive control for rougher flotation, *Powder Technology* **69**(1): 33–46.

Jämsä-Jounela, S.-L., Dietrich, M., Halmevaara, K. and Tiili, O. (2001). Control of pulp levels in flotation cells, *IFAC Proceedings Volumes* **34**(18): 175–180.

Jämsä-Jounela, S. L., Dietrich, M., Halmevaara, K. and Tiili, O. (2003). Control of pulp levels in flotation cells, *Control Engineering Practice* **11**(1): 73–81.

Jovanović, I. and Miljanović, I. (2015a). Contemporary advanced control techniques for flotation plants with mechanical flotation cells - A review, *Minerals Engineering* **70**: 228–249.

Jovanović, I. and Miljanović, I. (2015b). Modelling of flotation processes by classical mathematical methods - a review, *Archives of Mining Sciences* **60**(4): 905–919.

Kämpjärvi, P. and Jämsä-Jounela, S. L. (2003). Level control strategies for flotation cells, *Minerals Engineering* **16**(11): 1061–1068.

Koh, P. T. and Schwarz, M. P. (2006). CFD modelling of bubble-particle attachments in flotation cells, *Minerals Engineering* **19**(6-8): 619–626.

Krstić, M. and Wang, H. H. (2000). Stability of extremum seeking feedback for general nonlinear dynamic systems, *Automatica* **36**(4): 595–601.

Lara-Cisneros, G., Femat, R. and Dochain, D. (2017). Robust sliding mode-based extremum-seeking controller for reaction systems via uncertainty estimation approach, *International Journal of Robust and Nonlinear Control* **27**(16): 3218–3235.

Larsson, T. and Skogestad, S. (2000). Plantwide control - a review and a new design procedure, *Modeling, Identification and Control* **21**(4): 209–240.

Laurila, H., Karesvuori, J. and Tiili, O. (2002). Strategies for instrumentation and control of flotation circuits, *Mineral Processing Plant Design, Practice and Control* **2**: 2174–2195.

le Roux, J. D. and Craig, I. K. (2019). Plant-wide control framework for a grinding mill circuit, *Industrial and Engineering Chemistry Research* **58**(26): 11585–11600.

le Roux, J. D., Craig, I. K., Hulbert, D. G. and Hinde, A. L. (2013). Analysis and validation of a run-of-mine ore grinding mill circuit model for process control, *Minerals Engineering* **43-44**: 121–134.

Leblanc, M. (1922). Sur l'electrification des chemins de fer au moyen de courants alternatifs de frequence elevee, *Revue générale de l'électricité* **12**(8): 275–277.

Li, Y., Zhao, W., Gui, X. and Zhang, X. (2013). Flotation kinetics and separation selectivity of coal size fractions, *Physicochemical Problems of Mineral Processing* **49**(2): 387–396.

Lu, X., Krstic, M., Chai, T. and Fu, J. (2021). Hardware-in-the-loop multiobjective extremum-seeking control of mineral grinding, *IEEE Transactions on Control Systems Technology* **29**(3): 961–971.

Maldonado, M., Araya, R. and Finch, J. (2012). An overview of optimizing strategies for flotation banks, *Minerals* **2**(4): 258–271.

Maldonado, M., Desbiens, A. and del Villar, R. (2009). Potential use of model predictive control for optimizing the column flotation process, *International Journal of Mineral Processing* **93**(1): 26–33.

Maldonado, M., Sbarbaro, D. and Lizama, E. (2007). Optimal control of a rougher flotation process based on dynamic programming, *Minerals Engineering* **20**(3): 221–232.

Matthews, B. and Craig, I. K. (2013). Demand side management of a run-of-mine ore milling circuit, *Control Engineering Practice* **21**(6): 759–768.

McIvor, R. E. and Finch, J. A. (1991). A guide to interfacing of plant grinding and flotation operations, *Minerals Engineering* **4**(1): 9–23.

McKee, D. J. (1991). Automatic flotation control - a review of 20 years of effort, *Minerals Engineering* **4**(7-11): 653–666.

Moase, W. H. and Manzie, C. (2012). Fast extremum-seeking for Wiener-Hammerstein plants, *Automatica* **48**(10): 2433–2443.

Moase, W. H., Manzie, C. and Brear, M. J. (2010). Newton-like extremum-seeking for the control of thermoacoustic instability, *IEEE Transactions on Automatic Control* **55**(9): 2094–2105.

Muller, D., De Villiers, P. G. and Humphries, G. (2010). A holistic approach to flotation mass pull and grade control, *IFAC Proceedings Volumes* **43**(9): 133–136.

Muñoz, C. and Cipriano, A. (1999). An integrated system for supervision and economic optimal control of mineral processing plants, *Minerals Engineering* **12**(6): 627–643.

Neethling, S. J. and Cilliers, J. J. (2008). Predicting air recovery in flotation cells, *Minerals Engineering* **21**(12-14): 937–943.

Neethling, S. J., Lee, H. T. and Cilliers, J. J. (2003). Simple relationships for predicting the recovery of liquid from flowing foams and froths, *Minerals Engineering* **16**(11): 1123–1130.

Nelder, J. A. and Mead, R. (1965). A simplex method for function minimization, *The Computer Journal* **7**(4): 308–313.

Nešić, D., Mohammadi, A. and Manzie, C. (2010). A systematic approach to extremum seeking based on parameter estimation, *Proceedings of the IEEE Conference on Decision*

and Control pp. 3902–3907.

Norori-McCormac, A., Brito-Parada, P. R., Hadler, K., Cole, K. and Cilliers, J. J. (2017). The effect of particle size distribution on froth stability in flotation, *Separation and Purification Technology* **184**: 240–247.

Olivier, L. E. and Craig, I. K. (2017). A survey on the degree of automation in the mineral processing industry, *2017 IEEE AFRICON: Science, Technology and Innovation for Africa, 18–20 Sep 2017*, Cape Town, South Africa, pp. 404–409.

Oosthuizen, D. J. (2023). *A dynamic flotation model for online estimation, control and optimisation*, PhD thesis, University of Pretoria.

Oosthuizen, D. J., Craig, I. K., Jämsä-Jounela, S. L. and Sun, B. (2017). On the current state of flotation modelling for process control, *IFAC-PapersOnLine* **50**(2): 19–24.

Oosthuizen, D. J., le Roux, J. D. and Craig, I. K. (2021). A dynamic flotation model to infer process characteristics from online measurements, *Minerals Engineering* **167**: 106878.

Pauw, O. G., King, R. P., Garner, K. C. and Van Aswegen, P. C. (1985). The control of pebble mills at Buffelsfontein Gold Mine by use of a multivariable peak-seeking controller, *Journal of The South African Institute of Mining and Metallurgy* **85**(3): 89–96.

Pérez-Correa, R., González, G., Casali, A., Cipriano, A., Barrera, R. and Zavala, E. (1998). Dynamic modelling and advanced multivariable control of conventional flotation circuits, *Minerals Engineering* **11**(4): 333–346.

Pérez-García, E. M., Bouchard, J. and Poulin, É. (2020). A mineral liberation distribution estimator for monitoring and process control applications, *Powder Technology* **367**: 527–538.

Phillpotts, D., Whitehead, B. and Ramatsoma, S. (2020). Monitoring of air recovery for froth flotation optimisation on an industrial circuit, *XXX International Mineral Processing Congress, 18–22 Oct 2020*, Cape Town, South Africa, pp. 3348–3357.

Polat, M. and Chander, S. (2000). First-order flotation kinetics models and methods for estimation of the true distribution of flotation rate constants, *International Journal of Mineral Processing* **58**(1-4): 145–166.

Putz, E. and Cipriano, A. (2015). Hybrid model predictive control for flotation plants, *Minerals Engineering* **70**: 26–35.

Qin, S. J. and Badgwell, T. A. (2003). An overview of industrial model predictive control technology, *Control Engineering Practice* **11**(7): 733–764.

Qu, X., Wang, L. and Nguyen, A. V. (2013). Correlation of air recovery with froth stability and separation efficiency in coal flotation, *Minerals Engineering* **41**: 25–30.

Quintanilla, P., Neethling, S. J. and Brito-Parada, P. R. (2021a). Modelling for froth flotation control: A review, *Minerals Engineering* **162**(September 2020): 106718.

Quintanilla, P., Neethling, S. J., Mesa, D., Navia, D. and Brito-Parada, P. R. (2021b). A dynamic flotation model for predictive control incorporating froth physics. Part II: Model calibration and validation, *Minerals Engineering* **173**: 107190.

Quintanilla, P., Neethling, S. J., Navia, D. and Brito-Parada, P. R. (2021c). A dynamic flotation model for predictive control incorporating froth physics. Part I: Model development, *Minerals Engineering* **173**: 107192.

Savassi, O. N., Alexander, D. J., Franzidis, J. P. and Manlapig, E. V. (1998). An empirical model for entrainment in industrial flotation plants, *Minerals Engineering* **11**(3): 243–256.

Schena, G., Casali, A. and Vallebuona, G. (1996). Optimal throughput policies for a copper concentrator, *Minerals Engineering* **9**(11): 1105–1117.

Schubert, J., Henning, R., Hulbert, D. and Craig, I. (1995). Flotation control - a multivariable stabilizer, *XIX International Mineral Processing Congress, 23–27 Oct 1995*, San Francisco, CA, USA.

Schuhmann, R. (1942). Flotation kinetics. I: Methods for steady-state study of flotation problems, *Journal of Physical Chemistry* **46**(8): 891–902.

Shean, B., Hadler, K. and Cilliers, J. J. (2017). A flotation control system to optimise performance using peak air recovery, *Chemical Engineering Research and Design* **117**: 57–65.

Shean, B., Hadler, K., Neethling, S. and Cilliers, J. J. (2018). A dynamic model for level prediction in aerated tanks, *Minerals Engineering* **125**: 140–149.

Shean, B. J. and Cilliers, J. J. (2011). A review of froth flotation control, *International Journal of Mineral Processing* **100**(3-4): 57–71.

Skogestad, S. (2004). Control structure design for complete chemical plants, *Computers and Chemical Engineering* **28**(1-2): 219–234.

Smith, C. D., Hadler, K. and Cilliers, J. J. (2010). Flotation bank air addition and distribution for optimal performance, *Minerals Engineering* **23**(11-13): 1023–1029.

Smith, G. C., Jordaan, L., Singh, A., Vandayar, V., Smith, V. C., Muller, B. and Hulbert, D. G. (2004). Innovative process control technology for milling and flotation circuit operations, *Journal of The South African Institute of Mining and Metallurgy* **104**(6): 353–365.

Somasundaran, P. and Lin, I. J. (1973). Method for Evaluating Flotation Kinetics Parameters, *Trans Soc Mining Eng AIME* **254**(2): 181–184.

Sosa-Blanco, C., Hodouin, D., Bazin, C., Lara-Valenzuela, C. and Salazar, J. (2000). Economic optimization of a flotation plant through grinding circuit tuning, *Minerals Engineering* **13**(10): 999–1018.

Supomo, A., Yap, E., Zheng, X., Banini, G., Mosher, J. and Partanen, A. (2008). PT Freeport Indonesia's mass-pull control strategy for rougher flotation, *Minerals Engineering* **21**(12-14): 808–816.

Tan, Y., Moase, W. H., Manzie, C., Nešić, D. and Mareels, I. M. (2010). Extremum seeking from 1922 to 2010, *Proceedings of the 29th Chinese Control Conference* pp. 14–26.

Tan, Y., Nešić, D. and Mareels, I. (2006). On non-local stability properties of extremum seeking control, *Automatica* **42**(6): 889–903.

Thivierge, A., Bouchard, J., Desbiens, A. and Pérez, E. M. (2019). Modeling the product net value of a grinding-flotation circuit, *IFAC-PapersOnLine* **52**(14): 18–23.

Thornton, A. J. (1991). Cautious adaptive control of an industrial flotation circuit, *Minerals Engineering* **4**(12): 1227–1242.

Tian, Y., Luan, X., Liu, F. and Dubljevic, S. (2018). Model predictive control of mineral column flotation process, *Mathematics* **6**(6): 1–17.

van Schalkwyk, T. (2002). *Multivariable Control of a Rougher Flotation Cell*, Master's thesis, University of Cape Town.

Ventura-Medina, E. and Cilliers, J. J. (2002). A model to describe flotation performance based on physics of foams and froth image analysis, *International Journal of Mineral Processing* **67**(1-4): 79–99.

Wang, G., Ge, L., Mitra, S., Evans, G. M., Joshi, J. B. and Chen, S. (2018). A review of CFD modelling studies on the flotation process, *Minerals Engineering* **127**: 153–177.

Wang, H.-H., Krstić, M. and Bastin, G. (1999). Optimizing bioreactors by extremum seeking, *International Journal of Adaptive Control and Signal Processing* **13**(8): 651–669.

Wei, D. and Craig, I. K. (2009). Economic performance assessment of two ROM ore milling circuit controllers, *Minerals Engineering* **22**(9-10): 826–839.

Wepener, D. A., le Roux, J. D. and Craig, I. K. (2021). Disturbance propagation through a grinding-flotation circuit, *IFAC-PapersOnLine* **54**(21): 19–24.

Wepener, D. A., le Roux, J. D. and Craig, I. K. (2022). Extremum seeking control of a flotation circuit using peak air recovery, *IFAC PapersOnLine* **55**(21): 61–66.

Wills, B. A. and Finch, J. (2015). *Wills' mineral processing technology: an introduction to the practical aspects of ore treatment and mineral recovery*, 8th edn, Butterworth-Heinemann, Oxford, UK.

Woods, R. (2003). Electrochemical potential controlling flotation, *International Journal of Mineral Processing* **72**(1-4): 151–162.

Wright, B. (1999). *The Development of a Vision-Based Flotation Froth Analysis System*, PhD thesis, University of Cape Town.

Xiong, Q. and Jutan, A. (2003). Continuous optimization using a dynamic simplex method, *Chemical Engineering Science* **58**(16): 3817–3828.

Yianatos, J., Carrasco, C., Bergh, L., Vinnett, L. and Torres, C. (2012). Modelling and simulation of rougher flotation circuits, *International Journal of Mineral Processing* **112-113**: 63–70.

Zhang, C. and Ordóñez, R. (2009). Robust and adaptive design of numerical optimization-based extremum seeking control, *Automatica* **45**(3): 634–646.

Zhang, C. and Ordóñez, R. (2012). *Extremum-seeking control and applications: a numerical optimization-based approach*, Springer Science & Business Media, London, UK.

Ziolkowski, L., le Roux, J. D. and Craig, I. K. (2021). Optimizing grinding mill performance using extremum seeking control, *IFAC-PapersOnLine* **54**(11): 43–48.

Ziolkowski, L., le Roux, J. D. and Craig, I. K. (2022). Extremum seeking control for optimization of an open-loop grinding mill using grind curves, *Journal of Process Control* **114**: 54–70.

APPENDIX A ADDITIONAL RESULTS

A.1 SISO AIR RECOVERY SURFACE PLOTS

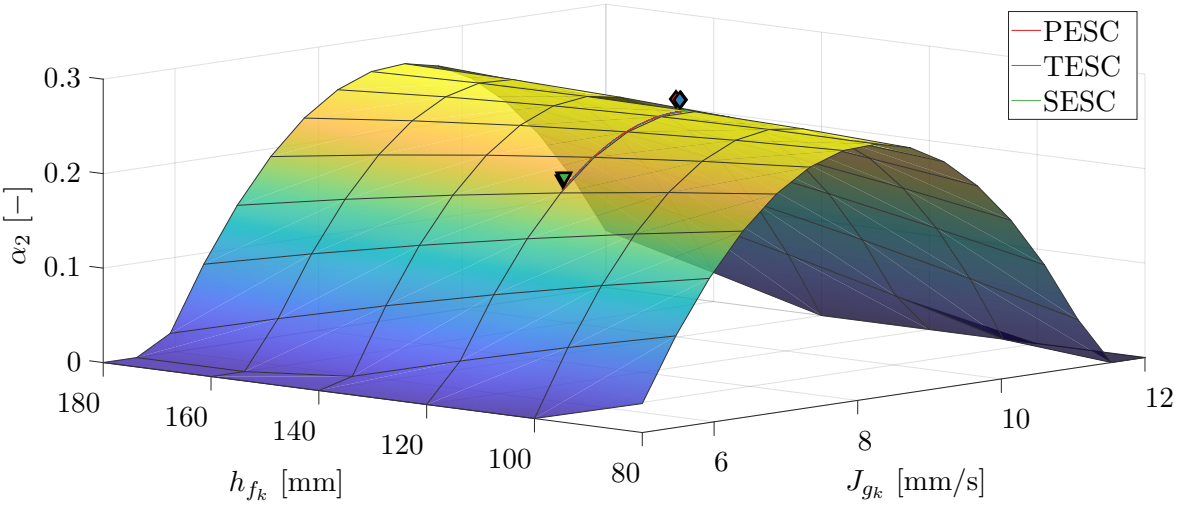

Figure A.1. Air recovery surface plot for cell 2 showing SISO air recovery optimization. The initial conditions are indicated by ∇ and the final optimized operating points by ◊.

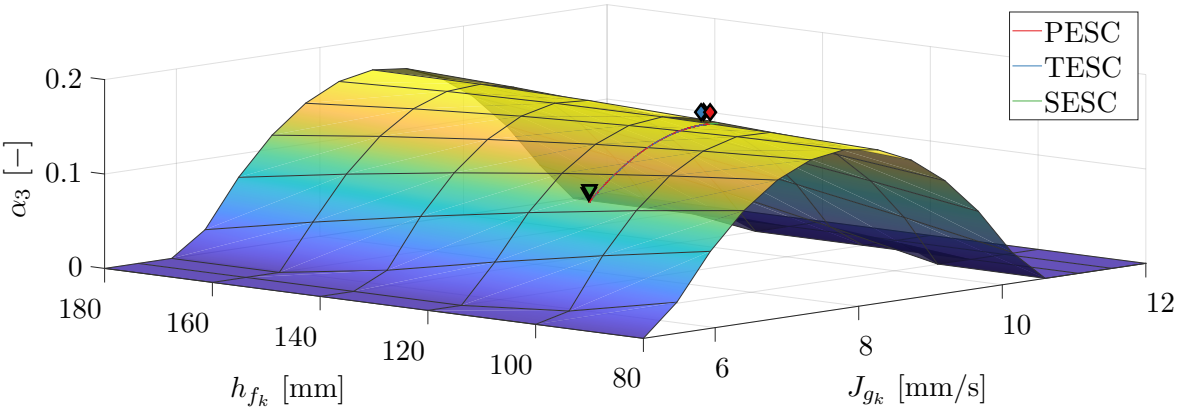

Figure A.2. Air recovery surface plot for cell 3 showing SISO air recovery optimization. The initial conditions are indicated by ∇ and the final optimized operating points by ◊.

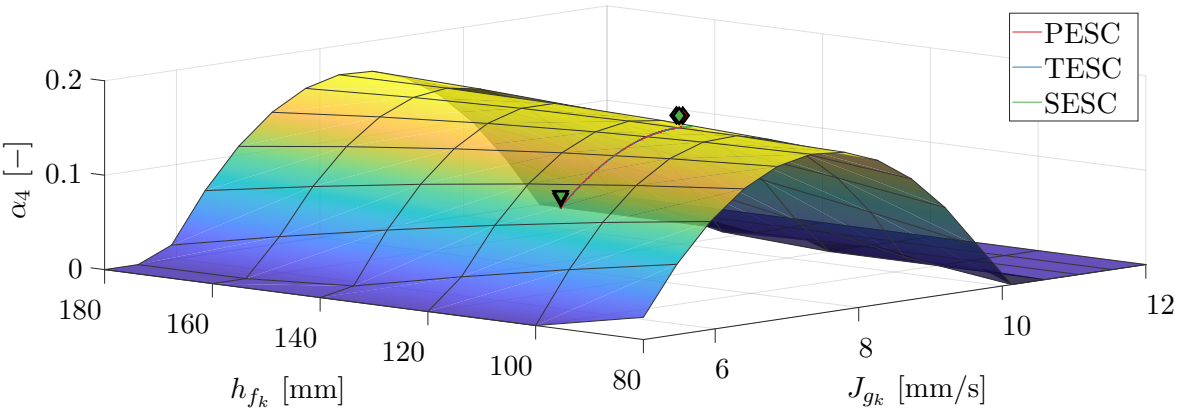

Figure A.3. Air recovery surface plot for cell 4 showing SISO air recovery optimization. The initial conditions are indicated by ∇ and the final optimized operating points by ◊.

A.2 MISO AIR RECOVERY SURFACE PLOTS

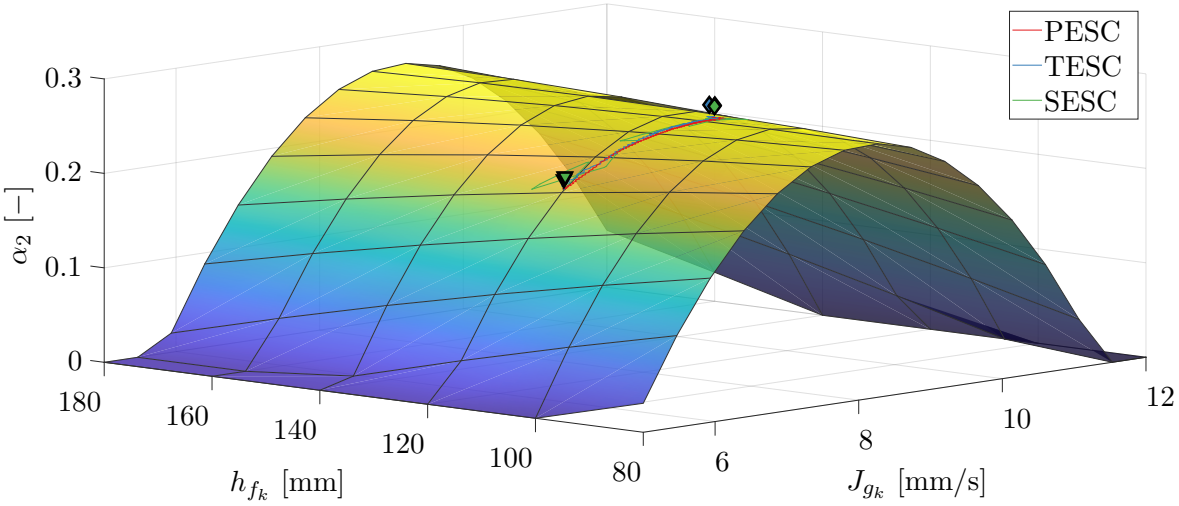

Figure A.4. Air recovery surface plot for cell 2 showing MISO air recovery optimization. The initial conditions are indicated by ∇ and the final optimized operating points by ◊.

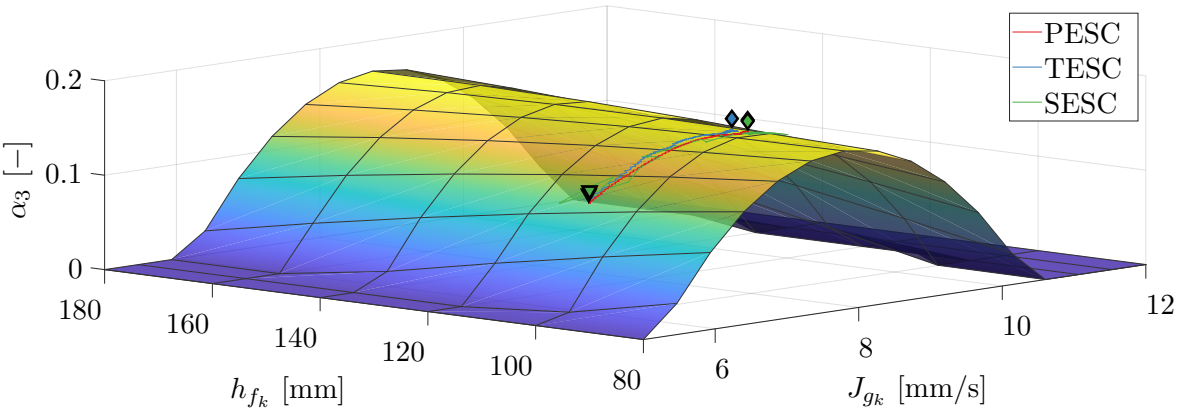

Figure A.5. Air recovery surface plot for cell 3 showing MISO air recovery optimization. The initial conditions are indicated by ∇ and the final optimized operating points by ◊.

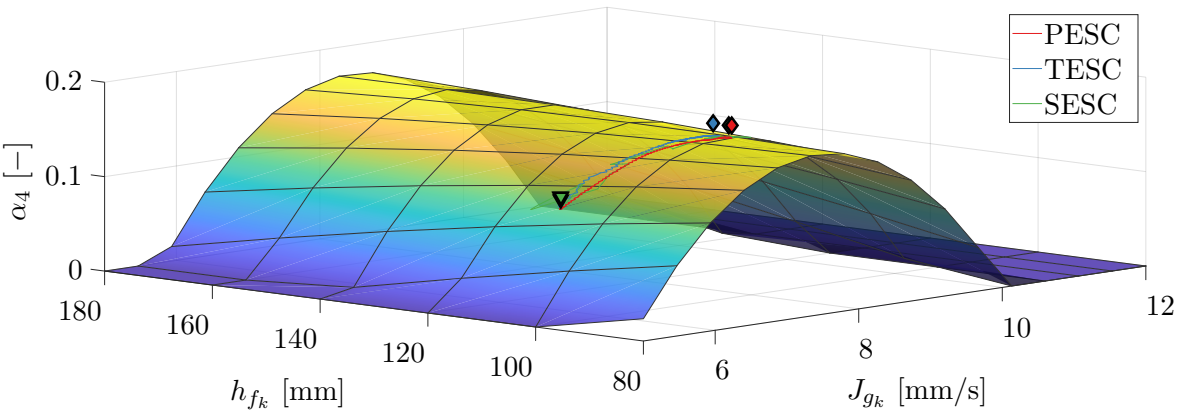

Figure A.6. Air recovery surface plot for cell 4 showing MISO air recovery optimization. The initial conditions are indicated by ∇ and the final optimized operating points by ◊.

APPENDIX B DISTURBANCE PROPAGATION THROUGH A GRINDING-FLOTATION CIRCUIT

In this appendix, the propagation of common disturbances in a grinding circuit connected to a flotation circuit and the effects of these disturbances on flotation cell levels are simulated and analyzed. The disturbances include changes in the mineral ore feed as well as a step change in the cyclone operating condition and spillage water added to the sump. The effect of the disturbances on the cell levels remains relatively small, but it is clear that multivariable control is required to prevent the propagation of the disturbances through the cells. Since few plant-wide simulation platforms for mineral processing plants exist, a contribution of this appendix is to present a simple simulation framework of a grinding mill circuit combined with a flotation circuit. The simulation of a grinding-flotation circuit is useful to simulate the effects of disturbance propagation which is an important consideration when designing flotation and plant-wide controllers (Wepener et al., 2021). A brief overview of the mineral processing process is given in section B.1. The grinding and flotation circuit models are described in sections B.2 and B.3. The simulation setup and results are shown in section B.4 and discussed in section B.5.

B.1 PROCESS DESCRIPTION

The two main stages of the mineral processing chain in Figure 2.1 are the comminution stage and the separation stage. In this appendix, a specific configuration of these two stages will be simulated together, which consists of a grinding circuit and a flotation circuit. The grinding and flotation processes have been described in Sections 2.2.2 and 2.2.3, respectively.

The grinding circuit used in this appendix is a single-stage closed run-of-mine (ROM) ore grinding circuit shown in Figure B.1. The grinding circuit includes three main components: a semi-autogenous (SAG) grinding mill, a sump and a hydrocyclone. The model and parameters for the grinding circuit are given in Section B.2. The model classifies the ore into different size classes. Firstly the ore is divided into rocks and solids where solids are defined as ore material small enough to pass through the mill end-discharge screen and rocks are too large to be discharged by the mill. Solids can then further be divided into coarse and fine ore, where fine ore is all ore smaller than the final product specification size (75 μm), and coarse ore is ore larger than the product specification size. The flotation circuit in this appendix consists of seven cells connected in series to form a rougher flotation bank, as shown in Figure B.2. The output of the grinding circuit, the cyclone overflow, flows directly into the first flotation cell. The model and parameters for the flotation circuit are given in Section B.3.

B.2 GRINDING CIRCUIT MODEL DESCRIPTION

The *Hulbert* grinding mill model of le Roux et al. (2013) will be used here to simulate the grinding circuit and is divided into three modules: mill, sump and hydrocyclone. Fig. B.1 shows the configuration of the grinding circuit including the mill, sump and cyclone modules.

In the model, the flow rates in m^3/h are given by Q and the volumetric states in m^3 by V. The first subscript of Q and V indicate the module (**m**ill, **s**ump or **c**yclone). The second subscript specifies the state (**w**ater, **s**olids, **c**oarse, **f**ines, **r**ock, **b**alls or **t**otal). The flow rates have a third subscript that indicates if the flow is an **i**nflow, **o**utflow or **u**nderflow.

B.2.1 Mill

The changes in the mill states are given by,

$$\dot{V}_{mw} = MIW + Q_{cwu} - Q_{mwo}, \tag{B.1a}$$

$$\dot{V}_{ms} = \frac{MFO}{\rho_O}(1-\alpha_r) + Q_{csu} - Q_{mso} + Q_{RC}, \tag{B.1b}$$

$$\dot{V}_{mf} = \frac{MFO}{\rho_O}\alpha_f + Q_{cfu} - Q_{mfo} + Q_{FP}, \tag{B.1c}$$

$$\dot{V}_{mr} = \frac{MFO}{\rho_O}\alpha_r - Q_{RC}, \tag{B.1d}$$

$$\dot{V}_{mb} = \frac{MFB}{\rho_B} - Q_{BC}, \tag{B.1e}$$

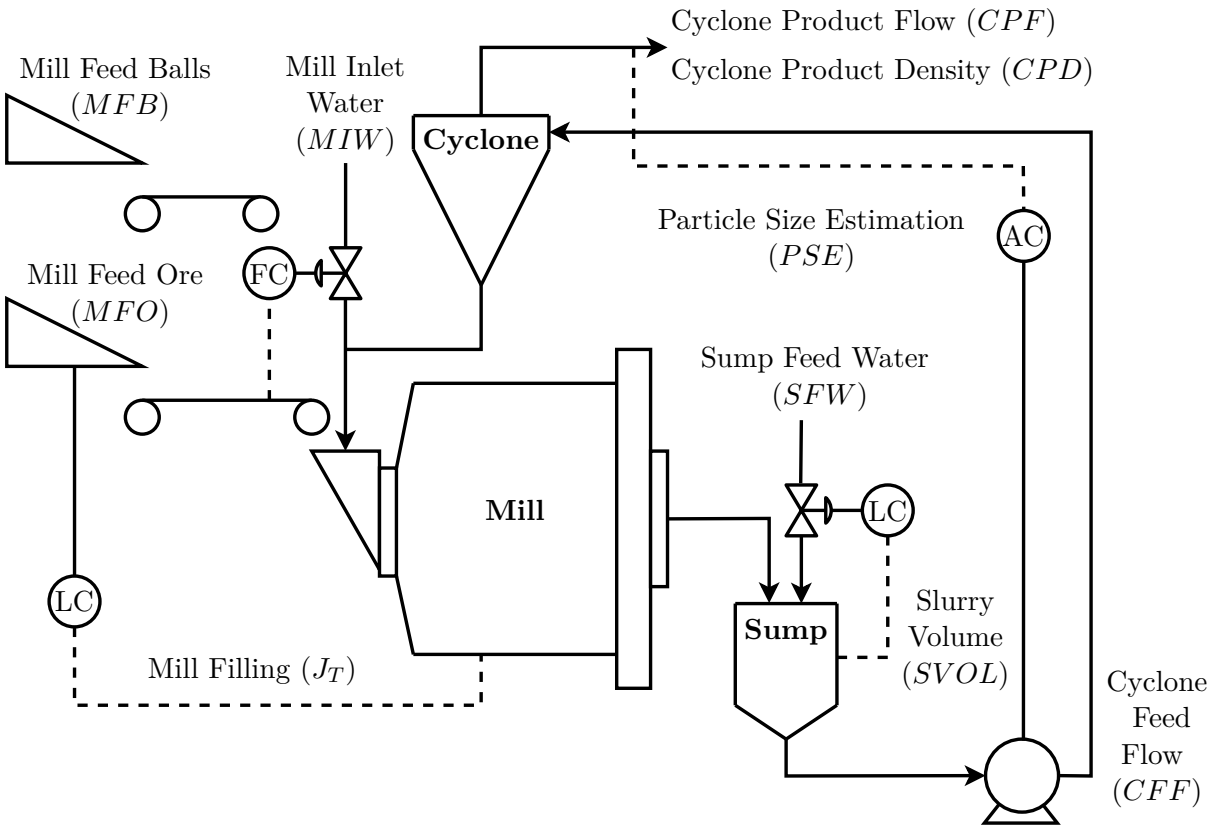

Figure B.1. Grinding circuit configuration with regulatory controllers

where MIW (m^3/h) is the Mill Inlet Water, MFO (t/h) is the Mill Feed Ore, MFB (t/h) is the Mill Feed Balls, ρ_O (t/m^3) is the density of ore, ρ_B (t/m^3) is the density of balls, α_r is the fraction of rock in the ore, and α_f the fraction of fines in the ore. Q_{RC} represents the rock consumption, Q_{BC} is the ball consumption, and Q_{FP} is the fines production in the mill. The mill rheology factor is,

$$\varphi = \begin{cases} \sqrt{1 - \left(\varepsilon_0^{-1} - 1\right) \frac{V_{ms}}{V_{mw}}} & ; \quad \frac{V_{ms}}{V_{mw}} \leq \left(\varepsilon_0^{-1} - 1\right)^{-1} \\ 0 & ; \quad \frac{V_{ms}}{V_{mw}} > \left(\varepsilon_0^{-1} - 1\right)^{-1} \end{cases} \tag{B.2}$$

where ε_0 is the fraction of solids by volume of slurry. The mill power draw is,

$$\begin{aligned} P_{mill} = (1 - \delta_{Pv} Z_x^2 - 2\chi_P \delta_{Pv} \delta_{Ps} Z_x Z_r - \delta_{Ps} Z_r^2) \\ \cdot P_{max} (\alpha_{speed})^{\alpha_P}, \end{aligned} \tag{B.3}$$

where P_{max} (kW) is the maximum mill motor power draw, δ_{Pv} is the power-change parameter for volume, δ_{Ps} is the power-change parameter for fraction solids, χ_P is the cross-term for maximum power draw, α_{speed} is the fraction of critical mill speed, and α_P is the fractional power reduction per fractional reduction from maximum mill speed. The effect of the total

charge on mill power (Z_x) is,

$$Z_x = \frac{LOAD}{v_{mill} \cdot v_{P_{max}}} - 1, \tag{B.4}$$

where v_{mill} (m^3) is the total mill volume, $v_{P_{max}}$ is the fraction of the mill filled for maximum power draw and the load in the mill is,

$$LOAD = V_{mw} + V_{mr} + V_{ms} + V_{mb} \tag{B.5}$$

with the fraction of the mill filled given by,

$$J_T = \frac{LOAD}{v_{mill}}. \tag{B.6}$$

The effect of the slurry rheology on mill power (Z_r) is,

$$Z_r = \frac{\varphi}{\varphi_{P_{max}}} - 1, \tag{B.7}$$

where $\varphi_{P_{max}}$ is the rheology factor for maximum mill power draw. The breakage function for rock consumption is,

$$Q_{RC} = \frac{P_{mill} \cdot \varphi}{\rho_O \phi_r} \left(\frac{V_{mr}}{V_{mr} + V_{ms}} \right), \tag{B.8}$$

where ϕ_r (kWh/t) is the rate of rock consumption in the mill. The breakage function for ball consumption is given by,

$$Q_{BC} = \frac{P_{mill} \cdot \varphi}{\phi_b} \left(\frac{V_{mb}}{\rho_O \cdot (V_{mr} + V_{ms}) + \rho_B \cdot V_{mb}} \right), \tag{B.9}$$

where ϕ_b (kWh/t) is the rate of ball consumption in the mill. The production of fines in the mill is,

$$Q_{FP} = \frac{P_{mill}}{\rho_O \cdot \left(\phi_f \cdot \left(1 + \alpha_{\phi_f} \cdot \left(\frac{LOAD}{v_{mill}} - v_{P_{max}} \right) \right) \right)}, \tag{B.10}$$

where ϕ_f (kWh/t) is the power needed per tonne of fines produced, and α_{ϕ_f} is the fractional change in power per fines produced per change in the fractional filling of the mill. The discharge flow rates out of the mill are given by,

$$Q_{mwo} = d_q \cdot \varphi \cdot V_{mw} \cdot \left(\frac{V_{mw}}{V_{ms} + V_{mw}} \right), \tag{B.11a}$$

$$Q_{mso} = d_q \cdot \varphi \cdot V_{mw} \cdot \left(\frac{V_{ms}}{V_{ms} + V_{mw}} \right), \tag{B.11b}$$

$$Q_{mfo} = d_q \cdot \varphi \cdot V_{mw} \cdot \left(\frac{V_{mf}}{V_{ms} + V_{mw}} \right), \tag{B.11c}$$

$$Q_{mro} = 0, \tag{B.11d}$$

$$Q_{mbo} = 0, \tag{B.11e}$$

where d_q is the discharge constant.

B.2.2 Mixed-sump

The changes in the sump states are given by,

$$\dot{V}_{sw} = Q_{swi} - Q_{swo} + SFW, \tag{B.12a}$$

$$\dot{V}_{ss} = Q_{ssi} - Q_{sso}, \tag{B.12b}$$

$$\dot{V}_{sf} = Q_{sfi} - Q_{sfo}, \tag{B.12c}$$

where SFW (m^3/h) is the Sump Feed Water and the input flow rates to the sump are equal to the mill output flow rates given by,

$$Q_{swi} = Q_{mwo}, \tag{B.13a}$$

$$Q_{ssi} = Q_{mso}, \tag{B.13b}$$

$$Q_{sfi} = Q_{mfo}. \tag{B.13c}$$

The Cyclone Feed Density (t/m^3) is,

$$CFD = \frac{V_{sw} + \rho_O \cdot V_{ss}}{SVOL}, \tag{B.14}$$

where the volume of slurry in the sump is,

$$SVOL = V_{sw} + V_{ss}. \tag{B.15}$$

The sump discharge flow rates are given by,

$$Q_{swo} = CFF \cdot \left(\frac{V_{sw}}{SVOL}\right), \tag{B.16a}$$

$$Q_{sso} = CFF \cdot \left(\frac{V_{ss}}{SVOL}\right), \tag{B.16b}$$

$$Q_{sfo} = CFF \cdot \left(\frac{V_{sf}}{SVOL}\right), \tag{B.16c}$$

where CFF is the cyclone feed flow rate.

B.2.3 Hydrocyclone

The cyclone coarse ore underflow is,

$$\begin{aligned} Q_{ccu} = &\left(1 - C_1 e^{\left(\frac{-CFF}{\varepsilon_c}\right)}\right)\left(1 - \left(\frac{F_i}{C_2}\right)^{C_3}\right) \\ &\left(1 - P_i^{C_4}\right)(Q_{sso} - Q_{sfo}), \end{aligned} \tag{B.17}$$

where ε_c (m^3/h) is a parameter related to coarse split, $F_i = \frac{Q_{sso}}{CFF}$, $P_i = \frac{Q_{sfo}}{Q_{sso}}$ and C_1, C_2, C_3 and C_4 are constant cyclone parameters. The underflow of water and fines are given by,

$$Q_{cwu} = \frac{Q_{swo}(Q_{ccu} - F_u Q_{ccu})}{F_u Q_{swo} + F_u Q_{sfo} - Q_{sfo}} \tag{B.18a}$$

$$Q_{cfu} = \frac{Q_{sfo}(Q_{ccu} - F_u Q_{ccu})}{F_u Q_{swo} + F_u Q_{sfo} - Q_{sfo}}, \tag{B.18b}$$

where

$$F_u = 0.6 - (0.6 - F_i) \cdot e^{\left(\frac{-Q_{ccu}}{\alpha_{su}\varepsilon_c}\right)} \tag{B.19}$$

and α_{su} is the fraction of solids in the underflow. The outflow flow rates can be determined by subtracting the underflows from the inflows. The Cyclone Product Flow (CPF) (m^3/h), product Particle Size Estimation (PSE) (fraction of fines in the product) and Cyclone Product Density (CPD) (t/m^3) are given by,

$$CPF = Q_{cwo} + Q_{cso} \tag{B.20a}$$

$$PSE = \frac{Q_{cfo}}{Q_{cco} + Q_{cfo}} \tag{B.20b}$$

$$CPD = \frac{Q_{cso}\rho_O + Q_{cwo}}{CPF}. \tag{B.20c}$$

B.2.4 Grinding circuit parameters

Table B.1 shows the plant data obtained from an industrial milling circuit, and Table B.2 shows the estimated model parameters for the *Hulbert* model and the initial states.

Table B.1. Grinding circuit plant data.

Parameter	Value	Unit	Parameter	Value	Unit
MIW	373	m^3/h	V_{mill}	497	m^3
MFO	759	t/h	J_T	0.307	–
α_r	0.7464	–	J_B	0.12	–
α_f	0.00015	–	SFW	858	m^3/h
ρ_O	2.63	t/m^3	V_{sump}	54	m^3
ρ_B	7.84	t/m^3	$SVOL$	35	m^3
P_{mill}	12.6	MW	CFF	3141	m^3/h
P_{max}	14	MW	CFD	1.65	t/m^3
α_{speed}	0.82	–	PSE	0.60	–

B.3 FLOTATION CIRCUIT MODEL DESCRIPTION

The flotation model of Jämsä-Jounela et al. (2003) gives a very simple way to model the level of flotation cells in series by considering the flow rates into and out of each flotation cell and

Table B.2. Grinding circuit estimated parameters and initial states.

Parameter	Value	Unit	Parameter	Value	Unit
Mill and feeder parameters					
MFB	50.297	t/h	$\varphi_{P_{max}}$	0.49	–
ε_0	0.6	–	ϕ_r	5.496	kWh/t
δ_{pv}	0.5	–	ϕ_b	90	kWh/t
δ_{ps}	0.5	–	ϕ_f	27.675	kWh/t
χ_P	0	–	α_{ϕ_f}	0.01	–
α_P	0.53	–	d_q	185.09	h^{-1}
$v_{P_{max}}$	0.307	–			
Cyclone parameters					
ε_c	487.228	–	C_3	4	–
C_1	0.6	–	C_4	4	–
C_2	0.7	–	α_{su}	1.099	–
States					
V_{mw}	28.175	m^3	V_{mf}	6.810	m^3
V_{mb}	59.640	m^3	V_{sw}	21.043	m^3
V_{mr}	32.655	m^3	V_{ss}	13.957	m^3
V_{ms}	32.109	m^3	V_{sf}	2.960	m^3

is used in this simulation study. The concentrate flow rate is much lower than the tailings flow rate and its effect on the cell level is ignored in this simulation study. The simulated plant has seven flotation cells in series as shown in Fig. B.2.

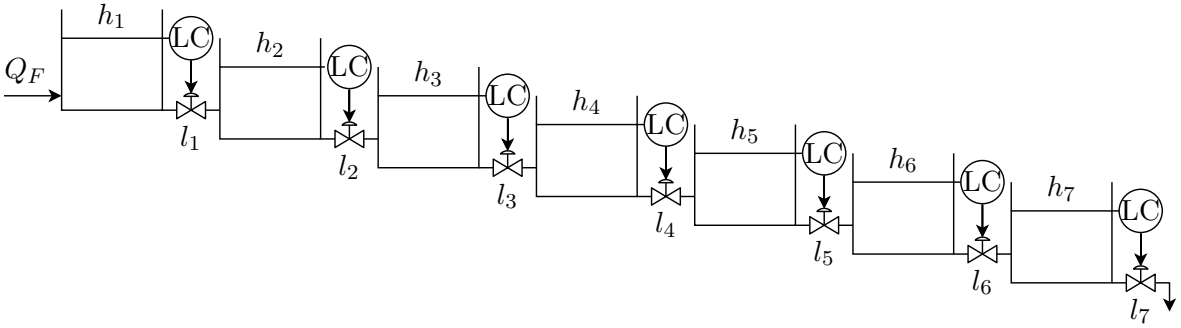

Figure B.2. Flotation bank configuration with regulatory controllers

The change in volume of the first cell is,

$$\dot{V}_1 = Q_F - \left(K \cdot C_v \cdot f_c(l_1) \cdot \sqrt{h_1 - h_2 + H_1}\right), \tag{B.21}$$

where Q_F (m^3/h) is the feed flow rate to the first cell and is equal to the CPF (assuming no storage or conditioning tank is used between the milling and flotation circuits). h_i (m) is

the pulp level in the i^{th} cell, H_i (m) is the physical difference in height between cell i and cell $i+1$, K is a constant coefficient, and C_v is the valve capacity coefficient. l_i is the valve control signal of the i^{th} cell and is a value between zero and one with zero being completely closed and one completely open. Linear valves are assumed, therefore $f_c(l_i) = l_i$. For cells, 2 to 6 where i is the cell number, the change in volume is,

$$\begin{aligned}\dot{V}_i = &\left(K \cdot C_v \cdot f_c(l_{i-1}) \cdot \sqrt{h_{i-1} - h_i + H_{i-1}}\right) \\ &- \left(K \cdot C_v \cdot f_c(l_i) \cdot \sqrt{h_i - h_{i+1} + H_i}\right),\end{aligned} \tag{B.22}$$

and for cell 7 the change in volume is,

$$\begin{aligned}\dot{V}_7 = &\left(K \cdot C_v \cdot f_c(l_6) \cdot \sqrt{h_6 - h_7 + H_6}\right) \\ &- \left(K \cdot C_v \cdot f_c(l_7) \cdot \sqrt{h_7 + H_7}\right).\end{aligned} \tag{B.23}$$

The cross-section of the cells (A_i) is assumed to be constant. The change in pulp levels in the cells is therefore,

$$\dot{h}_i = \frac{\dot{V}_i}{A_i}. \tag{B.24}$$

The valve capacity coefficient (C_v) is calculated according to ISA-75.01.01-2007,

$$C_v = 1.17 \cdot Q_m \cdot \sqrt{\frac{\rho_P}{\Delta p}}, \tag{B.25}$$

where ρ_P is the pulp density (t/m^3). The pressure difference over the valve (Δp) is assumed to be a function of the physical height difference of the cells and pulp density only and is,

$$\Delta p = \rho_P g H_i, \tag{B.26}$$

where $g = 9.81\,\text{m/s}^2$. Q_m is the mean flow rate (m^3/h) through the cell,

$$Q_m = 1.2\frac{V_i}{\tau/60}, \tag{B.27}$$

where τ (min) is the pulp retention time in the cell.

The flotation model parameters and initial states were obtained from an industrial flotation circuit and are given in Table B.3.

B.4 SIMULATION

The circuit models are simulated with different disturbances in the grinding circuit to monitor the changes in the levels of the flotation cells. Fig. B.3 shows the inputs and the disturbances during the simulation. A step disturbance in ϕ_f of +10 kWh/t is introduced for 1 h at $t = 1$ h under normal operating conditions. Then from $t = 3$ h for 1 h a step disturbance of +3 kWh/t

Table B.3. Flotation circuit parameters and initial states.

Parameter	Value	Unit	Parameter	Value	Unit
Q_F	1519.6	m^3/h	$K_{i=1..6}$	7.6895	$m^{2.5}/s$
V_{cell}	76	m^3	K_7	2.6847	$m^{2.5}/s$
A_i	12	m^2	h_i	6.123	m
H_i	0.85	m	V_i	73.476	m^3
τ	5	min	l_i	0.5	–

is introduced in ϕ_r. The first two disturbances simulate an increase in the power needed per tonne of fines and rocks produced respectively. This reflects a change in the hardness of the ore. Spillage water of 10 % of SFW is added to the sump from $t = 5$ h for 1 h and from $t = 7$ h for 1 h the PSE setpoint is increased by 0.03 %. Lastly, the ϕ_f, ϕ_r, as well as the spillage water disturbance, are simulated simultaneously from $t = 9$ h for 2 h.

A PI-controller is used to regulate the charge inside the mill (J_T) by manipulating the feed ore and water flow rates into the mill (MFO and MIW). The flow rates are controlled in a constant ratio of $MIW/MFO = 0.49$ to ensure that the change in slurry density is kept as small as possible. A second PI-controller is used to control the sump level with the sump feed water (SFW) and a third control the PSE with the CFF. On each of the seven flotation cells, a PI-controller is implemented to control the level of the cell to a setpoint of 6.123 m by adjusting the linear valves limiting the outflow of each cell. The PI-controllers have the form,

$$MV(t) = MV(0) + K_c \left(E(t) + \frac{1}{\tau_I} \int_0^t E(t)dt \right), \tag{B.28}$$

where $E(t) = SP(t) - CV(t)$, MV is the manipulated variable, SP is the setpoint, CV is the controlled variable, K_c is the proportional gain, and τ_I is integration constant. Table B.4 gives the controller parameters for the PI-controllers.

Table B.4. PI-controller parameters.

CV	SP	MV	MV(0)	K_c	τ_I
J_T	0.307 %	MFO	759 t/h	36365	0.116
$SVOL$	35 m^3	SFW	858 m^3/h	145.5	0.04
PSE	0.6 %	CFF	3414 m^3/h	2500	0.08
h_i	6.123 m	l_i	0.5	−1	0.02

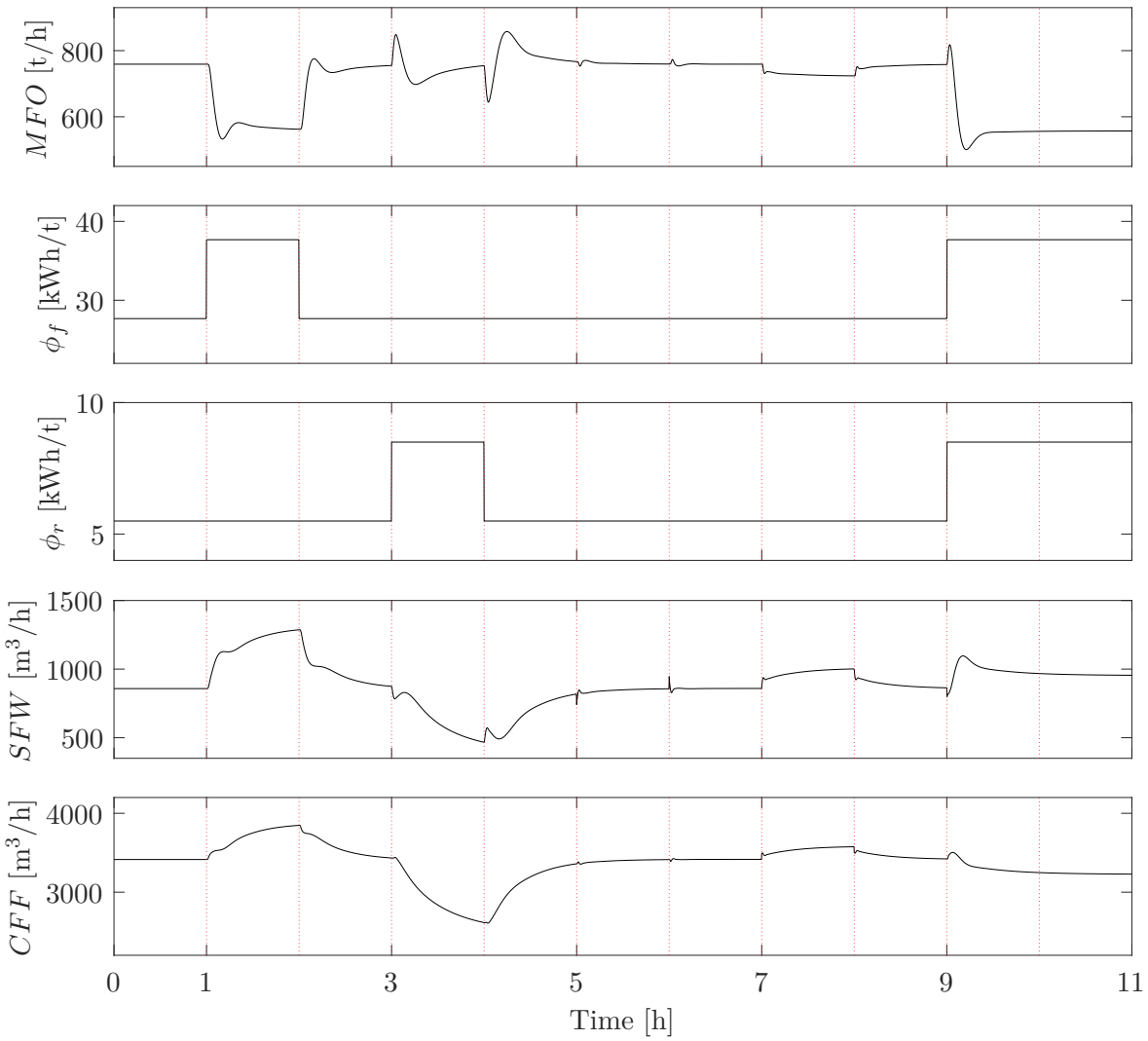

Figure B.3. Grinding circuit input simulation result

The circuit models are simulated in MATLAB and Simulink for 11 h with a sampling interval of 10 s using the Runge-Kutta 4^{th} order numerical integration method. The simulation results of the grinding mill and flotation cells can be seen in Fig. B.4 and Fig. B.5 respectively.

B.5 DISCUSSION AND CONCLUSION

The change in hardness of the ore simulated by the step disturbance in ϕ_f reduces the amount of fines produced which increases the charge in the mill (J_T). The controller adjusts to this change by decreasing the input feed MFO and MIW to keep the charge in the mill at the setpoint. The reduced flow volume into the mill causes a drop in the sump level and thus an increase in SFW as shown in Fig. B.3 and Fig. B.4. The increase in ore hardness also causes a decrease in PSE for which the controller compensates by increasing CFF. The increased

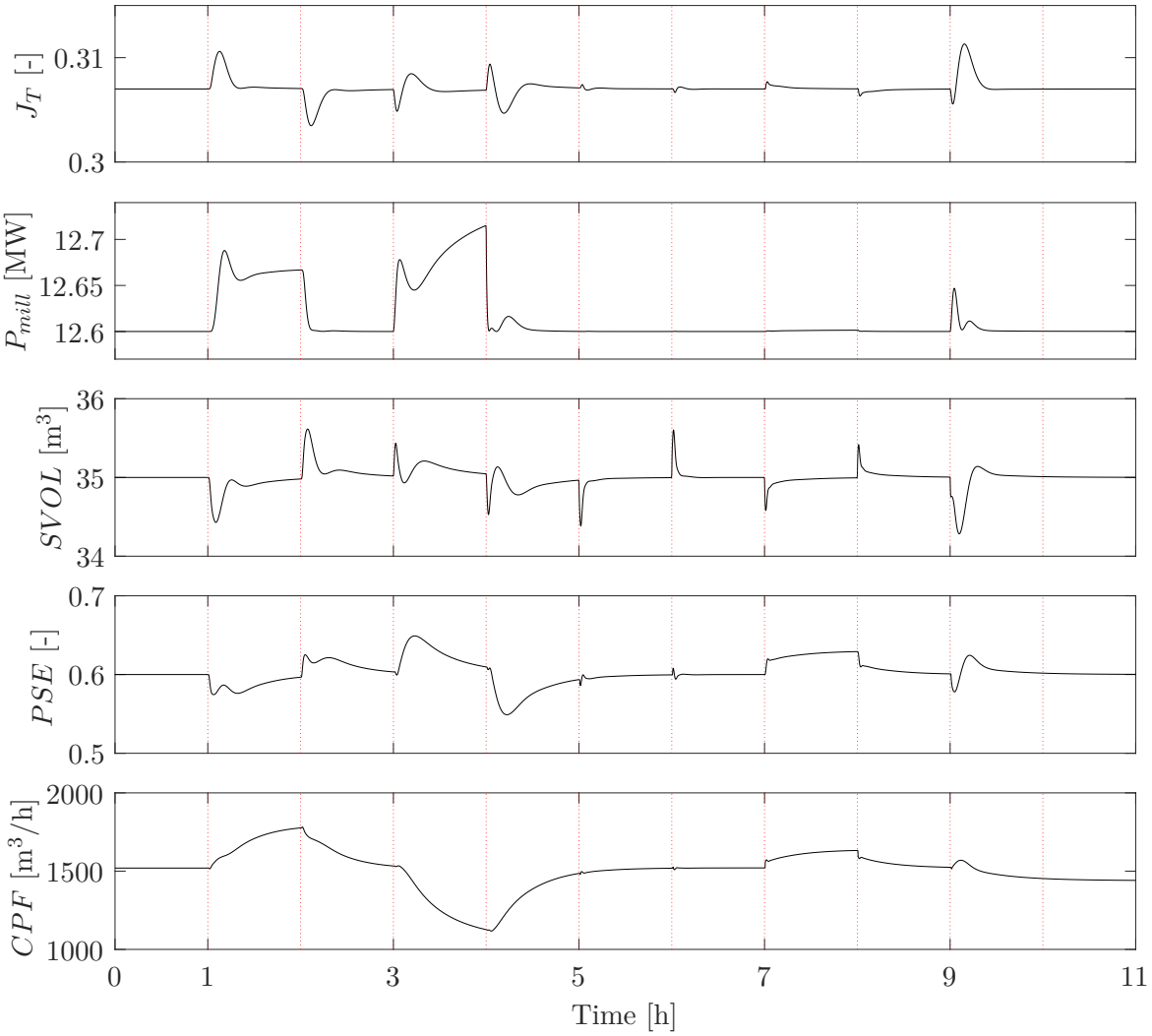

Figure B.4. Grinding circuit output simulation result

cyclone feed rate results in an increased cyclone outflow and the flotation levels start to rise as shown in Fig. B.5. The disturbance in ϕ_r has a similar effect on the mill as the disturbance in ϕ_f but in the opposite direction. The disturbances in ϕ_f and ϕ_r cause an increase in P_{mill} since more power is used to grind the harder ore.

The effect of the sump spillage water disturbance is negated by the sump level controller which acts quickly by decreasing SFW and bringing the sump level back to the setpoint. The step disturbance in PSE and subsequent increase in CFF to correct it directly affects the cyclone by increasing both the underflow and overflow and a slight increase in the cell levels can be seen. The combination of different disturbances almost cancels each other out since the individual disturbances cause changes in opposite directions and only a small increase in

Figure B.5. Flotation bank simulation result

the flotation levels can be seen.

As expected, Fig. B.5 shows how the disturbances of the grinding mill circuit propagate through the flotation cells. Although the cell level variations are relatively small, at least in this simulation scenario, it is clear that the effect of the disturbances on CPF propagates from the first cell to the last cell. The disturbance of the ore hardness via ϕ_f and ϕ_r has the largest overall impact on the flotation cell, while the sump spillage water disturbance

results in the largest sudden change in the cell levels. It is not visible in this graph, but there is a small delay in the propagation of the disturbance from one cell to the next. It is clear that multivariable control is required to optimally control the flotation levels and prevent the propagation of the disturbance through the flotation cells (Schubert et al., 1995; Smith et al., 2004).

Possible future work can include the effect of the disturbances on the final grade and recovery and not only the cell levels. The model can also be expanded to include a more comprehensive flotation model, such as by Oosthuizen et al. (2021) and validating the plant-wide model with industry data. A better control framework can be designed using an expanded plant-wide model to optimize the economic performance of the plant. Control actions for extreme cases such as a complete stop in ore feed can also be explored and included in the control framework.